The American Mineralogist

Journal of the Mineralogical Society of America

Vol. 37 JULY-AUGUST, 1952 Nos. 7 and 8

Contents

Published bi-monthly by the Society

Mineralogical Society of America

ASSOCIATED WITH THE GEOLOGICAL SOCIETY OF AMERICA

President: Michael Fleischer, U. S. Geological Survey, Washington 25, D. C.
Vice President: J. D. H. Donnay, The Johns Hopkins University, Baltimore, Maryland.
Secretary: C. S. Hurlbut, Jr., Harvard University, Cambridge, Massachusetts.
Treasurer: Earl Ingerson, U. S. Geological Survey, Washington 25, D. C.
Editor: Walter F. Hunt, University of Michigan, Ann Arbor, Michigan.
Councillors: Lewis S. Ramsdell, University of Michigan, Ann Arbor, Michigan.
E. F. Osborn, School of Mineral Industries, Pennsylvania State College, Pennsylvania.
George T. Faust, U. S. Geological Survey, Washington 25, D. C.
Victor T. Allen, Institute of Geophysical Technology, St. Louis, Missouri.
Adolf Pabst, University of California, Berkeley, California

The enlarged issues of this journal for 1952 are made possible by a grant from the Penrose Fund of the Geological Society of America.

The American Mineralogist—Journal of the Mineralogical Society of America

A journal containing articles on mineralogy, crystallography, petrography, and allied sciences, is issued every two months. Contributions are invited from everyone.
Office of Publication, Mineralogical Laboratory, Ann Arbor, Mich.

The general conduct of the journal is in the hands of the editor, **Walter F. Hunt**, Ann Arbor, Michigan, to whom all manuscripts should be submitted. To assist the editor the council of the Mineralogical Society has appointed **Lewis S. Ramsdell**, Ann Arbor, Michigan, assistant editor, and the following board of associate editors:

Michael Fleischer, U. S. Geological Survey, Washington, D. C.
Esper S. Larsen, Jr., U. S. Geological Survey, Washington, D. C.
Austin F. Rogers, 2412 Durant Ave., Berkeley, California.
George Tunell, University of California at Los Angeles, California.

Contributors of leading articles are given without charge 100 reprints (without covers) of their article. If additional reprints are desired these can be purchased at the following rates:

Pages	*1–4*	*5–8*	*9–12*	*13–16*	*17–20*	*21–24*	*25–28*	*29–32*	*Covers*
Copies									
25	$3.50	$5.00	$ 8.00	$ 9.50	$11.00	$13.00	$15.00	$16.00	$4.90
50	3.80	5.55	8.80	10.40	12.10	14.20	16.40	17.50	5.50
75	4.10	6.10	9.60	11.30	13.20	15.40	17.80	19.00	6.10
100	4.00	6.65	10.40	12.20	14.30	16.60	19.20	20.50	6.70
Addl. C's	1.20	2.20	3.20	3.60	4.40	4.80	5.60	6.00	2.40

Cover Composition $1.55.

Sent to all members and fellows of the Mineralogical Society of America. Subscription price, $4.00 per year (single copies of normal issues, $1.00 plus postage).

Entered as second class matter at the post office at Menasha, Wis., under Act of March 3, 1879. Acceptance for mailing at the special rate of postage provided for in section 1103, Act of Oct. 3, 1917, paragraph 4 section 429 P. L. & R. authorized March 13, 1922.

Notice of change of address, orders, and remittances should be sent to Dr. Earl Ingerson, U. S. Geological Survey, Washington 25, D. C.

Printed by the George Banta Publishing Company, Menasha, Wisconsin
Printed in the United States of America

THE AMERICAN MINERALOGIST

JOURNAL OF THE MINERALOGICAL SOCIETY OF AMERICA

Vol. 37 JULY-AUGUST, 1952 Nos. 7 and 8

FORMATION TEMPERATURES OF SOUTHERN ILLINOIS BEDDED FLUORITE AS DETERMINED FROM FLUID INCLUSIONS[1]

ROBERT M. GROGAN AND RAYMOND S. SHRODE

ABSTRACT

Fluid inclusions in fluorite crystals were studied principally to determine the range of temperature of formation of individual crystals. Measurements were made by heating specimens and recording temperatures at which vapor bubbles within the inclusions disappeared. Over-all accuracy, excluding pressure corrections, was of the order of $\pm 2.5°$ C.

Some of the fluid inclusions are arranged in geometrically regular planes parallel to cube faces. These are apparently of primary origin. Others form bands along former fractures which approximately parallel the cleavage directions and which cut across each other and the primary planes alike. Historically such inclusions have been called "secondary" although "subsequent" is considered a more meaningful designation. Most of the primary inclusions are smoothly rounded and contain petroleum, whereas "subsequent" inclusions range from jagged to smooth in outline and contain principally a clear fluid.

Measurements on primary inclusions indicate that temperatures at which the crystals grew generally ranged from 83° to 115° C., with a mean around 100° C. Commonly the indicated growth temperature increased slightly for some distance outward from the crystal center and then dropped off toward the exterior. Measurements on subsequent inclusions gave results in the range of 112° to 172° C., generally higher than those shown by primary inclusions.

Incomplete bulk analyses of the fluid from inclusions, probably mostly of the subsequent variety, show a preponderance of Ca, Na, and Cl ions, and a total concentration of dissolved material amounting to 45,000 parts per million.

INTRODUCTION

Investigations of the temperature of formation of fluorite from deposits in southern Illinois have been carried on in the laboratories of the Illinois State Geological Survey at intervals for a number of years. The method used in all the studies is that in which liquid inclusions within cleavage or sawed plates of the mineral are observed through a microscope equipped with a heating stage, and the temperatures are recorded at which the vapor bubbles within the liquid inclusions disappear. These temperatures are considered to be approximately those at which the fluorite was deposited.

[1] Published with the permission of the Chief, Illinois State Geological Survey.

Initial investigations involving the use of cleavage flakes of fluorite from crystals in different parts of several mines yielded temperature data which, although informative, seemed to lack any pattern or internal consistency. It was decided, therefore, to work out the thermal history of a number of individual crystals in an effort to obtain more useful data. This article describes the major results of this most recent phase of the work and discusses some of its implications.

Fluid inclusions in minerals result from imperfect crystal growth. The fluid in each is assumed to have filled its containing cavity at the above-atmospheric temperature and pressure prevailing when the cavity was closed off. At room temperature the contracted fluid occupies less space than it did at the temperature of entrapment, and a vapor bubble is present in consequence. When the mineral is heated in the laboratory the fluid expands and the vapor bubble shrinks and disappears at a temperature which approximates that prevailing when the cavity was filled and sealed. This temperature is low, however, by an amount proportional to the magnitude of the original pressure, by which the fluid had been somewhat compressed. The true formation temperature is not attained until heating has continued to the point where the pressure exerted by the fluid within the cavity again equals the original pressure. If it is possible to estimate the magnitude of this original pressure, an appropriate correction may be added to the cavity-filling temperature to arrive at a closer approximation of the true temperature of formation.

Work of Previous Investigators

Sorby[2] demonstrated, by artificially crystallizing a number of compounds, that crystals formed in free space frequently contain fluid inclusions developed during growth of the crystals, and that the size of the vapor bubbles in the inclusions at room temperature was determined by the temperature and pressure conditions prevailing when the crystal was grown. He concluded that similar fluid inclusions in natural crystals might be used to determine the temperature-pressure relations when those natural crystals were formed.

After a long period in which the nature and importance of Sorby's work was generally overlooked, Newhouse[3] brought to light and applied the method to the study of fluid inclusions in sphalerite crystals from zinc-lead deposits in the Mississippi Valley region. Since that time numerous investigators have employed the principle in studies of formation temperature of various types of crystals and mineral deposits.

[2] Sorby, H. C., On the microscopical structure of crystals: *Quart. Jour., Geol. Soc. London*, **14**, 453–500 (1858).

[3] Newhouse, W. H., Temperature of formation of Mississippi Valley lead-zinc deposits: *Econ. Geol.*, **28**, 744–750 (1933).

Ingerson[4] discussed theoretical aspects of the method as applied to geologic thermometry and prepared curves showing the relationship between temperature of disappearance of the vapor bubbles and temperature and pressure at the time of formation of the inclusions. Twenhofel[5] investigated a number of inclusions within a slice sawed from a well-formed fluorite crystal and observed decreasing temperature zones from the center to the outside of the crystal. He also noted a change in crystal habit from octahedral in the interior to cubic at the exterior. Bailey[6] applied the method to the quartz of granites, but was handicapped by the small number of inclusions which could be accurately determined as primary. Dreyer, Garrels, and Howland[7] investigated the temperature of formation of halite crystals from undisturbed beds in various salt mines.

Scott,[8] Peach,[9] and Smith[10] employed a decrepitation technique differing from the visual method used by other investigators. They heated mineral fragments in a furnace and recorded the intensity of sound produced by decrepitation of the mineral at various temperatures. From the resulting data, they believe estimates of formation temperature may be made. Kennedy[11] discussed some of the limitations of the decrepitation method and presented new charts, based on recent experimental work, for determining the true temperature of formation from observational data plus estimates of the pressures at the time of crystal growth.

Technique

Selection and preparation of specimens. Six crystals were chosen for study on the basis of variety of geographic and stratigraphic location, the

[4] Ingerson, Earl, Liquid inclusions of geologic thermometry: *Am. Mineral.*, **38,** 375–388 (1947).

[5] Twenhofel, W. S., The temperature of crystallization of a fluorite crystal from Luna County, New Mexico: *Econ. Geol.*, **42,** 78–82 (1947).

[6] Bailey, Sturges W., Liquid inclusions in granite thermometry: *Jour. Geol.*, **57,** 304–307 (1949).

[7] Dreyer, R. M., Garrels, R. M., and Howland, A. L., Liquid inclusions in halite as a guide to geologic thermometry: *Am. Mineral.*, **34,** 26–34 (1949).

[8] Scott, H. S., The decrepitation method applied to minerals with fluid inclusions: *Econ. Geol.*, **43,** 637–645 (1947).

[9] Peach, P. A., A decrepitation geothermometer: *Am. Mineral.*, **34,** 413–442 (1949).

———, Geothermometry of some pegmatite minerals of Hybla, Ontario: *Jour. Geol.*, **59,** 32–38 (1951).

[10] Smith, F. G., and Peach, P. A., Apparatus for the recording of decrepitation in Minerals: *Econ. Geol.*, **44,** 449–451 (1949).

Smith, F. G., Laboratory testing of "pneumatolytic" deposits: *Econ. Geol.*, **44,** 624–625 (1949).

[11] Kennedy, George C., "Pneumatolysis" and the liquid inclusion method of geologic thermometry: *Econ. Geol.*, **45,** 533–548 (1950).

fact that they grew on the walls of vugs and projected freely into open spaces, and the fact that they had at least three well-defined cube faces. Cube faces were the only forms present. All crystals came from bedding replacement deposits of the Cave in Rock district of eastern Hardin County.

From these selected crystals slices about 2.5 mm. thick were cut with a diamond saw. The slices were cut as nearly as possible through the growth centers of the crystals, perpendicular to one crystallographic axis and parallel to the other two.

Measurement of temperatures. The sawed slices were supported horizontally on a piece of 8-mesh copper screen about one-sixteenth of an inch above the bottom of a shallow Pyrex dish about $2\frac{1}{2}$ inches in diameter. Wooden pegs stuck into the screen kept the specimens from moving laterally. Thus the silicone oil, of refractive index close to that of fluorite, which was employed as the heating medium was able to circulate freely around the specimens. The Pyrex dish was placed in a thin transite collar held in the jaws of a mechanical stage. The regular stage on the microscope was replaced by an independent box-like stage of transite, which supports the mechanical stage, a modified Leitz hot stage, and a mirror. When in use, the Pyrex dish was in contact with the surface of the hot stage and could be moved about in a controlled, measurable manner by means of mechanical stage. A thin glass plate placed over the dish cut down loss of heat and spattering of hot oil.

The amount and rate of heat input to the hot stage was controlled by a powerstat. Temperatures were measured with a copper-constantan thermocouple inserted between the specimen and the copper screen and connected through a zero-degree reference junction to a Leeds and Northrup K-2 potentiometer.

During the heating process, the inclusions were observed by transmitted light with a microscope equipped with a long focal length heat-resisting objective. The temperature was allowed to rise slowly to the point of disappearance of the vapor bubble, and the temperature at that instant recorded. The current was then turned off until the temperature had fallen low enough for the bubble to reform, and subsequently raised again to the disappearance point to provide a check on the first reading.

By employing coordinates read from the vernier scales on the mechanical stage, it was possible to prepare accurate diagrams of the sections showing the exact location of inclusions used in temperature measurements.

Accuracy of measurements. Tests involving placing the thermocouple at various points within the bath, both in contact with and away from the copper screen, indicated no measurable temperature gradient within

the bath when the heating was slow. When the vapor bubble of an inclusion was clearly visible down to the point of disappearance, duplicate temperature measurements consistently showed a variation of less than 0.5° C. When the visibility of the vapor bubble near the end point was reduced by dark "relief" borders around the inclusion or by small opaque masses within the inclusion, less accuracy was obtainable. By comparing results obtained from partially obscured inclusions with adjacent clear inclusions, it was estimated that the expectable variation due to poor visibility was of the order of ±2° C. or less. Thus the probable variation observed from true end-point temperatures was about ±2.5° C.

Results

The results of the study of one typical crystal slice are shown in Fig. 1. Two well-formed cube faces have been cut and a third is parallel to the plane of the section. Lines representing planes of inclusions connect circles representing individual inclusions used, and the numbers indicate the temperatures of vapor bubble disappearance. There are two kinds of planes of inclusions. One, represented by lines A–A' and B–B', is parallel

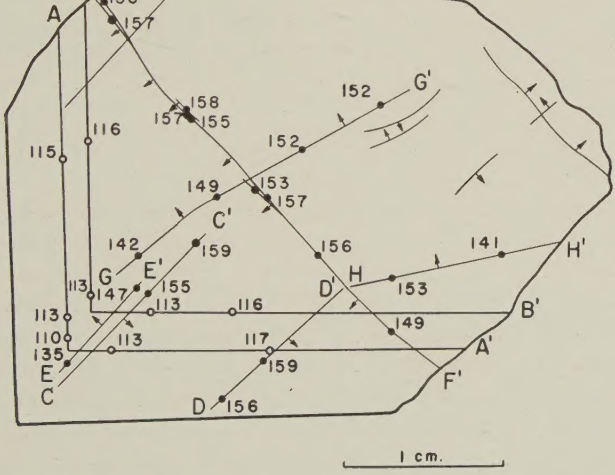

Fig. 1. Slice from a typical fluorite crystal, showing location of planes of fluid inclusions and of inclusions for which temperature determinations were made. Open circles indicate primary inclusions along lines A–A' and B–B', parallel to cube faces. Solid circles indicate subsequent inclusions along lines C–C' to H–H' which follow fairly closely the directions of octahedral cleavage and are inclined to the plane of the slice as shown by the dip arrows. Numbers indicate temperatures in °C. The slice is about one inch square.

to the cube faces and vertical to the plane of the section. The other, represented by lines *C–C′* to *H–H′*, trends at angles to the cube faces and to the plane of the section as shown by the dip arrows. The vertical planes make right angles following the cubic contour of the crystal, but do not cross each other. They parallel bands of coloration which are usually considered zonal growth phenomena. The inclusions along them are ellipsoidal and vary in size from sub-microscopic to megascopic.

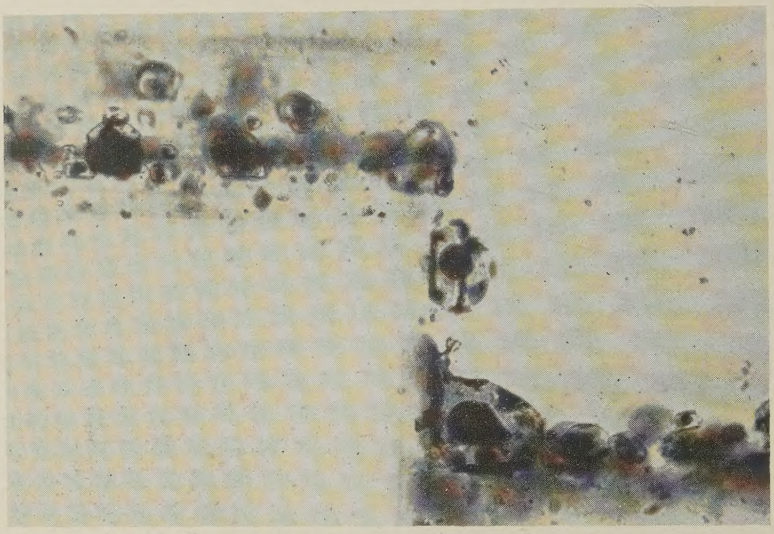

FIG. 2. Primary fluid inclusions along planes vertical to the plane of the slice and parallel to cube faces of the crystal. The offset pattern apparently mirrors an irregularity in a former surface of the crystal. The faint bands paralleling the planes of inclusions are zones of purple coloration common in fluorite crystals. The inclusions contain petroleum, a rounded vapor bubble which photographed black, and small masses of dark opaque material which is probably bitumen.

Many are flattened on the side toward the interior of the crystal, some on two sides where they lie in an interior angle. Figure 2 shows how they look through the microscope. They contain yellow petroleum, small masses of opaque material presumably bitumen, and, at room temperature, a vapor bubble. The petroleum fluoresces under ultra-violet light, contains a low boiling fraction that evaporates quickly when inclusions are opened, and has a carbon-hydrogen ratio of approximately 1:2, as indicated by micro-analysis of a tiny sample.[12] Although all the inclusions in vertical planes examined in this study contained only petroleum, it is possible that inclusions which contain some other liquid might be found.

[12] Analysis by H. S. Clark, Assoc. Chemist, Illinois State Geological Survey.

The inclusions along planes parallel to the cube faces are considered to be of primary origin and the planes in which they lie to mark successive stages in the growth of the crystals.

The inclined planes of inclusions, Fig 1, frequently intersect and cross each other, as well as planes parallel to cube faces. Most of them follow more or less closely the octahedral direction of cleavage characteristic of the mineral. Some of these planes are remarkably flat and straight, whereas others undulate or curve somewhat. The appearance under the microscope of crossing inclined planes is shown in Fig. 3 and that of an inclined plane crossing two vertical planes in Fig. 4. Frequently these inclined planes terminate within the crystal along lines paralleling cube faces as shown in Fig. 5. The inclusions on these inclined planes are of various shapes from smoothly oval to irregular and even sharply jagged. Figure 6 shows a group of them which have rather regular shapes. All these inclusions used in the present study contained only a colorless watery liquid and a bubble, but from work on other fluorite crystals from the same district it is known that some contain in addition a drop of yellow petroleum.

It is postulated that these inclusions were formed at various times in

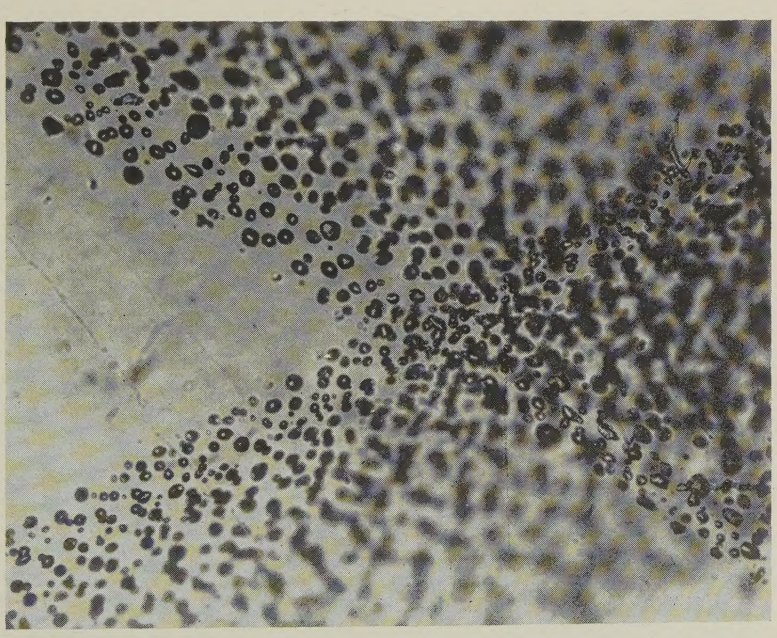

FIG. 3. Appearance of crossing inclined planes of fluid inclusions. Note the continuation without deviation of each plane beyond the line of intersection. Line of sight is normal to one cube face and parallel to two others.

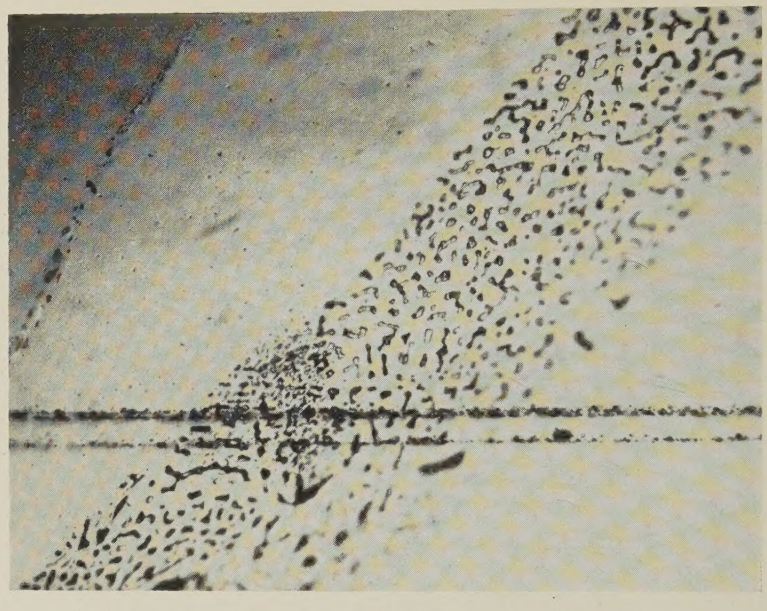

FIG. 4. Inclined plane of fluid inclusions crossing two vertical planes. The vertical planes appear as narrow lines because they lie parallel to the line of sight.

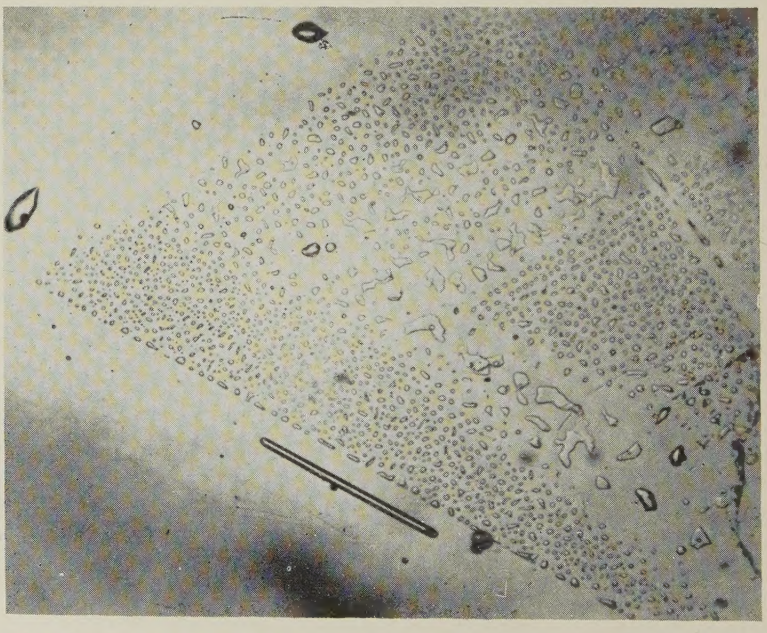

FIG. 5. Inclined plane of fluid inclusions terminating along interior lines parallel to cube faces of a fluorite crystal. As the view is of a cleavage flake instead of a sawed slice, the inclined plane lies normal to the line of sight.

FIG. 6. Group of subsequent inclusions of typical sub-regular outline. The inclusions contain vapor bubbles (the dark round objects) and a colorless watery fluid.

the history of the crystal, along intersecting cleavage and related fracture planes resulting from twisting or warping stresses set up by differential subsidence during formation of the deposit, or to shocks incident to faulting, or sudden temperature changes, even though all the crystals studied were found projecting into open cavities. Liquid inclusions of this type have been called "secondary," but the term "subsequent" inclusions is preferred because they were formed in a different manner from the primary inclusions and subsequent to that part of the crystal in which they are contained. This also avoids possible confusion arising from the many and various geologic meanings already given to the term "secondary."

In the crystal slice diagrammed in Fig. 1, it was found that the average of the temperatures along primary planes *A*–*A'* and *B*–*B'* are 113° C. and 115° C. respectively, whereas along the subsequent planes *C*–*C'* to *H*–*H'* they ranged from 135° C. to 159° C., some twenty to forty degrees higher. In general, similar features were noted in the other five crystals studied. One, however, contained only subsequent inclusions, some in planes which crossed the boundary between portions of two crystals without break or deviation.

The results of the temperature measurements on the six crystals studied is summarized in graphic form in Fig. 7. The open circles in the

columns represent average temperatures along planes of primary inclusions, with the circle nearest the left, in each case, representing the plane nearest the outside of the crystal, that farthest to the right representing the plane closest to the center of the crystal. A rise in temperature from the center outward and then a drop toward the surface is apparent in crystals 2, 3, and 6, the only ones for which data adequate to show that

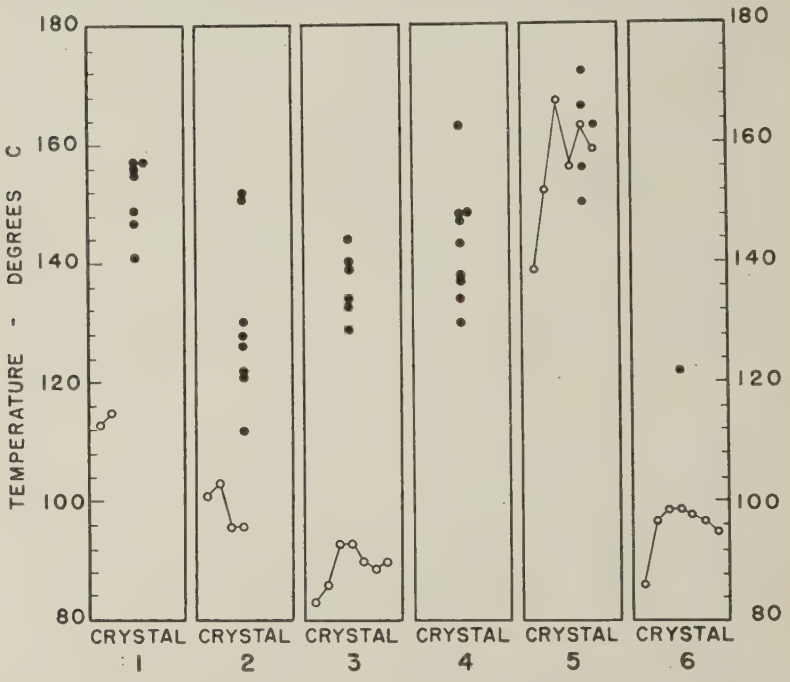

FIG. 7. Graphs of results of temperature measurements on six fluorite crystals. Open circles indicate average temperatures on individual planes of primary inclusions, solid circles the same for planes of subsequent inclusions. In each column the open circle nearest the left represents the primary plane nearest the outside of the crystal, and those to the right represent planes farther toward the interior of the crystal. The relative positions of the subsequent planes cannot be similarly shown.

feature are available. The average temperatures along planes of subsequent inclusions are shown by solid circles. In all but one crystal the average subsequent inclusion temperatures are higher than the corresponding average primary inclusion temperatures. Because there are so many planes of subsequent inclusions in crystal 6, only the average of all inclusions from these planes is shown. The range of primary temperatures was from 83° to 115° C. in four crystals, and from 139° to 167° C. in the fifth. No primaries were present in the sixth crystal, crystal 4 of

Fig. 7. The subsequent inclusions gave temperatures in the range of 112° to 172° C.

Pressure Corrections

None of the temperatures listed in the preceding section have been corrected for the compression of the liquid in the inclusions caused by pressure on it at the time the inclusions were formed. As explained by Ingerson and others, the temperatures measured in the laboratory are somewhat lower than the actual temperatures prevailing when the inclusions were formed.

The amount of pressure on a crystal growing at depth, even though the depth were known exactly, is a matter which can only be guessed at in many cases. It could be greater or less than either the weight of the superincumbent rock or the hydrostatic pressure exerted by a column of water extending to the surface. If in the present instance, however, it is assumed that the rock cover on the forming deposit was 3000 feet thick and that the pressure exerted was midway between hydrostatic and that equivalent to the weight of the overlying rock, calculation yields a figure of 2375 pounds per square inch or about 160 bars. Using the correction curves published by Kennedy,[13] we find that this pressure would necessitate adding between 9° and 10° C. to the measured temperature values in order to arrive at the true formation temperature. If the pressure is calculated on the basis of the weight of the overlying rock, the corresponding figures are 3450 pounds per square inch, 235 bars, and 14° C. Either of these temperature corrections is too small to alter in any significant way the geologic implications of the relatively low temperatures recorded by the inclusions.

Composition of Fluid in Inclusions

An attempt has been made to determine the chemical composition of the liquid in the inclusions in a specimen of fluorite from the Cave in Rock district of Illinois. This work was done by B. Brunn at the University of Chicago under the direction of Professor Tom. F. W. Barth. The total amount of liquid in the inclusions was found to be 0.54% of the specimen. The total amount of dissolved salts in the inclusions was found to be 4.5 grams per hundred grams of included liquid, equivalent to 45,000 p.p.m. The analysis was not complete, but showed that the elements in largest amount were Cl, Na, and Ca, with lesser amounts of F, S, Si, Mg, and Fe or Al. Evidently the liquid in the inclusions, excepting the yellow petroleum, is a saline solution containing principally sodium and calcium chlorides.

[13] Kennedy, George C., *op. cit.*, p. 540.

Conclusions

Fluorite crystals contain primary inclusions along growth planes parallel to cube faces and subsequent inclusions along octahedral and other fracture planes produced by fracturing during crystal growth. In the six specimens studied, the primary inclusions show uncorrected growth temperatures in the range of 83° to 115° C., whereas subsequent inclusions indicate formation temperatures of 112° to 172° C. These results reemphasize the need for cautious discrimination between primary and secondary inclusions in using any method of geologic thermometry based on liquid inclusions.

Manuscript received Oct. 2, 1951

OPAQUE OXIDES IN SOME ROCKS OF THE BASEMENT COMPLEX, TORRICELLI MOUNTAINS, NEW GUINEA

GEORGE BAKER, *University of Melbourne, Australia.*

ABSTRACT

A study of polished surfaces of the plutonic and metamorphic rocks that form part of the basement complex as exposed in the Torricelli Mountains of New Guinea, reveals magnetite, ilmenite, hematite, rutile, and spinel in various associations and showing a range of textural relationships. Apart from simple crystallization, complex intergrowths have arisen in parts from the unmixing of solid solutions of different pairs of some of the oxides and from eutectic crystallization of others. Among these are already well-known intergrowths, also examples of the rarely observed (insofar as they occur in parent rocks) ex-solution intergrowth of magnetite and hematite and the hitherto unrecorded ex-solution intergrowth comprised of ex-solved rutile lamellae in ilmenite proper. The relationships of the opaque oxides to one another and to the silicate minerals in the different rocks examined, reveal that the oxides have various positions in the crystallization sequence.

A collection of intermediate, basic, and ultrabasic igneous rocks and acid and basic metamorphic rocks from the Torricelli Mountains, has been found to contain a variety of opaque oxides showing interesting textural relationships.

The rocks were collected by A. Coulson in 1944. Some were in situ, others were waterworn pebbles obtained from the Finsch Coast (Fig. 1) and regarded as being derived from the basement complex rocks in the

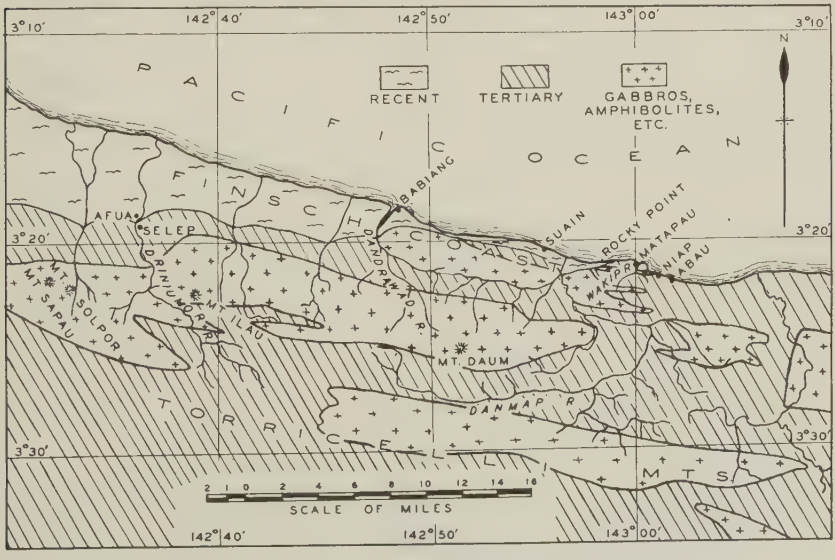

FIG. 1. General geological map of the Finsch Coast-Torricelli Mountains Region on the northern coast of Eastern New Guinea.

Torricelli Mountains, two or three miles away where similar rocks outcrop.

Among the rocks examined for their opaque mineral content are gabbros from Afua on the Driniumor River, Matapau on the Wakip River, Babiang on the Dandrawad River (all these localities are marked on Fig. 1), and from Solyaliu Hill on Tumleo Island (15 to 20 miles northwest of the area shown in Fig. 1). Peridotite was collected from Babiang, amphibolite and granulite from Matapau, and diorite (in situ) from Rocky Point at the eastern end of the Finsch Coast (Fig. 1).

In most of these rocks, magnetite, ilmenite, hematite, spinel, and rutile[1] are present in the proportions and grain sizes normal to basic igneous and metamorphic rocks. They generally do not constitute more than 4 to 5 per cent in each of the rocks examined, but in one or two of the gabbro specimens, they comprise up to 25 per cent of some parts of the rock. Minor amounts of sulfides are present in some of the rocks, but comprise only a fraction of a per cent of any one rock.

The opaque oxides are associated in a variety of intergrowths. Most of the intergrowths revealed by polished surfaces are a direct consequence of crystallization. The following list (Table 1) summarizes the types of textures encountered among the opaque oxides observed in the rocks from the Torricelli Mountains.

It is evident from Table 1 that the more complex relationships among the opaque oxides occur in the Babiang gabbro. This is largely due to the association of rutile with the other oxides. In gabbros lacking rutile, the relationships are simpler, as in the Afua gabbro, where the principal textures are ex-solution intergrowths of magnetite (host) and ilmenite (lamellae). In the Matapau gabbro, magnetite, the principal opaque oxide mineral, is devoid of ex-solution textures and in the Tumleo gabbro, spinel largely takes the place of magnetite. An occurrence of ex-solved hematite lamellae in magnetite host, unusual in natural occurrences, is found in amphibolite from Matapau and occasionally in peridotite from Babiang. Ilmenite acting as host to ex-solved lamellae of hematite, was observed in diorite from Rocky Point. Martitization is confined solely to the metasomatized granulite from Matapau.

The nature and relationships of the opaque oxides and sulfides in these various rock types, are as follows:

Opaque Minerals in Gabbros

Whereas Newhouse (5, p. 16) noted that ilmenite was the dominant opaque oxide in over two dozen gabbros, crystals of magnetite and mag-

[1] The rutile is practically opaque, likewise the spinel.

TABLE 1

No.	Texture or Intergrowth	Containing Rock
(i)	Magnetite with ex-solved ilmenite lamellae	Afua gabbro
(ii)	Magnetite and ilmenite in micrographic intergrowth	
(iii)	Structureless magnetite, without (i) or (ii)	
(iv)	Magnetite with ex-solved hematite lamellae (Also magnetite and ilmenite as in (ii))	Matapau amphibolite
(v)	Magnetite graphically intergrown with olivine and augite, but free of ex-solution phenomena	Matapau gabbro
(vi)	Ex-solved rutile lamellae in the ilmenite lamellae (of ex-solution origin) in magnetite	Babiang gabbro
(vii)	Sub-graphic intergrowths (eutectic) of rutile and ilmenite in the ex-solution lamellae of ilmenite contained in magnetite	
(viii)	Ditto of rutile and hematite in similar lamellae	
(ix)	Magnetite lamellae in the ex-solved ilmenite lamelae contalined in host magnetite	
(x)	Micrographic intergrowths (eutectic) of rutile and magnetite in the cores of ilmenite crystals enveloped by magnetite	
(xi)	Micrographic intergrowths of magnetite—rutile—ilmenite	
(xii)	Micrographic intergrowths of magnetite—rutile—ilmenite—hematite	
(xiii)	Rutile cores to ilmenite crystals enveloped by magnetite (Also excellent examples of (i))	
(xiv)	Granular intergrowths of spinel and magnetite (Also occasional examples of (iv))	Babiang peridotite
(xv)	Spinel the most common oxide. Rare chromite. Structureless magnetite	Tumleo gabbro
(xvi)	Ilmenite with ex-solved bodies of hematite.	Rocky Point diorite
(xvii)	Ilmenite in subgraphic intergrowth with hornblende	
(xviii)	Martitized magnetite	Matapau granulite

netite (host) with ilmenite (lamellae) predominate in six New Guinea gabbros examined.

Afua. Magnetite forms primary crystals and secondary dust-like streaks in a partially serpentinized olivine-hypersthene gabbro from Afua, which is a little over 4 miles inland from the mouth of the Driniumor River. The dust-like streaks of magnetite have been formed along serpentinized cracks in olivine. Primary crystals of magnetite, up to

0.30×0.70 mm. in size and usually of irregular shape, are scattered throughout the rock.

The primary crystals of magnetite contain occasional ex-solution lamellae of ilmenite along octahedral directions. Some magnetite crystals also show occasional micrographic intergrowths with ilmenite. These intergrowths are just detectable under a 1/10 Fl. oil immersion lens, but the lamellae and granules of ilmenite are of sufficient abundance to cause the host magnetite to appear a darker grayish-brown in reflected light than is usual for magnetite.

Certain of the magnetite crystals are free of ilmenite intergrowths. The amount of magnetite present is such that small pieces of the gabbro (measuring $1'' \times 1'' \times \frac{1}{2}''$) can be attracted to an Alnico hand magnet.

Pyrrhotite, pyrite, and chalcopyrite occur in the Afua gabbro as small, isolated grains averaging 0.04×0.08 mm. in size.

Matapau. Minor amounts of small crystals of primary magnetite, chalcopyrite, and pyrrhotite are present in a hornblende-augite-hypersthene-olivine gabbro from Matapau.

The magnetite crystals are occasionally micrographically intergrown with both olivine and augite, but are free of ex-solution intergrowths with other iron oxides. The chalcopyrite in parts replaces some of the pyrrhotite, crystals of which do not exceed 0.12×0.35 mm. in size.

Rare, small particles of a hard and creamy-white mineral, much more brightly reflecting than neighbouring sulfide grains, are found in the Matapau gabbro. The particles are too small for precise determination, the largest being 4 μ across, but the properties indicate a platinoid metal.

Thin sections of the Matapau gabbro, reveal that opaque streaks of dust-like material have been developed along cracks in altered portions of the olivine crystals. In many gabbros, such material is composed of fine particles of magnetite, but in the Matapau gabbro, it consists largely of narrow stringers composed of specks of chalcopyrite and pyrrhotite. Evidently during deuteric alteration of the olivine, sulfur and copper were available in small quantities for combination with the iron released during breakdown of the olivine.

Tumleo Island. An ejected block of gabbro caught up from the basement complex and thrown out by the Lower Miocene volcano at Solyaliu Hill, Tumleo Island (15 to 20 miles northwest of Afua), contains a few grains of opaque oxide minerals.

The most frequent of these rarely occurring oxides is spinel, a few crystals of which are scattered through the rock. The spinel is an iron-rich variety with low reflecting properties and in one or two places, brilliant green internal reflections. The intensity of coloration of the spinel is so great, that in thin microscope sections, no transmitted light

passes through even the thinnest edges of the crystals. Some of the spinel shows rather brownish-green internal reflections resembling those characteristic of chrome-spinel. In places there occur rare, almost opaque chromite grains showing faint brownish-red internal reflections only at crystal edges and rarely along cracks, when observed in polished surfaces.

Grains of magnetite are sparse and of minute size in the Tumleo Island gabbro. No ilmenite was detected and the only sulfides are infrequent blebs of chalcopyrite and one or two small crystals of bornite partly altered to covellite.

Babiang. Three different specimens of gabbro were examined from Babiang. In (i), hornblende gabbro, the main opaque oxides consist of occasional magnetite crystals enclosing broad lamellae of ilmenite, with granular intergrowths of rutile. In (ii), an altered olivine gabbro, there is little magnetite and rare pyrrhotite, but in (iii), a partly metasomatized hornblende gabbro, occurs the best array of opaque minerals in the series of rocks under consideration. In this rock, a little epidote has been formed, the hornblende is partly chloritized and the plagioclase feldspars have been slightly altered. The opaque minerals consist of magnetite, ilmenite, rutile, hematite, pyrite, pyrrhotite, chalcopyrite, and a little limonite. The rock is strongly magnetic, due largely to abundant magnetite which is intergrown with ilmenite and rutile. The opaque oxides, which make up to 25 per cent of some polished surfaces of the partially altered hornblende gabbro (Plate I, photo. 1), show complex eutectic and ex-solution intergrowths. Individual areas occupied by the iron and titanium oxides measure up to 15×10 mm. and appear to be moulded around the silicates. They frequently enclose small amounts of hornblende and plagioclase (Plate I, photo. 1), thus indicating fairly late crystallization of the opaque oxides in this gabbro.

The magnetite contains ex-solution lamellae of ilmenite ranging from minute (short and narrow) lamellae in many of the magnetite crystals to broad, long lamellae in a few of them. All the ilmenite lamellae lie along (111) directions in the magnetite, and some of them have been partly altered to leucoxene. The ex-solved lamellae of rutile in ilmenite are few in number, small in size and lie obliquely across the length of the ilmenite lamellae in a regular pattern corresponding to the rhombohedral directions of the ilmenite. Subgraphic intergrowths of rutile and ilmenite (vii in Table 1) and of rutile and hematite, occur in strings and irregular elongated patches along the principal direction of the broader of the ilmenite lamellae. They are sometimes centrally placed, sometimes situated to one side of the broader lamellae, but do not interrupt the finer rutile lamellae.

A few of the ilmenite crystals show well-developed twin lamellae. Twin

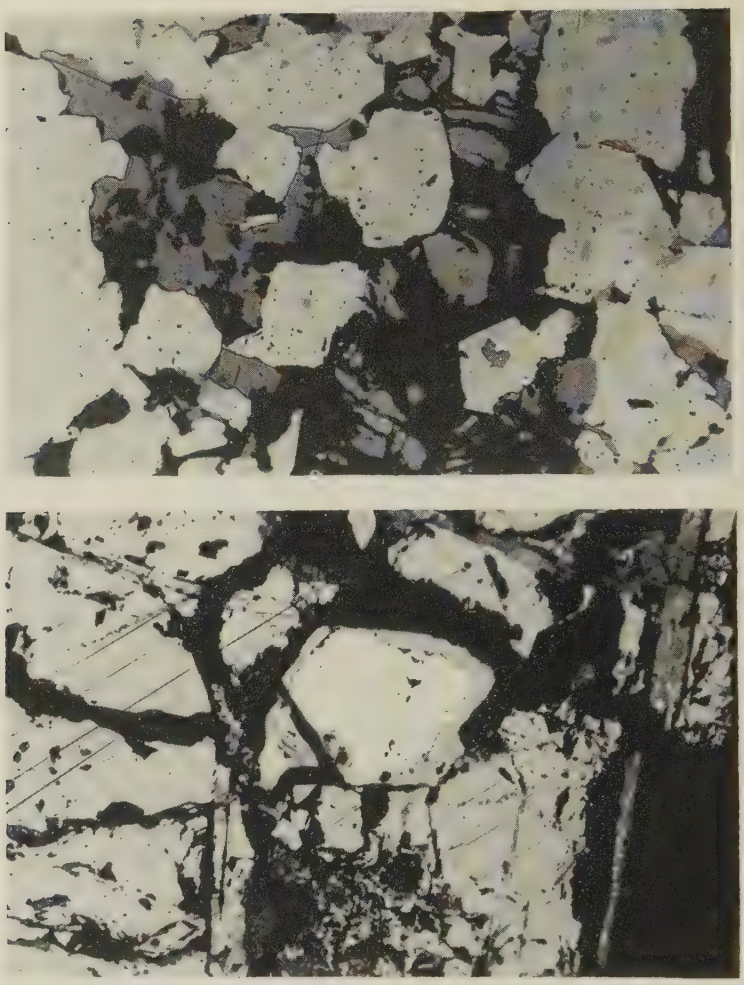

EXPLANATION OF PLATE I

Photo. 1. Opaque oxides (grayish-white) in partially altered hornblende gabbro from Babiang, New Guinea. (×150).

Photo 2. Partially altered pyrite crystal (white) with rim of limonite (gray). From partially altered hornblende gabbro, Babiang, New Guinea. (×150). (Other light gray areas are magnetite-ilmenite intergrowths).

lamellae are also well-developed in the rutile crystals associated with magnetite and ilmenite in micrographic intergrowths (xi of Table 1). This twinning often extends through individual portions of rutile having the same optical orientation in the intergrowths, but separated by areas of magnetite.

Whereas Edwards (2, p. 62) records eutectic relationships between

rutile and hematite in occasional specimens from Western Australia and Olary, South Australia, in some of which the rutile is in excess and crystallized first as coarse crystals, the sub-graphic intergrowths between this pair of oxides in the ilmenite lamellae of the Babiang partially altered hornblende gabbro, are rather different. Apart from the minuteness of the component crystals in the intergrowths, there is little difference in the amounts of the components, hematite, if anything, being perhaps a little more abundant in most of the micrographic intergrowths, and the two components evidently separated out together at much the same time in the ilmenite lamellae.

Most of these textures in the opaque iron and titanium oxide minerals are already well-known (cf. Edwards, 2, pp. 57–66). It is of interest to note, however, the relationships between the ilmenite lamellae in the host magnetite and the rutile intergrowths and lamellae in the ilmenite lamellae. Graphic intergrowths between rutile and ilmenite (see (vii) in Table 1) are already known (likewise the graphic intergrowths between rutile and hematite), and would indicate the development of eutectoid relationships between rutile and ilmenite (and between rutile and hematite). The ex-solved lamellae of rutile within the broader of the ilmenite lamellae are of interest in that, whereas Edwards (1, Figs. 13 and 14) noted the development of such ex-solution lamellae of rutile in ilmenite-hematite solid solutions, the occurrence of such lamellae in ilmenite proper has not been noted previously. There is here evidence that this slight solubility of rutile in ilmenite-hematite solid solutions, at high temperatures, extends over the whole range of composition from hematite-rich solutions to ilmenite. Within the confines of the narrow walls of ilmenite lamellae, the evidence points to the close spatial association of the two processes—(*a*) eutectic intergrowth and (*b*) ex-solution intergrowth as between rutile and ilmenite. The lamellae of rutile in the ilmenite lamellae are small and cease abruptly against contacts between ilmenite lamellae and host magnetite, while their arrangement indicates precipitation along $(10\bar{1}1)$ directions in the ilmenite.

The pyrite crystals, which were originally euhedral, are surrounded by thin crusts of limonite (Plate I, photo. 2) and contain occasional rounded bodies of pyrrhotite and chalcopyrite.

Opaque Minerals in Peridotite

A partially altered peridotite from Babiang, contains occasional iron oxide minerals, spinel, and rare sulfides.

Ilmenite occurs as occasional small, irregularly shaped grains. Magnetite appears as occasional crystals and as fine particles forming thin stringers in serpentinized portions of the peridotite.

The crystals of magnetite contain minute ex-solution lamellae of hema-

tite, so small that they are only made visible by the use of a 1/10 Fl. oil immersion lens. Some of the larger magnetite crystals, which are up to 0.35×0.60 mm. in size, contain patches of crystals having cubic outline and greenish-brown internal reflections. In reflected light, these cubic crystals have a lower reflecting power than chromite and are evidently the spinel observed in thin sections. Occasionally, the spinel and magnetite form granular intergrowths.

Rare specks of chalcopyrite are up to 5 μ across. Pyrrhotite of similar dimensions is partially replaced by chalcopyrite and in places peripherally altered to limonite.

Specks of a silver white metallic mineral with a creamy tinge, up to 4 μ across, occur more abundantly in this peridotite than in the gabbros and amphibolite from the Torricelli Mountains. They are hard and scale-like and presumably represent particles of platinoid metal.

Opaque Minerals in Amphibolite

An amphibolite from Matapau contains numerous small crystals of magnetite with ex-solution lamellae of hematite, shot through the albite, and larger clots of magnetite and ilmenite crystals as granular aggregates in the hornblende. Smaller grains of magnetite and ilmenite are sometimes confined to cleavage planes in the hornblende.

Some of the larger, as well as many smaller crystals of magnetite, contain lamellae of hematite along (111) planes. The hematite occurs as blades of uniform size and even distribution, thus forming a regular triangular lattice structure in the magnetite (cf. Edwards, 2, Fig. 71). There is no concentration of hematite at the crystal margins of the magnetite, such as occurs where magnetite has been martitized during supergene or hypogene oxidation (cf. Edwards, 2, Fig. 72), so that the intergrowth is evidently due to ex-solution.

Edwards (3, p. 759) has recently described natural ex-solution intergrowths of magnetite and hematite in Fijian beach sands (presumably derived from andesites[2]) and in a waterworn crystal of magnetite from river gravel in the Cairns district of Queensland, Australia. Such intergrowths occur in situ in some abundance in amphibolite from Matapau, New Guinea, and occasionally also in peridotite from Babiang. The specimens examined are waterworn pebbles derived from the nearby Torricelli Mountains.

The proportion of host magnetite to unmixed hematite lamellae in the intergrowth, measured micrometrically, is 88:12, indicating a tempera-

[2] These intergrowths have not been observed in polished surfaces of Fijian basalts and andesitic dykes.

ture of formation of 1,200° C., according to the experimental data of Greig et alia (4). As pointed out by Edwards (3, p. 761), the temperature of formation indicated for intergrowths having approximately 80:20 ::magnetite:hematite, is unduly high for igneous rocks. Although somewhat lower (88:12), the hematite content of these intergrowths also indicates a rather high temperature of formation in the Matapau amphibolite. Some additional, at present unknown factor must have operated, to allow the formation of solid solution under natural conditions at temperatures lower than those found in the laboratory by Greig and his associates (4).

Much of the ilmenite is surrounded by alteration rims of sphene and many of the coarser grains of ilmenite are located in granular aggregates with magnetite, without showing ex-solution intergrowths.

Opaque Minerals in Diorite

A diorite from Rocky Point on the Finsch Coast contains ilmenite, magnetite and chalcopyrite. The rock, which was in situ, shows incipient metasomatism, and is similar to diorite outcropping along the coast easterly to Niap.

The magnetite, which is rare and structureless under oil immersion lenses, ranges up to 0.03×0.06 mm. in size.

Ilmenite crystals up to 0.25×0.35 mm. in size, contain ex-solved, irregularly elongated bodies of hematite arranged in parallel rows along (0001) planes in the host mineral in the same manner as illustrated by Edwards (1, Fig. 4). Occasional, very irregular areas of hematite in the ilmenite, are evidently due to the coalescence of several smaller lamellae. The ilmenite has been partially altered to sphene. Some crystals of ilmenite show subgraphic intergrowths with hornblende (cf. Newhouse, 5, Fig. 1, plate 13), while smaller grains sometimes lie along cleavage directions in the hornblende. Such occurrences indicate that the ilmenite crystallized partly before, partly during hornblende crystallization. The formation of the ilmenite was thus a relatively early phase in the crystallization history of the diorite, as also noted by Newhouse (5, p. 14) in a number of American and other diorites.

Pyrite is the most abundant opaque mineral present in the Rocky Point diorite. It occurs in isolated grains and crystals ranging up to 0.15×0.30 mm. in size. Occasional chalcopyrite grains range up to 0.06 ×0.12 mm.

Opaque Minerals in Granulite

A garnetiferous granulite from Matapau contains magnetite closely associated with epidote throughout the rock. Metasomatic alteration of

the rock has resulted in much of the magnetite becoming martitized. The alteration of the magnetite to hematite during this process, has penetrated from the peripheries of the magnetite crystals, inwards along (111) planes, giving partial pseudomorphs. Sometimes complete, sometimes only partial rims of hematite surround the altered magnetite, and from them, hematite lamellae of uneven width, taper off towards the interiors of the magnetite crystals along the octahedral planes. No crystals of magnetite in the granulite have escaped some degree of martitization and in many, the replacement process is advanced, leaving only a few, small remnants of magnetite. The existence of hematite lamellae as evenly distributed blades of uniform size in a few of the partially altered magnetite crystals, makes it difficult to assess whether such hematite lamellae are due to ex-solution intergrowth or to fortuitous, even alteration along octahedral planes of the magnetite in this granulite from Matapau.

Summary and Conclusions

The opaque oxides in the igneous rocks from the Torricelli Mountains bear out the earlier conclusions of Newhouse (5, p. 33) that the opaque oxides in igneous rocks vary in amount, grain size, habit, species, and position in the sequence of crystallization in rocks of different composition and texture. Of these, perhaps the most fundamental variation is that of the crystallization sequence of the opaque oxides in relation to the silicate minerals, insofar as this must have an important bearing on both ore genesis and petrogenesis. The opaque oxides have crystallized during and shortly after the silicate minerals in some of the rocks (cf. Babiang partially altered hornblende gabbro), prior to them in others (as in the Babiang peridotite), during and prior to them in yet others (e.g. as in the Rocky Point diorite).

The presence in one and the same rock (e.g. the Babiang partially altered hornblende gabbro) of oriented intergrowths arising from the unmixing of solid solutions and of micrographic intergrowths caused by eutectic crystallization, indicates the complexities that may arise during the crystallization of iron and titanium oxides in some rocks, while in most of the rocks, the textural relationships have remained relatively simple. The main factors affecting these differences, are probably to be ascribed to the temperatures of formation of each particular rock, the availability of particular ions required in the intergrowths and the time taken for cooling and crystallization under the prevailing pressures in the basement complex rocks, whether igneous or metamorphic. Where the iron content of the basic gabbroic magma in the Torricelli Mountains region was low (cf. Tumleo gabbro), ample supplies of magnesia and alumina combined with the available iron to form spinel at the expense

of magnetite. Where, however, excess of iron occurred (cf. Babiang gabbro) and abundant titania was available, the textural relationships became complex, with the development of magnetite-ilmenite-rutile intergrowths, and the, so far, rarely observed phenomenon of exsolved rutile in ilmenite.

No conclusive evidence is to hand to account for the occurrence of natural ex-solution intergrowths between magnetite (host) and hematite (lamellae) at the temperatures of formation of the containing rocks (amphibolite and peridotite).

Acknowledgments

The author is indebted to Dr. A. B. Edwards of the Mineragraphic Section, Commonwealth Scientific and Industrial Research Organization, for aid in the interpretation of the microstructures revealed by the opaque oxides discussed in this paper.

References

1. Edwards, A. B. (1938), Some ilmenite micro-structures and their interpretation: *Austr. Inst. Min. and Met., proc. n.s.*, no. **110,** 39–58 (16 figures).
2. Edwards, A. B. (1947), Textures of the ore minerals and their significance: *Austr. Inst. Min. and Met.* (Inc.), Melbourne, 1947.
3. Edwards, A. B. (1949), Natural ex-solution intergrowths of magnetite and hematite: *Am. Mineral.*, **34,** 759–761.
4. Greig, J. W., Posnjak, E., Merwin, H. E., and Sosman, R. B. (1935), Equilibrium relationships of Fe_3O_4, Fe_2O_3 and oxygen: *Am. Jour. Sci.*, **30,** 239–316.
5. Newhouse, W. H. (1936), Opaque oxides and sulphides in common igneous rocks: *Bull. Geol. Soc. Am.*, **47,** 1–52 (18 plates).
6. Ramdohr, P. (1950), Die Erzmineralien und ihre Verwachsungen: Akademie-Verlag. Berlin.

Manuscript received Aug. 21, 1951

IRIS AGATE

FRANCIS T. JONES, *244 Trinity Ave., Berkeley 8, California.*

ABSTRACT

Iris agate owes its spectral colors to the presence of a diffraction grating structure. The lines in the grating are the edges of thin lamellae having alternately high and lower refractive indices. The rhythmic segregation of opal among the crystals may account for the index variation. The chalcedony needles are always perpendicular to the lamellae. The optical properties of the chalcedony associated with the grating structure indicate that the aggregate is pseudo-orthorhombic, probably being made up of needles of quartz elongated perpendicular to *c*, but not being perfectly parallel. Form-birefringence may account for the difference of the refractive indices from those of quartz. Maximum and minimum indices are given.

Iris agate is agate whose thin section shows spectral colors when viewed in transmitted light. These colors are not thin-film colors such as those of precious opal. Specimens of iris agate were observed in 1933 by Fred S. Young,[1,2] then publisher of the *Oregon Mineralogist*, during the preparation of cabochons. Short articles were published on the subject by H. C. Dake,[3,4] editor of the journal. These articles were largely devoted to the occurrence and cutting of such material. Microscopic study by Dr. E. W. Lazell revealed the lamellar structure of iris agate but no detailed study was made of the specimens.[1]

In 1935 when Fred S. Young and Dr. H. C. Dake first showed the author thin slices of iris or rainbow agate, the display of colors recalled the similar appearance of a diffraction grating. Microscopical examination soon confirmed the opinion that a periodic banded structure existed in the agate, and revealed interesting correlations with the chalcedony structure and variations in fineness and regularity. No satisfactory explanation of the formation of this regularly banded structure has yet been devised although the theory proposed by Hedges[5] may apply in a general way.

OCCURRENCE

It is probable that some specimens of agate from any locality may show the iris structure. Those used in this study were from Oregon, Montana, and California. Some amygdules from an outcrop near the

[1] Young, Fred S., Private communication.

[2] Young, Fred S., *Oregon Mineralogist*, **2**, 22 (April 1934).

[3] Dake, H. C., *Oregon Mineralogist*, **1**, 1 (July 1933).

[4] Dake, Fleener and Wilson, Quartz Family Minerals, McGraw-Hill Book Co., **(1938)**.

[5] Hedges, E. S., Liesegang Rings and Other Periodic Structures, London, Chapman & Hall, Ltd. **(1932)**.

junction of Grizzly Peak Blvd. and Fish Ranch Road in Berkeley, Calif., provide good iris agate specimens.

The iris grating structure, when present, is usually associated with the "turtleback" type of chalcedony crystallization. It has often been found in the chalcedony layers adjacent to quartz layers in the center of an agate amygdule or geode. It has never been observed in opal bands in agate. It has only been found in colorless, or nearly colorless, chalcedony although patches of the reddish brown to black gelatinous appearing type of "moss" have been observed between the bands containing the grating structure.

Quality Factors

In order to produce the best play of colors the slice of iris agate must be cut so that the thin layers, whose edges are the lines of the diffraction

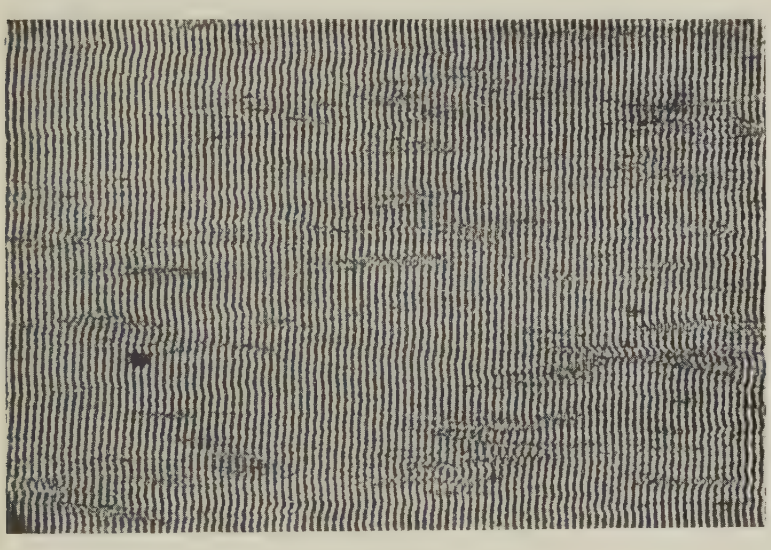

Fig. 1. Iris agate 9,600 lines to the inch. 370×.

grating, as shown in Figs. 1 to 5, will be at right angles to the polished surface. The slice will show the brightest colors if it is thin (1 mm. or less) because the absorbing and scattering effect of any milkiness will then be at a minimum. If the line spacing is uniform, as in Fig. 1, a very thin slice will show primary colors even if the layers in the agate are somewhat inclined to the polished or lacquered surface, although the slice may have to be tilted to correct for the inclination. A specimen which shows primary colors in very thin section may show only pastel colors if it is cut too thick. If the line spacing is not quite uniform only pastel

colors may be seen, and if it is very irregular only a chatoyance will be observed.

A single band of uniform spacing will show only one color for a given position but any adjacent band of uniform but different spacing will give a different color for the same position because a fine spacing will diffract any one wave length through a larger angle than a coarser grating. In addition, the finer gratings separate the colors from each other more than do the coarser gratings, consequently they give purer, more saturated colors.

FIG. 2. Iris agate between crossed nicols showing single lines and turtleback. 80×.

LINES PER INCH

The fineness of structure observed in iris agates ranges from about fifteen thousand to as few as four hundred lines per inch. Figure 1 shows a specimen having about 10,000 lines per inch. Part of Fig. 2 shows only 400 lines per inch. Finer and coarser spacings may exist in some agates but any spacing in this range will show the grating effect. A grating of only 100 lines per inch will show diffraction colors but they will be so close to the illuminating beam that they will be difficult to see. Gratings as fine as 30,000 lines per inch have been observed by the author in some crystalline organic materials.

A variation in spacing of the lines such as shown in Figs. 2 and 3 may possibly be caused by changes in the rate of crystallization of the chalced-

ony, either because changes in temperature occurred or because the composition (concentration) of the solution (perhaps a gel) varied, or both. It is also possible that the coarse spacing shown in Fig. 2 may be of the ordinary successive deposition type with the grating structure starting but failing to continue in each of the broad layers which happen to be fairly uniform in thickness. The fact that the needles seem to be continuous across several layers may be explained in the same way phantom lines in single crystals are explained.

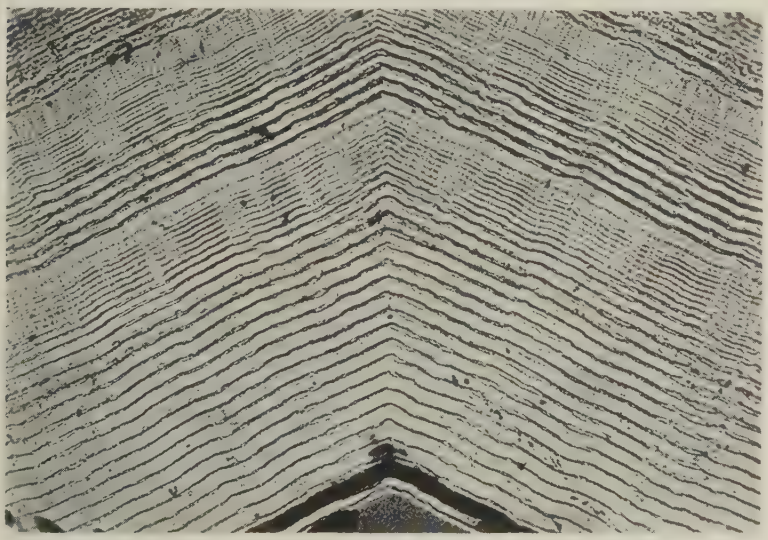

FIG. 3. Iris agate showing spacing differences and change of direction at grain boundary. 80×.

CORRELATION OF GRATING LINES AND CRYSTALS

The lines in iris agate are always at right angles to the length of the needle-like crystals of chalcedony. Figure 1 shows an unusually straight set of lines but even these are slightly wavy because the crystals are not all exactly parallel to each other. It should be pointed out also that the waves run along the layers within the specimen at right angles to the cut surface, but the amplitude of the waves is small and a thin slice will give good color in spite of the front to back waviness. Figure 2 shows lines that curve because the crystals have grown in radiating clusters. This structure is sometimes termed "turtleback" or "spherulitic." Figure 3 shows a relatively coarse structure of varying fineness and also reveals that the banding is continuous across adjacent groups of crystals in spite of abrupt changes in direction. Figure 4 is the same specimen as Fig. 1

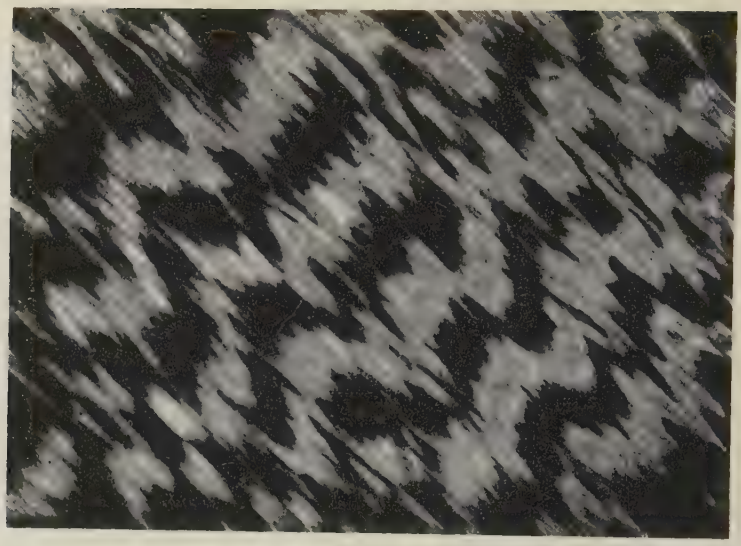

FIG. 4. Iris agate between crossed nicols. 80×.

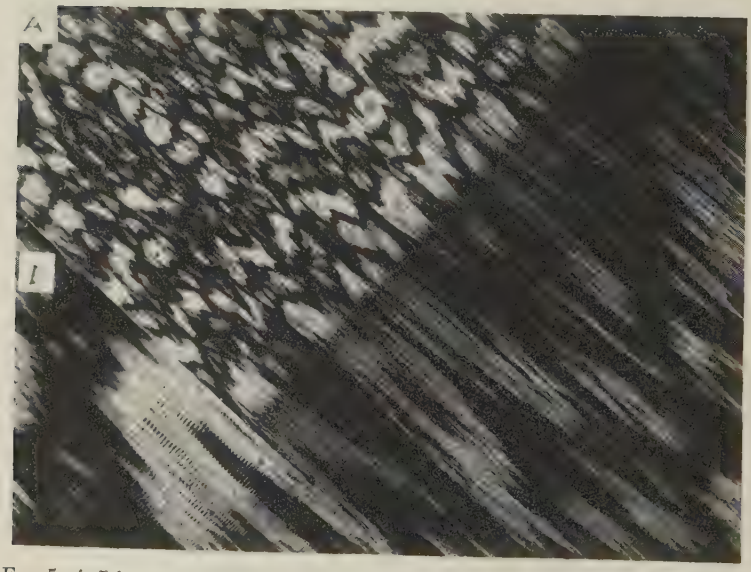

FIG. 5. *A*. Iris agate between crossed nicols showing start of narrow band where crystal size changes. 80×. *B*. Start of grating band seen in *A*. 200×.

but seen between crossed nicols and at only 80×. The irregular, ragged black bands indicate changes in polarization colors of the chalcedony but do not correlate with the grating structure. (See Fig. 5.) Such coarse

patterns appear to the unaided eye as a woven cloth such as burlap.

Figure 5*A* shows a band of iris starting where short, relatively jumbled crystals change to long, nearly parallel crystals. Figure 5*B* shows the start of the grating band at higher magnification. In most specimens the iris bands show a higher order of polarization color and more uniform orientation than adjacent bands which do not show the iris grating structure; however, these differences are not always noticeable. The band of iris which begins where the crystal size changes (Fig. 5) becomes finer where a band of cloudy material extends across the field but becomes coarser again beyond the cloudy zone. This cloudy material may be opal which can exist between the crystals of chalcedony.[6] Colloidally dispersed impurities such as the brown ferric hydroxide type of gelatinous appearing "moss" often occur in the bands between the iris bands, but very little such colored impurity is ever present in the iris bands themselves. In any case it appears that the chalcedony in which the grating structure is present must be quite pure and sufficiently free from porosity to prevent much diffusion of iron stain or dyes between the crystals.

The observations above indicate that the grating lines must have been formed while the crystals were growing but it is the author's opinion that the manner of their deposition is not the same as the irregular deposition of the ordinary bands in agate. Organic materials such as cholesteryl acetate melted under a cover glass have been observed crystallizing rapidly in rhythmically banded structures which produce a display of rainbow colors just as does iris agate. Probably a similar process proceeding at a slower rate is responsible for the grating structure in iris agate.

Nature of the Lines

The lines in iris agate are optical inhomogeneities but are not layers of opaque impurities. If they are impurities they must be of transparent material.

The crystals appear to be crossed by grating lines without any disturbance of their optical properties. The lines are visible because an abrupt change in refractive index occurs on both sides of each "line" which must be the edge of a thin layer of material. The boundaries between layers of differing refractive indices cause the black lines in the photomicrographs. The layers of higher index must necessarily alternate with those of lower index. Although a difference of composition could account for such an alternation of refractive index, it is also possible to have such a refractive index difference with constant composition but

[6] Donnay, J. D. H., Le birefringence de forme dans la calcedoine: *Ann. Soc. Geol. Belgique*, **59**, B 289 (1936).

change in orientation caused by twinning. The grating structure in the amethyst of Fig. 6 is too coarse to show colors but it is conceivable that similar but much finer structures might exist. In this example there are uniform overlapping layers of alternately left- and right-handed quartz. An important difference to be noted is that the grating lines in iris agates go from crystal to crystal whereas the twinning of amethyst is within a single crystal. Zapffe and Worden[7] describe banded structures of somewhat similar appearance revealed by fractography. These structures are

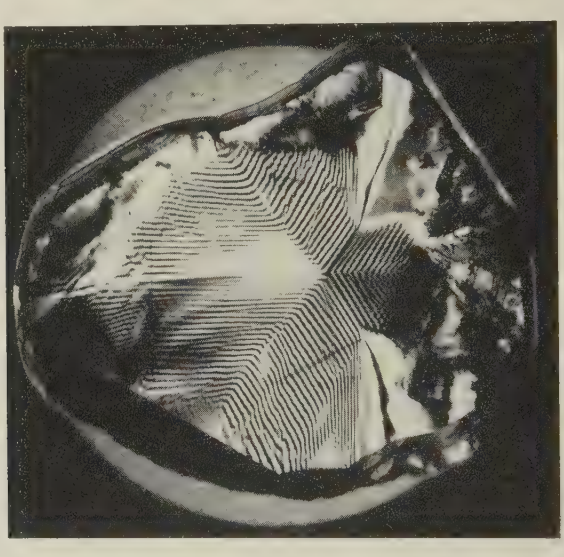

FIG. 6. Brazilian twinning in amethyst. (X nicols.) 2×.

confined to single crystals of ammonium dihydrogen phosphate containing some arsenate, but they may have something in common with the lamellar structure in iris agate because an opportunity existed for segregation of arsenate and phosphate in the solid solution which could account for the refractive index differences of the alternate layers. Neither structure has the appearance of twinning.

In Figs. 2 and 3 the single thin "lines" or layers have appreciable thickness and the refractive index of each thin layer is greater than the index of the broader crystalline zone on either side. This evidence rules out the possibility that the thin layers contain more opal than the adjacent material. On the contrary they have properties more nearly approaching those of quartz.

[7] Zapffe and Worden, *Acta Crystallographica*, **2**, 386 (1949).

Optical and Crystallographic Properties

Table 1 summarizes the optical and crystallographic properties and gives for comparison the corresponding values reported by Dana,[8] Rogers,[9] Winchell,[10] and Larsen.[11]

Winchell quotes the results of Washburn and Navias[12] who made a careful study of chalcedony from Yellowstone Park and concluded on the basis of *x*-ray powder diffraction photographs of their sample that chalcedony is quartz in spite of optical, thermal, and density differences. The more recent work of Correns and Nagelschmidt[13] indicates that the chalcedony fibers are quartz, elongated at right angles to the *c* axis. None of

Table 1. Optical and Crystallographic Properties of Chalcedony Aggregates

Crystal System: Pseudo-orthorhombic, or monoclinic, in needles; fibrous, clusters tending to radiate

Refractive Indices Sodium Light	This work	Rogers	Winchell	Dana	Larsen
α	1.5350±0.0005	1.532	n_e1.530		
β	1.537 ±0.001				1.537
γ	1.5430±0.0005	1.543	n_o1.533–1.539	1.537	
Birefringence	0.008	0.011	0.007		0.01
Axial Angle, 2E	50±5°				
Optical Character	(+)			(−)	
Sign of Elongation	(−)		(+) or (−)		
Optical Orientation	Axial plane & α lengthwise				

the authors cited above mention the presence of such a grating structure in agate as is described in this paper. The properties reported here were observed on chalcedony that contained the iris grating structure. Most of the measurements were made on chips broken off the edges of the thin section shown in Fig. 1. Immersion methods were used to observe the edges of the specimen. Sodium light was used for the index determinations

[8] Dana and Ford, Textbook of Mineralogy, 4th Ed., John Wiley and Sons, Inc., (1932).

[9] Rogers, Introduction to the Study of Minerals; 3rd Ed., McGraw-Hill Book Co. (1937).

[10] Winchell, Microscopic Characters of Artificial Minerals, John Wiley and Sons, Inc. (1931).

[11] Larsen and Berman, The Microscopic Determination of the Nonopaque Minerals *U.S.G.S., Bulletin 848* (1934).

[12] Washburn and Navias, *Proc. Nat'l. Acad. Sci.*, **8**, 1 (1922).

[13] Correns and Nagelschmidt, *Zeits. Krist.*, **85**, 199 (1933).

which could be made with a precision of ± 0.0005, but it should not be expected that all chalcedony specimens would have these values within such narrow limits. The maximum and minimum values observed are given.

The black areas in Figs. 4 and 5 reveal crystals oriented in positions which have very low retardation. The centers of these dark areas do not become bright when the specimen is rotated. Interference figures obtained from some of these areas by means of an oil immersion lens, although somewhat indistinct, were good enough to reveal that the crystals appear to be biaxial. The optic axial angle in oil, $2H = 34°$; in air $2E = 50 \pm 5°$; the optical character is (+) and the axial plane is lengthwise of the crystals, with the acute bisectrix perpendicular to the crystals. The sign of elongation is (−). The bright crystals which show sharp extinction give an "optic normal" interference figure. This combination of properties, if unqualified, would indicate that the crystals, or at least their aggregates, belong in the orthorhombic system, or the monoclinic system if the crystals are elongated in the direction of the *b* axis.

The refractive index for the lengthwise vibrations is always alpha and has a value of 1.5350 ± 0.0005.

The refractive index for crosswise vibrations measured on the crystals showing the greatest retardation and sharpest extinction (the "optic normal" view) is gamma and has a value of 1.5430 ± 0.0005. The beta index measured on crystals showing the "acute bisectrix" could not be determined as accurately but has a value of 1.537 ± 0.001. Indices measured on specimens shown in Figs. 2 and 3 show that the single "lines" or layers have a γ value of 1.544 compared to the portions of the crystals between the layers which showed a maximum value of 1.543.

The change from the "optic normal" to the "acute bisectrix" position occurs quite regularly along any one line of lengthwise (spiral?) growth, e.g. Figs. 4 and 5, although this periodicity is not so noticeable in some specimens, e.g. Fig. 2, where most of the dark crystals are simply near their extinction positions. As noted previously the grating structure does not correlate with this rough periodicity in the variation of orientation.

With axial illumination extinction was always parallel with respect to the individual crystals, or small bundles of essentially parallel needles, but in some crystal clusters extinction appeared oblique by about five degrees when observed in highly convergent illumination. These imperfections can be explained if it is recalled that the structure variations are the same perpendicular and horizontal to the cut surface. Any nearly "isotropic" area is composed of a bundle of needle-like crystals which are not perfectly arranged so as to act as a single crystal. The lower layers may contain a few crystals in a position to show the optic normal, others may be dipping slightly. If the needle-like crystals in these specimens of

chalcedony were quartz having the c axis lengthwise, then end views of the needles should be "isotropic." Sections cut to show this end view reveal that the crystals are not "isotropic" but show a retardation about equal to that seen on sections cut parallel to the length of the crystals.

The thin layers responsible for the grating structure do not show any variation in their extinction position as do twins, and as mentioned earlier, these lamellae have refractive indices greater than the zones between them. The maximum observed difference is only 0.001, but the contrast within the specimen would lead one to estimate a larger value.

Discussion

On the basis of the evidence given above one would conclude that: (1) The iris agate grating structure results from the segregation of alternate layers having higher and lower refractive indices during crystallization of the needles or fibers of chalcedony. (2) The crystallization is a rhythmic process affecting the entire aggregate of crystals uniformly. (3) Factors such as variations in rate of growth and percentage of impurity, such as opal, probably cause the difference of fineness in the different grating bands of a specimen.

If Donnay's[6] explanation of the influence of form-birefringence is accepted, the higher index of the thin layers in some specimens such as Figs. 2 and 3 cannot be attributed to an increased amount of opal but the lower index of adjacent material may be accounted for on that basis.

The optical properties of the aggregate would indicate that chalcedony is not quartz but an orthorhombic or monoclinic mineral. However, if allowance is made for the fact that these properties are measured on an aggregate of very small crystals instead of upon single crystals, and also considering the influence of amorphous intercrystalline material, probably opal, upon the index values[6] it is conceivable that the difference between these optical properties and those of quartz ($\epsilon = 1.553$, $\omega = 1.544$) can be accounted for. It is also necessary to explain the difference in habit of the chalcedony needles (c axis perpendicular to length) in contrast with that of ordinary quartz. It is to be noted that both quartz and chalcedony are optically positive.

Unless there is some ambiguity[14] in the x-ray data or possibly very slight but significant differences between the diffraction patterns of chalcedony and quartz, chalcedony crystals must be considered quartz in an unusual form. An x-ray fiber pattern obtained from a sliver of iris agate gave dimensions agreeing with those measured on a powder pattern of alpha quartz.

Manuscript received July 27, 1951

[14] Menzer, G. Z., Naturforsch: *4a*, 11–21 (April, 1949). (Only the abstract seen.)

RAPID DETERMINATION OF INTERPLANAR SPACINGS FOR TRIMETRIC CRYSTALS

F. Donald Bloss, *University of Chicago,* Chicago, Illinois.*

Abstract

A rapid and accurate technique of determining interplanar spacings for trimetric crystals by the use of a grid based on Peacock's graphical method is described. Interplanar spacings of chalcanthite were determined by such grid measurements and showed remarkable agreement with the calculated values. The procedure for keeping the method at its highest degree of accuracy is discussed. Miller indices are assigned to some of the lines of a powder film of chalcanthite on the basis of the spacing values.

Introduction

A graphical method of determining the interplanar spacings in trimetric lattices, given the values of the interaxial angles and the unit translations, has been described by M. A. Peacock (1938). This method is far more rapid than the laborious mathematical calculations necessitated by the standard formulae. Herewith is described a grid which greatly increases the speed of this graphical method yet maintains or improves its degree of accuracy. The ease with which lattices, regardless of symmetry, are handled by the method is illustrated by a triclinic example.

Principles of the Graphical Method

The procedure for the graphical method involves: (1) the drafting of a scale model of the reciprocal lattice, and (2) the measurement of distance between the lattice origin and the various "face poles" of the reciprocal lattice model.

The first step may be accomplished (Fig. 1*a*) by developing an ordinary gnomonogram into an orthographic projection of a gnomonic lattice[1] whose origin is at the center of the sphere of projection. On this scale the distance between adjacent levels of the reciprocal lattice (i.e. those parallel the plane of the gnomonogram) equals r, the radius of the fundamental sphere. These layers are termed 0-level, 1-level, 2-level, etc., according to the number of radii at which they are located above the origin. The 1-level in Fig. 1*a* is, of course, the gnomonogram of classical crystallography and the primed gnomonic projection constants p_0', q_0', etc., are used in its construction.

* Present address: Department of Geology, University of Tennessee, Knoxville, Tennessee.

[1] Here used to designate a reciprocal lattice on the same scale as a similarly oriented gnomonogram of the crystal.

The second step, measurement of the central distance[2] of the gnomonic lattice point, is accomplished essentially through use of cross sections similar to AB of Fig. 1*b*. These all involve right triangles (cf. OO_3P of Fig. 1*b*) with one apex at O, the lattice origin; another at O_n, the orthographic projection of O on the n-layer; and the third apex at P, a random lattice point in this n-layer which reciprocally represents the set of crystal

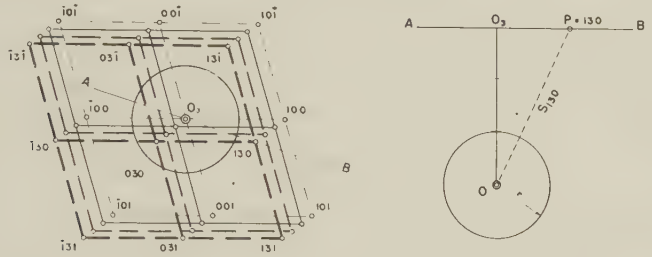

FIG. 1. (*a*) Orthographic projection of a triclinic lattice upon the $|h3l|$ plane; thus [*b*] is normal to the plane of the paper. The equator of the fundamental sphere appears as the circle centered on O_3, which is the projected position of the lattice origin (=center of sphere) upon the 3*d* level.

To add apparent depth to the lattice, the lines denoting the upper layers are successively heavier. Removal of all dashed lines and of line AB would leave a gnomonogram, with P' extending to right and R' extending downwards.

(*b*) A cross section through line AB of (*a*). O_3 is directly above O, the lattice origin, a distance of $3r$, where r is the radius of the fundamental sphere. For this [*b*]-vertical gnomonic lattice, S_{130} represents the central distance of the point, (130), generalized as P.

planes whose interplanar spacing is desired. The lengths of the two legs, O_nP and OO_n, of the right triangle are easily determined since O_nP is located in the plane of the orthographic projection and therefore directly measurable while OO_n is equal to nr. The hypotenuse OP, which represents S_{hkl}, the central distance of point P, is then secured from the two legs by Peacock's (1938, pp. 97–98) clever graphic method.

The grid scales (Fig. 2) offer a further short cut. For this same point P, located in the n-layer of the gnomonic lattice, it is only necessary to measure the leg O_nP with a photographic positive of the n-level grid scale; the resulting grid scale reading, G_{hkl}, is the value of the ratio S_{hkl}/r.

PREPARATION OF GNOMONOGRAM FOR USE WITH GRID

The basic gnomonogram from which the gnomonic lattice is to be developed should be drawn with a fundamental sphere of a radius equal to

[2] The distance of the point from the gnomonic lattice origin.

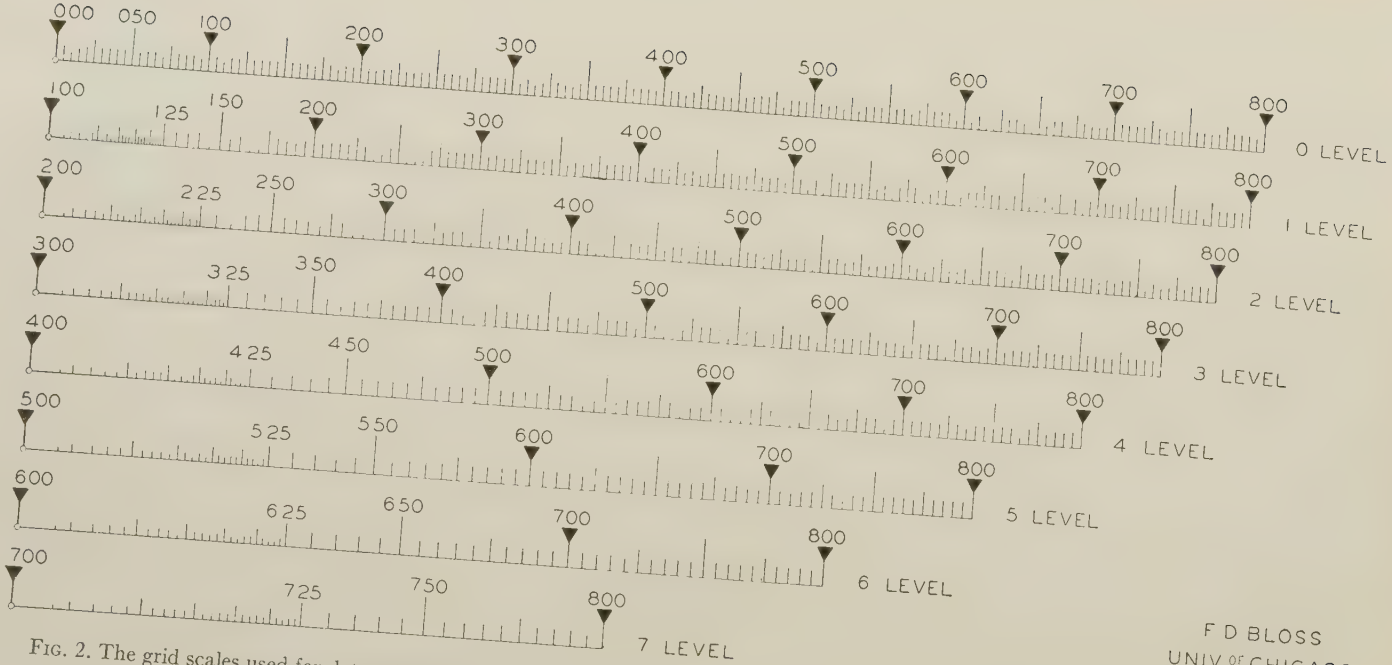

FIG. 2. The grid scales used for determining the G_{hkl} values, i.e., the ratio of S_{hkl}, the central distance, to r, the vertical distance between levels of the lattice.

unit distance on the 0-level grid scale. The vertical distance between layers of the gnomonic lattice, which always equals r, thus becomes equal to 1 unit on the 0-level grid scale, a condition necessary to permit use of the grid scale. This is most easily done by calculating the gnomonic projection elements (Table 1) for unit radius and then setting off these distances in terms of 0-level scale units of the positive copy (Fig. 2) being used for the measurements.

That gnomonogram which has the direct axis of largest unit translation normal to it will be found to yield the most accurate results; reasons for this are discussed in a later section.

The development of a gnomonogram into an orthographic projection of a gnomonic lattice is readily apparent from Fig. 1*a*. A more quickly prepared substitute (Fig. 3) of equal utility may be developed merely by assuming the basic gnomonogram to represent different levels ($0, 1, 2 \cdots n$) of the gnomonic lattice and locating the orthographically projected positions ($O, O_1, O_2, \cdots O_n$) of the lattice origin upon each of these layers. These projected positions are quickly located. For example, the origin of the 0-level coincides with the projected and actual positions of the gnomonic lattice origin; for the remaining levels, projected lattice origin positions ($O_1, O_2, \cdots O_n$) are located along a line extending outward from the origin of the basic gnomonogram at a ϕ angle equal but opposite in sign to that of the pinacoid nearest horizontality; they are periodically spaced outward along it, in order of their subscripts, at intervals equal to tan ρ in 0-level units for this cited pinacoid.

Because of this convention of considering the gnomonogram to represent different layers, it is convenient to label its points with only partial Miller indices, leaving a blank for the index referring to the crystal axis normal to the gnomonogram.

Preparation of Grid

Prepare a positive of Fig. 2 on heavy base film, preferably so it can be used with the emulsion side down (to reduce parallax).[3] A thin coat of shellac sprayed on the emulsion side will protect it from wear and moisture. Carefully pierce the "minimum point" (encircled left end) of each grid scale with a fine sharp-pointed needle; use a magnifying lens to locate this hole exactly on the point.

Measurement of G_{hkl} with the Grid Scales

G_{hkl} values for all the points in a given layer, e.g., the n-level, can be secured rapidly by transfixing the "minimum point" of the n-level grid

[3] Copies from a glass plate negative of Fig. 1 are available from the author at the cost of preparation and handling.

scale (Fig. 2) to the O_n point of the orthographically projected gnomonic lattice and then slowly rotating this scale around O_n. On a form similar to that used in Table 2, record the Miller indices and the values of the intercepts of the points on the n-scale during its rotation. The former are

TABLE 1

Axis normal to gnomonogram	Elements to be calculated in order to construct gnomonogram		Orientation of reciprocal axes in gnomonogram		
	Symbol	Formula number[a]	Symbol	Coordinates	
				Phi	Rho
		Standard Orientation			
c	γ^*	(3)			
	p_0'	(10)	a^*	$+\gamma^*$	90°
	q_0'	(9)	b^*	0°	90°
	$\tan \rho_0$	(4)			
	ϕ_0	(5)			
		First Permutation			
a	α^*	(1)			
	q_1'	(17)	b^*	$+\alpha^*$	90°
	r_1'	(18)	c^*	0°	90°
	$\tan \rho_1$	(12)			
	ϕ_1	(13)			
		Second Permutation			
b	β^*	(2)			
	p_2'	(26)	a^*	0°	90°
	r_2'	(27)	c^*	$+\beta^*$	90°
	$\tan \rho_2$	(21)			
	ϕ_2	(22)			

[a] Refer to formulae in Fisher (1952) from which element may be calculated.

secured by inserting the value of n into the blank of the partial Miller index. To measure G_{hkl} values for points in the n-1 layer, transfix the minimum point of the n-1 level scale to the O_{n-1} point and repeat the above procedure. Figure 3 shows the grid in a position to read G_{h4l} values for the points in a gnomonic lattice normal to [b].

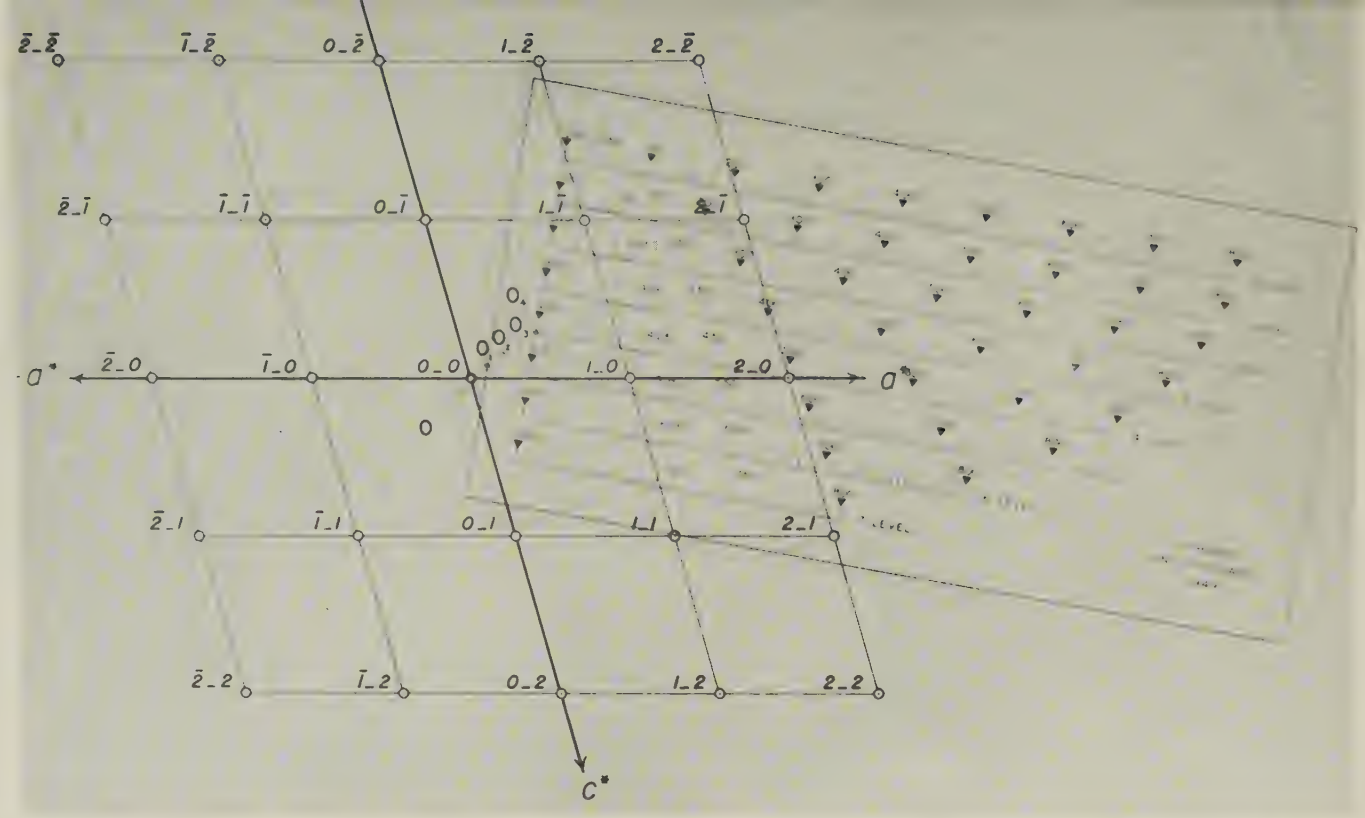

FIG. 3. Conversion of ordinary gnomonogram (center of its sphere of projection would be at O_1 and blanks in indices would be filled with 1's) into the equivalent of a series of orthographic projections of the lattice origin upon various levels of the reciprocal lattice. Thus O_1, O_2, O_3 represent these projected origin positions as the gnomonogram is respectively considered to represent the 1st, 2nd, and 3rd layers of the gnomonic lattice.

The grid has been placed over it with the 4-level scale in position to measure G_{hkl} values for all the "face poles" in the gnomonic lattice plane $|h4l|$ merely by rotation around the projected origin position, O_4. The pin ordinarily used to transfix the minimum point of the scale to O_4 has here been removed for illustrative purposes only. G_{240} can be seen to be equal to 5.02.

Relationship Between G_{hkl} and d_{hkl}

For the unit reciprocal lattice where the proportionality constant is set equal to unity (Buerger, 1942, p. 117), the following relations hold:

$$d_{001}^* = \frac{1}{c_0}, \quad d_{100}^* = \frac{1}{a_0}, \quad \text{and} \quad d_{010}^* = \frac{1}{b_0}.$$

For the various gnomonic lattices $d_{001}^G = r$, $d_{100}^G = r$, or $d_{010}^G = r$ depending upon whether the c, a, or b axis is oriented normal to the basic gnomonogram. Thus for these three different orientations, the derived gnomonic lattices represent vastly increased models of the unit reciprocal lattice on a scale $rc_0 : 1$, $ra_0 : 1$, or $rb_0 : 1$ respectively; or in general $ru_0 : 1$, where u_0 is the unit translation along the direct crystal axis normal to the gnomonogram.

Thus to translate S_{hkl}, a central distance measured in the gnomonic lattice, into σ_{hkl}, the analogous distance in the unit reciprocal lattice, it is necessary to divide the former by ru_0 which is the magnification constant, i.e., $\sigma_{hkl} = S_{hkl}/ru_0$. Therefore, since $\sigma_{hkl} = S_{hkl}/r$ and since by definition $d_{(hkl)} = 1/\sigma_{hkl}$, $d_{(hkl)} = u_0/G_{hkl}$. A 20-inch slide rule is generally adequate for this calculation. For the example of Fig. 3,

$$d_{(240)} = \frac{b_0}{G_{240}} = \frac{10.72\text{A}}{5.02} = 2.14 \text{ Å}.$$

The magnification constant, ru_0, of a gnomonic lattice is largest, and therefore the accuracy in this graphical determination of $d_{(hkl)}$ values is highest, when the gnomonic lattice is developed from a gnomonogram which is normal to the direct crystal axis of largest unit translation. Thus the basic gnomonogram for trimetric crystals with axes chosen as recommended by Donnay (1943) should generally be one normal to [b]. The ratios b_0/a_0 and b_0/c_0 indicate the ratio of size of a [b] vertical gnomonic lattice to those lattices developed from [a] and [c] vertical gnomonograms respectively. They thus indicate the relative importance of a constant plotting or measuring error in an [a] and a [c] vertical gnomonic lattice with respect to the same error in the [b] vertical one.

Bravais Sphere

Most of the planes encountered in morphology are those of maximum spacing and therefore with simple Miller indices. They are represented in the reciprocal lattice by the points closest to the origin. To avoid needless measurement of closely spaced planes it is well to decide upon a minimum spacing, $d_{\min}$, and upon a device to avoid measurement of planes spaced less than this minimum value.

The grid is automatically such a device, supplanting the limiting circles

Peacock constructed for this purpose. A minimum spacing limitation of direct lattice planes is expressed in the reciprocal lattice by a limiting maximum distance from the origin, beyond which no points will be measured. Thus the choice of a value for $d_{\min}$ automatically circumscribes in the gnomonic lattice an origin-centered sphere (Bravais sphere of Peacock, 1938, pp. 95–96) within which all points will have scale readings less than $G_{\max}$, where $G_{\max} = u_0/d_{\min}$ in grid units. Only the points in the gnomonic lattice denoting planes having spacings greater than $d_{\min}$ will have $G_{hkl} < G_{\max}$ and therefore fall within the sphere.

Example

Three differently oriented [a], [b], and [c] normal gnomonograms were constructed from Fisher's (1952) data on chalcanthite. The one normal to [b] is reproduced in Fig. 3 with the partial Miller indices indicated. The minimum spacing decided upon was 2.41 Å. Since the size of the gnomonogram and therefore the gnomonic lattice varies with the orientation, the value of $G_{\max}$ must similarly vary. For the gnomonic lattice with [a] normal,

$$G_{\max} = \frac{a_0}{d_{\min}} = \frac{6.104 \text{ Å}}{2.41 \text{ Å}} = 2.53;$$

for the gnomonic lattice with [b] normal,

$$G_{\max} = \frac{b_0}{d_{\min}} = \frac{10.72}{2.41} = 4.45;$$

and for the gnomonic lattice with [c] normal

$$G_{\max} = \frac{c_0}{d_{\min}} = \frac{5.949}{2.41} = 2.47.$$

Thus, for Fig. 3 no points, excluding the example (240), were measured if their G_{hkl} values exceeded 4.45; for the [c] normal gnomonic lattice, no points were measured if their G_{hkl} values exceeded 2.47, etc.

Table 2 presents the results of grid scale determinations on two differently oriented gnomonic lattices of chalcanthite. Results for the [a] normal gnomonic lattice were similar in accuracy to those for the [c] normal gnomonic lattice and therefore omitted. As was expected, results for the [b] normal gnomonic lattice are more accurate in general. The column entitled "d_{calc}" refers to the interplanar spacings calculated from the formula

$$\frac{1}{d_{hkl}^2} = h^2a^{*2} + k^2b^{*2} + l^2c^{*2} + 2\,k\,l\,b^*c^* \cos\alpha^* + 2\,l\,h\,c^*a^* \cos\beta^* + 2\,h\,k\,a^*b^* \cos\gamma^*$$

(Int. Tables, 1935, p. 69) using Fisher's (1952) data.

TABLE 2

Miller indices	c-axis normal gnomonic lattice		b-axis normal gnomonic lattice		d_{calc} (from formula)
	G_{hkl}	$\frac{c_0}{G_{hkl}}$	G_{hkl}	$\frac{b_0}{G_{hkl}}$	
010	0.57	10.44	1.027	10.44	10.44
100	1.035	5.75	1.87	5.73	5.73
001	1.05	5.67	1.89	5.67	5.67
110	1.08	5.51	1.95	5.50	5.48
020	1.14	5.22	2.055	5.22	5.22
$0\bar{1}1$	1.15	5.18	2.08	5.15	5.14
011	1.235	4.82	2.205	4.86	4.84
$\bar{1}01$	1.26	4.72	2.26	4.75	4.74
$\bar{1}\bar{1}1$	1.25	4.76	2.27	4.72	4.72
$\bar{1}10$	1.27	4.69	2.30	4.66	4.67
120	1.38	4.31	2.505	4.28	4.28
$\bar{1}11$	1.49	4.00	2.675	4.01	4.00
$02\bar{1}$	1.48	4.02	2.69	3.99	3.98
$\bar{1}21$	1.49	4.00	2.70	3.97	3.96
021	1.61	3.69	2.88	3.72	3.71
101	1.67	3.56	3.00	3.57	3.56
$1\bar{2}0$	1.67	3.56	3.025	3.54	3.54
030	1.71	3.48	3.08	3.48	3.48
111	1.73	3.44	3.10	3.46	3.45
$1\bar{1}1$	1.79	3.33	3.25	3.30	3.30
130	1.82	3.27	3.29	3.26	3.26
$\bar{1}21$	1.88	3.17	3.37	3.18	3.18
$\bar{1}31$	1.87	3.18	3.405	3.15	3.15
$03\bar{1}$	1.925	3.09	3.495	3.07	3.07
121	1.95	3.05	3.51	3.05	3.05
$2\bar{1}1$	1.99	2.99	3.61	2.97	2.98
210	2.05	2.90	3.69	2.91	2.91
$\bar{1}12$	2.05	2.90	3.695	2.90	2.90
$\bar{2}01$	2.05	2.90	3.69	2.91	2.90
$\bar{1}02$	2.073	2.87	3.723	2.88	2.88
200	2.075	2.87	3.74	2.87	2.87
031	2.08	2.86	3.725	2.88	2.87
$\bar{1}21$	2.07	2.87	3.77	2.84	2.85
002	2.10	2.83	3.775	2.84	2.83
$\bar{2}21$	2.095	2.84	3.80	2.82	2.82
$0\bar{1}2$	2.13	2.79	3.85	2.79	2.79
$1\bar{3}0$	2.16	2.76	3.89	2.76	2.75
220	2.16	2.76	3.92	2.74	2.74
$\bar{1}22$	2.18	2.73	3.945	2.74	2.72
012	2.22	2.68	3.98	2.69	2.69

TABLE 2—*Continued*

Miller indices	*c*-axis normal gnomonic lattice		*b*-axis normal gnomonic lattice		d_{calc} (from formula)
	G_{hkl}	$\frac{c_0}{G_{hkl}}$	G_{hkl}	$\frac{b_0}{G_{hkl}}$	
$\bar{1}12$	2.246	2.65	4.02	2.67	2.66
$\bar{2}11$	2.25	2.64	4.055	2.65	2.65
$2\bar{1}0$	2.25	2.64	4.07	2.64	2.64
040	2.28	2.61	4.107	2.61	2.61
131	2.31	2.58	4.14	2.59	2.58
$0\bar{2}2$	2.31	2.58	4.18	2.56	2.57
140	2.325	2.56	4.18	2.56	2.56
$\bar{1}31$	2.35	2.53	4.19	2.56	2.55
$\bar{1}41$	2.335	2.55	4.24	2.53	2.53
$\bar{2}31$	2.34	2.54	4.25	2.52	2.53
230	2.43	2.45	4.38	2.45	2.45
$0\bar{4}1$	2.43	2.45	4.40	2.44	2.44
$\bar{1}32$	2.44	2.44	4.42	2.43	2.43
$\bar{2}12$	2.45	2.43	4.435	2.42	2.43
022	2.47	2.41	4.425	2.42	2.42
$1\bar{3}1$	2.46	2.42	4.45	2.41	2.41

ASSIGNMENT OF MILLER INDICES TO POWDER FILM LINES

Several powder films (114 mm. diameter camera) of chalcanthite were measured and the *d* values of the more intense lines are given in Table 3. Lines with *d* values of less than 2.41 Å were not measured. The graphically determined *d* values of Table 2 were then used to determine, where possible, the Miller indices of the plane (or planes) responsible for the respective powder lines.

Comparison of Tables 2 and 3 indicates that one may often unequivocally assign a set of Miller indices to the powder lines of greater *d* values whereas this possibility lessens as the powder lines of smaller *d* values are considered. However, extinction data may help eliminate some of the ambiguity. The powder line of $d=2.55$ Å, e.g., could be caused by any one or combination of the planes $(0\bar{2}2)$, (140), $(\bar{1}31)$, $(\bar{1}41)$, and/or $(\bar{2}31)$. The spread of the several calculated or graphically measured *d* values around 2.55 Å is such that the disparity between any of them and the 2.55 Å powder photo measured value could be caused by small inaccuracies in the single crystal data, in the measurement of the powder line, or in the graphical determination of the *d* value. This latter effect may be eliminated by calculating the ambiguous *d* value from the stand-

TABLE 3

d measured from powder films	I/I_1 by visual estimation of intensities	Assignment of Miller indices to powder lines on basis of Table 2
10.45 Å	.3	010
5.70	.6	100 and/or 001
5.45	.7	110
5.15	.4	$0\bar{1}1$
4.70	1.0	$\bar{1}\bar{1}1$ (less likely $1\bar{1}0$)[a]
4.26	.4	120
3.97	.7	$0\bar{2}1$ and/or $\bar{1}\bar{2}1$
3.69	.7	021
3.53	.35	$1\bar{2}0$[b] and/or 101
3.45	.3	111[a]
3.29	.4	$1\bar{1}1$[a]
3.24	.3	130
3.17	.2	$\bar{1}21$ and/or $\bar{1}\bar{3}1$
3.04	.4	121 and/or $0\bar{3}1$
2.89	.05	210, $\bar{1}\bar{1}2$ and/or $\bar{2}01$
2.86	.15	200;[b] possibly (031, $\bar{1}02$ and/or $1\bar{2}1$)
2.82	.4	$\bar{2}\bar{2}1$ and/or 002
2.78	.15	$0\bar{1}2$
2.74	.4	220 and/or $1\bar{3}0$
2.72	.05	$\bar{1}22$
2.66	.4	$2\bar{1}0$[b] possibly ($\bar{2}11$ and/or $\bar{1}12$) also 012
2.55	.15	Numerous possibilities
2.52	.05	Numerous possibilities
2.45	.3	Numerous possibilities
2.41	.6	Numerous possibilities

[a] Crystal with [c] parallel to the rotation axis was mounted in powder camera after removal of powder rod so that, in effect, a c-axis rotation picture was superimposed upon the powder film. No ($hk0$) spot was observed to fall on this line.

[b] Under same conditions as above, an ($hk0$) spot was observed to fall on or very near a powder line.

ard interplanar spacing formulae. Extinction data, if available, may be of considerable use in eliminating some of the ambiguities due to the cited inaccuracies.

ACKNOWLEDGMENTS

The author is heavily indebted to Professor D. Jerome Fisher for his recent data on chalcanthite, for critically reading the manuscript, and for suggestions and advice freely given during the construction and testing of the scale. Thanks are due Mr. Frederick A. Johnson for drafting the original of Fig. 1, from which the scale was made.

References

Buerger, M. J. (1942), *X*-Ray Crystallography: John Wiley and Sons, Inc., New York.

Donnay, J. D. H. (1943), Rules for the conventional orientation of crystals: *Am. Mineral.*, **28,** 313–328.

Fisher, D. Jerome (1952), Triclinic gnomonostereograms. *Ibid.*, **37,** 83–94.

International Tables, Vol. **1,** 1935.

Peacock, Martin A. (1938), A general graphical method for determining the spacings of lattice planes: *Zeit. Krist.*, **100,** 93–103.

Manuscript received Aug. 21, 1951

STUDY OF HOEGBOMITE

GERALD M. FRIEDMAN, *University of Cincinnati, Cincinnati, Ohio.*

ABSTRACT

Hoegbomite occurrences in New York, Virginia, and North Carolina were investigated. The North Carolina locality is a new hoegbomite discovery.

Hoegbomite occurs in emery or hornfels associated with emery. It formed at the expense of an earlier spinel. In North Carolina two varieties of hoegbomite were discovered, hoegbomite *A* and hoegbomite *B*. Hoegbomite *A* appears to be transitional between spinel and hoegbomite *B*. The hoegbomite of the New York emery deposits was formed later than the emery but earlier than the high-temperature quartz veins which represent the last stages of the intrusion that gave rise to the emery.

Some of the properties of hoegbomite are discussed.

INTRODUCTION

Hoegbomite was first described by Gavelin[1] from Lapland, Sweden, in 1916. The only description of an American occurrence is that by Watson[2] from Virginia in 1925.

In recent years hoegbomite has been reported from a number of localities. Gillson and Kania[3] noted its occurrence in the hornfels of Cortlandt township, New York. De Lapparent[4] reported the discovery of a new mineral which he termed taosite on the island of Samos in the Aegean, but which on further investigation[5] proved to be hoegbomite. Oenay[6] noted hoegbomite in the Turkish emery and Nel[7] in corundum-spinel-chlorite rocks in the corundum fields of eastern Transvaal. Hoegbomite has also been reported from the corundum-rich magnetite ore at Roedstand, Soendmoere, Norway.[8] Sandrea[9] discovered hoegbomite in the spilites of Kamerun, West Africa.

[1] Gavelin, A., Ueber Hoegbomit. Ein neues gesteinbildendes Mineral aus dem Ruoutevarre-Gebiet in Lappland: *Bull. Geol. Inst., University of Upsala*, **15,** 289–316 (1916).

[2] Watson, T. L., Hoegbomite from Virginia: *Am. Mineral.*, **10,** 1–9 (1925).

[3] Gillson, J. L., and Kania, J. E. A., Emery deposits near Peekskill, N. Y.: *Econ. Geol.*, **25,** 518 (1930).

[4] De Lapparent, J., Les étapes du métamorphisme des émeris de Samos: *Comptes Rend. Acad. Sci.*, **201,** 154–157 (1935).

[5] De Lapparent, J., Composition minéralogique, structure et origine des émeris de Turquie: *Comptes Rend. Acad. Sci.*, **223,** 227–228 (1946).

[6] Oenay, T. S., Ueber die Smirgelgesteine SW-Anatoliens: *Schweizer. min. pet. Mitt.*, **29,** 387 (1949).

[7] Nel, H. J., Papers on the mineralogy of Southern Africa: *S. Africa Geol. Survey, Mem.* **43,** 1–8 (1949).

[8] Palache, C., Berman, H., & Frondel, C., System of Mineralogy; 7 ed., 1, 723, John Wiley & Sons, New York (1946).

[9] Sandrea, A., Sur la présence de hoegbomite dans une spilite du Cameroun: *Comptes Rend. Acad. Sci.*, **230,** 2306–2307 (1950).

In most of these localities hoegbomite occurs as a rare accessory constituent. In several of the above cases its occurrence in a particular area was merely noted by the respective authors and was incidental to the general discussion. This may be the reason why Sandrea who discovered the Kamerun hoegbomite considered it its third reported occurrence whereas eight others had previously become known.

On a ten-day field trip in the crystalline area of Alabama and neighboring Georgia in 1896, Clements[10] collected three samples of hornblende-olivine rock on the road between Lafayette and Oakbowery. Microscopic study showed the rock to be a granular aggregate of hornblende, olivine, pleonaste, and magnetite. Of interest is Clements' observation of the alteration of spinel into a brownish-yellow mineral which he could not identify. He noted: "No such alteration has ever been described for pleonaste in any rock." The mineral he discussed is undoubtedly hoegbomite. His description of that mineral is probably the first on record.

In the course of this study three hoegbomite localities were investigated along the Appalachian belt. They include a new hoegbomite locality in Macon County, North Carolina, the hoegbomite occurrence of Pittsylvania County, Virginia, previously described by Watson,[11] and a Westchester County, New York occurrence. Hoegbomite from Westchester County, New York, has been reported in the hornfels adjoining the emery deposits of Emery Hill by Gillson and Kania[12] but its mode of occurrence has not been described. In this study hoegbomite was noted in both the emery and hornfels of Emery Hill and on the south slope of Salt Hill. The Alabama occurrence could not be rediscovered as the descriptions of Clements were not sufficiently detailed.

New York Occurrence

Hoegbomite occurs as a very rare accessory mineral in the emery deposits and hornfels of Cortlandt township, Westchester County, New York. Cortlandt township is located to the south and southeast of the town of Peekskill, about 35 miles north of New York City. Two hoegbomite occurrences were noted, one at Emery Hill, the other on the south slope of Salt Hill.[13]

The Cortlandt emery is a corundum, titaniferous magnetite, spinel (pleonaste) aggregate that occurs in norite. The relative proportions of

[10] Clements, J. M., Notes on the microscopical character of certain rocks from northeast Alabama: *Geol. Survey of Alabama*, **5**, 156–157 (1896).

[11] Watson, T. L., *op. cit.* (1925).

[12] Gillson, J. L., and Kania, J. E. A., *op. cit.* (1930).

[13] For index map see Friedman, G. M., The sapphirine occurrence of Cortlandt, New York: *Am. Mineral.*, **37**, 244–249 (1952).

the constituent minerals vary. Hoegbomite was noted in the rock in which spinel was abundant and corundum scant. Sillimanite, cordierite, kyanite, magnetite, garnet, and sapphirine make up the hornfels.

The hoegbomite crystals are very small and must be studied with high power magnification. The length of the largest crystals does not exceed 0.04 mm., their width does not exceed 0.02 mm. They are pleochroic; ω = moderate brown, ϵ = moderate yellowish brown, $\omega > \epsilon$. The mineral is uniaxial negative.

Hoegbomite is a replacement product of spinel. The stages in the replacement of spinel can be traced. It usually formed around the margin of the spinel grains, the rest of the original crystal is typical spinel. Tabular plates which resemble biotite usually show the strongest pleochroism. They also occur along the margin of spinel grains. Many of the spinel grains are slightly fractured and tabular hoegbomite replaced the spinel between the fracture and the margin of the original spinel grain. The major difference in the composition between hoegbomite and spinel is that hoegbomite contains titanium. Titanium must have therefore been introduced subsequent to spinel formation.

Quartz veins that have cut the emery are bounded along their entire margin by reaction rims of garnet. The quartz is nowhere in direct contact with spinel. The reaction between spinel and quartz gave rise to garnet and sillimanite or to sapphirine, and occasionally to cordierite.[14] Quartz veins are surrounded by garnet, garnet in turn by sillimanite. Sapphirine was formed at the expense of the spinel farthest from the quartz vein. These quartz veins have cut the emery after the replacement of spinel by hoegbomite. This is evident from the following: it has been shown[15] that spinel and quartz are incompatible. Hoegbomite on the other hand is stable in the presence of free silica. Wherever quartz reacted with a spinel grain that was partially replaced by hoegbomite the spinel part was transformed into sapphirine, unless garnet or cordierite formed. The original grain is therefore, partially sapphirine and partially hoegbomite. As the quartz veins represent the last stages of the intrusion that was responsible for the formation of the emery, of which the spinel is a major constituent, the titanium emanations that gave rise to the hoegbomite can be deduced as being later than the formation of the spinel, but earlier than the high-temperature quartz veins.

Virginia Occurrence

The Virginia hoegbomite occurs in the emery deposits of Whittles, which are located in the north-central part of Pittsylvania County,

[14] Friedman, G. M., The sapphirine occurrence of Cortlandt, New York: *Am. Mineral.* **37**, 244–249 (1952).

[15] Friedman, G. M., *op. cit.*

about 20 miles north of Danville and 40 miles south of Lynchburg. As the Virginia hoegbomite has previously been described by Watson a detailed discussion is not necessary. The replacement features merely will be described.

The Virginia emery consists of corundum, spinel (of composition near hercynite), and titaniferous magnetite. The relative proportions of these

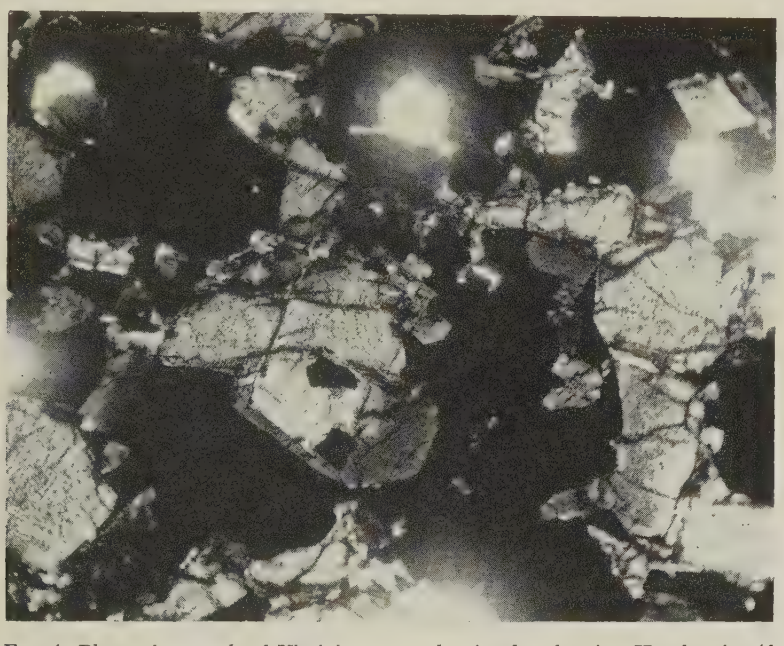

FIG. 1. Photomicrograph of Virginia emery showing hoegbomite. Hoegbomite (dark borders) rimming spinel (large grains). Prismatic hoegbomite (near left margin), magnetite (opaque). ×56 (W. B. Hall, photo).

three constituents vary widely, in some of the thin sections spinel was not observed and corundum was abundant, in others the reverse held true. Hoegbomite is invariably associated with spinel, or occurs in slides containing spinel relicts in which the spinel has almost been totally replaced by hoegbomite. The emery deposits, as at Cortlandt, New York, are associated with a basic rock, a gabbro.

That hoegbomite formed at the expense of earlier spinel is evident from the observation that spinel grains are mantled with hoegbomite and replacement nuclei of hoegbomite occur in some of the spinel grains. In some samples it can be noted that hoegbomite crystals have merely replaced the outer margin of spinel grains and entirely replaced only small spinel grains that were partially enclosed in magnetite. In other sections hoegbomite grains are molded on small remnants of spinel and corroded

spinel relicts are enclosed in the hoegbomite. Again, in a third type of section only occasional corroded spinel relicts are noted in hoegbomite, the bulk of the slide being made up of hoegbomite, magnetite, and corundum.

Measurement of the grain sizes of the hoegbomite differ substantially from the figures given by Watson. The largest crystals he observed[16] did not exceed 0.03 mm. in length and 0.01 mm. in width, while the corresponding measurements made in this study were 1 mm. and 0.3 mm., respectively. Many of the hoegbomite grains have entirely replaced spinel grains and consequently assumed the dimensions of the former.

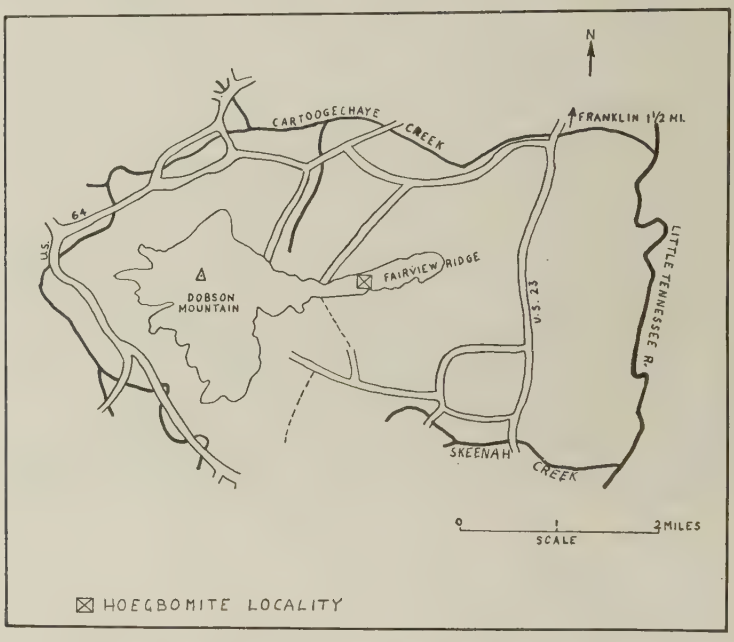

Fig. 2. Index map of the Dobson Mountain-Fairview Ridge tract, North Carolina, showing location of hoegbomite occurrence.

North Carolina Occurrence

The North Carolina hoegbomite occurs in the emery deposits of Macon County. The hoegbomite locality can be reached from Franklin by following Highway 23 south for about five miles, then turning west before crossing Skeenah Creek. About two miles west of Highway 23 a northward trending road leads to the top of the Fairview Ridge where the emery deposits are located.

[16] Watson, T. L., *op. cit.* (1925).

The North Carolina emery is very similar in composition to the New York and Virginia emery. Its chief mineral constituents are corundum, spinel (of composition near pleonaste), and titaniferous magnetite. Hoegbomite is common. Because of the deep weathering it was not possible to establish with certainty the nature of the rock in which the emery occurs. Outcrops of Roan gneiss, which in this area is of dioritic composition, were noted near emery occurrences.

FIG. 3. Photomicrograph of North Carolina emery showing hoegbomite. V-shaped mineral in center is hoegbomite *A* passing marginally into hoegbomite *B* (dark rim). Prismatic hoegbomite *B* in upper right. Corundum (white), magnetite (black, opaque). The rest of section is made up of spinel (example lower right and lower left) and hoegbomite (example top center, right margin). ×34. (W. B. Hall, photo.)

In hand specimen the hoegbomite cannot be distinguished from the associated iron oxides and spinel. Like these it is of black color. However, after the rock is crushed and examined with the aid of a binocular microscope, even without immersion into refractive index liquids, the brown color of the mineral becomes apparent. The grains have a metallic luster. Most of the hoegbomite crystals are anhedral, some, however, are of prismatic form. They are on the average larger than those from the Virginia locality. The largest grains exceed 1 mm. in length and are about 0.4 mm. in width. The cleavage is micaceous and well developed.

TABLE 1. OPTICAL PROPERTIES OF HOEGBOMITE

	Virginia	North Carolina		Transvaal		Kamerun	Turkey	Samos	Sweden (Lapland)
		A	*B*	*A*	*B*				
Pleochroism									
ω	dark brown	pale pink	deep brown	reddish brown	dark sepia brown	yellow	dark brown	brownish red	dark golden brown
ϵ	light golden brown to nearly colorless	light yellow pink to nearly colorless	moderate brown	pale golden brown	light sepia brown	yellow brown	light brown to yellow brown	yellow	light golden brown
Refractive Index									
ω	1.848	1.840–1.845	1.852	1.820	1.848	>1.845 <1.850	between 1.82+1.85	~1.78	1.853 ±0.003
ϵ	1.817	1.815 ±0.005	1.804	1.800	1.823	~1.804	~1.815		1.803 ±0.003
Absorption	$\omega>\epsilon$	$\omega>\epsilon$	$\omega>\epsilon$	$\omega>\epsilon$	$\omega>\epsilon$	$\omega>\epsilon$	$\omega>\epsilon$	$\omega>\epsilon$	$\omega>\epsilon$
$\omega-\epsilon$	0.031	0.020–0.035	0.048	0.020	0.025	0.047–0.048	0.032	0.035	0.050

Two varieties of hoegbomite can be distinguished. These differ somewhat in their optical properties. Nel,[17] in his study of the Transvaal hoegbomite likewise noted two varieties and referred to these as hoegbomite *A* and hoegbomite *B*. This nomenclature will be adopted in this study.

Hoegbomite *A* is weakly pleochroic, ω = pale pink, ϵ = light yellow pink to nearly colorless; absorption $\omega > \epsilon$. In contrast to hoegbomite *B* the interference colors of hoegbomite *A* are not masked by the color of the mineral. The indices of refraction[18] are variable; $\omega = 1.840$–1.845, $\epsilon = 1.815 \pm 0.005$. Double refraction: $\omega - \epsilon = 0.020$–$0.035$.

Hoegbomite *B* likewise is pleochroic, ω = deep brown, ϵ = moderate brown; absorption $\omega > \epsilon$. Hoegbomite *B* closely resembles the Virginia and New York hoegbomite, its brown color, however, is much deeper than that of those localities. Because of the deep brown color the interference colors of many grains are masked. The indices of refraction[19] are $\omega = 1.852$, $\epsilon = 1.804$; double refraction: $\omega - \epsilon = 0.048$.

Both varieties of hoegbomite are uniaxial negative. Hoegbomite *B* shows a greater absorption than hoegbomite *A*.

The North Carolina like the New York and Virginia hoegbomite was formed by replacement of spinel. Spinel grains are mantled with hoegbomite and replacement nuclei of hoegbomite occur in spinel grains. Many hoegbomite *B* grains pass marginally into hoegbomite *A* and these in turn into spinel. Hoegbomite *A* appears to be transitional between spinel and hoegbomite *B*.

Comparative Table of Optical Properties

For comparative purposes a table of the optical properties of hoegbomite has been compiled.

Association

The minerals that are immediately associated with the hoegbomite of the ten reported localities are noted in the table below.

At the New York, Virginia, North Carolina, Alabama, Lapland, and Samos localities hoegbomite is intimately associated with spinel and magnetite, corundum is abundant in most cases. Spinel has been reported from all the localities except Turkey.[20] The magnetite-spinel rocks in which the hoegbomite of the American localities occurs is associated with basic rocks.

[17] Nel, H. J., *op. cit.* (1949).

[18] Determined by Jewell J. Glass of the U. S. Geol. Survey.

[19] Determined by Jewell J. Glass of the U. S. Geol. Survey.

[20] No information has been available to the author on the Norwegian occurrence.

Table 2. Minerals Associated with Hoegbomite

	New York	Virginia	North Carolina	Alabama	Lapland	Norway	Samos	Turkey	Kamerun	Transvaal
Spinel	—	—	—	—	—	No Information	—		—	—
Corundum	—	—	—		—	—		—		—
Magnetite	—	—	—	—	—	—	—	—		
Pyroxene	—	—							—	
Diaspore							—	—		
Chlorite		—	—		—					—
Chloritoid							—	—		
Gibbsite					—					—

Discussion of Origin

Gavelin and Watson believed that hoegbomite was essentially a primary mineral but that some hoegbomite was formed by replacement of spinel. Examination of hoegbomite from New York, Virginia, and North Carolina indicates a secondary origin. The mineral appears to have formed at the expense of spinel. Hoegbomite *B* appears to be the ultimate product.

Nel ascribes the following formula to hoegbomite $(Fe,Mg)_6(Al, Fe)_{16}TiO_{32}$. The composition of pleonaste spinel is $(Mg, Fe)Al_2O_4$. If the formula of the spinel is written $(Mg, Fe)_8Al_{16}O_{32}$ it becomes apparent that the hoegbomite was formed from the spinel by the isomorphous substitution of Ti for 2(Mg, Fe) and Fe^3 for Al ions.

As shown at the New York locality the Ti emanations which reacted with the spinel to form the hoegbomite were later than the formation of the spinel-magnetite-corundum rock, but earlier than the high temperature quartz veins which represent the last stages of the intrusion that gave rise to that rock.

Acknowledgments

The author is greatly indebted to Miss Jewell J. Glass of the United States Geological Survey for the refractive index determinations that are cited in this paper. Grateful acknowledgment is extended to Mr. W. B. Hall for preparing the photographs.

Manuscript received Sept. 27, 1951

VISÉITE, A ZEOLITE WITH THE ANALCIME STRUCTURE AND CONTAINING LINKED SiO_4, PO_4 AND H_xO_4 GROUPS

DUNCAN MCCONNELL, *National Bureau of Standards, Washington, D. C., and The Ohio State University, Columbus, Ohio.*

ABSTRACT

By combining the chemical data given by Mélon with information obtained by powder diffraction methods, a structural analogy between viséite and analcime is established. The cubic or pseudocubic unit cell is 13.65 Å and probably contains: $(Na_2Ca_{10})[(AlO_2)_{20}(SiO_2)_6(PO_2)_{10}(H_3O_2)_{12}]\cdot 16H_2O$. It is concluded, therefore, that a significant number of tetrahedral hydroxyls (H_xO_4) groups) occur in the framework of this tectosilicate-phosphate.

INTRODUCTION

Recent concepts on the isomorphic relationships amongst silicates and phosphates make possible certain mineral correlations which are not consistent with the more restricted classification according to anionic groups. Of particular importance is the possible substitution of $(OH)_4$ groups for both SiO_4 and PO_4 groups. Substitutions of the type $SiO_4 \rightarrow (OH)_4$ have been adequately demonstrated in nesosilicates for plazolite (Pabst, 1937) and grossularoid (Hutton, 1943) and in a nesophosphate, griphite (McConnell, 1942). Complete replacement of SiO_4 by $(OH)_4$ in the garnet structure yields $Ca_3Al_2(OH)_{12}$ and similar isostructural compounds (Flint, McMurdie, and Wells, 1941). These concepts need no further discussion.

More recently, substitution of $(OH)_4$ statistically for SiO_4 has been proposed to account for certain properties of a phyllosilicate, montmorillonite (McConnell, 1950). The present results will indicate the applicability of these concepts to a tectosilicate-phosphate.

Viséite was assigned the composition of $5CaO\cdot 5Al_2O_3\cdot 3SiO_2\cdot 3P_2O_5\cdot nH_2O$ (where $30>n>25$) by Mélon (1942) on the basis of four partial analyses by himself and by A. Jorissen. With the exception of the water content, which appears to be excessive, Mélon's determinations are quite in accord with theoretical requirements. Nevertheless, no relationship to any other known mineral was suggested by Mélon and it has only been possible to establish such a relationship after obtaining further experimental data and after re-examining these data in light of the theoretical concepts already mentioned.

The writer is indebted to Professor H. Brasseur of the University of Liège, Belgium, for an adequate sample of this rare mineral,* which per-

* The residue of the sample of viséite has been presented to the U. S. National Museum and entered under catalogue No. 106,364.

mitted certain additional measurements. It must be admitted that a study of this type would be quite impossible were it not for the prior existence of structural analyses on analcime by Gruner (1928), Taylor (1930), and Hartwig (1931), and on pollucite by Strunz (1936), Náray-Szabó (1938), and Taylor (1938). My colleagues have furnished constructive criticism, particularly P. M. Harris and W. J. McCaughey in Columbus and Herbert Insley and H. F. McMurdie in Washington. Michael Fleischer of the Geological Survey read the manuscript and made several helpful suggestions.

Chemical Considerations

The chemical composition found by Mélon can be accepted without question in all respects except the water content. At 110° C. Mélon re-

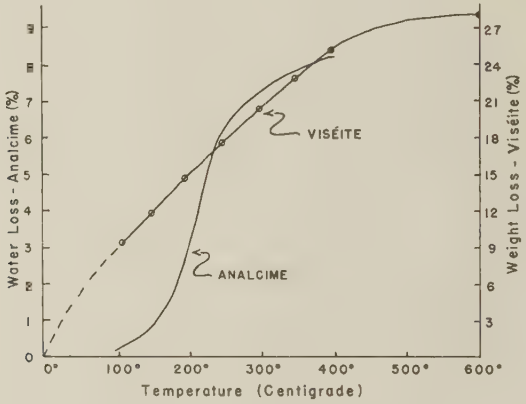

Fig. 1. Weight-loss data for viséite (Mélon) and selected, isobaric, water-loss data for analcime (Milligan and Weiser).

ports liberation of 9.02 per cent of H_2O after 2 hours of heating, but when his dehydration data are plotted (Fig. 1), it becomes immediately noticeable that a downward extension of the dehydration curve indicates loss of water at 0° C. unless the curve increases in slope at lower temperatures. This condition of greatest slope at temperatures below 110° C. is likely to occur only if free moisture is present, so it is deduced that all three of the water determinations are too high and that the average is too high by several per cent when compared with proposed theoretical composition.

A further complication which causes uncertainty in regard to Mélon's water determinations is the fact that the sample of viséite examined by the writer was found to contain organic matter, the presence of which was

indicated in two ways: (i) the pale yellowish-green powder turns brown on heating for several hours at 200° to 250° C. and (ii) when boiled in a solution of $AgNO_3$, small fragments of viséite turn black. Inasmuch as Mélon's water determinations appear to have been made solely by measuring loss in weight on heating, it seems highly probable that an unknown, though possibly significant, error may have resulted if organic material was present in his samples. The ability of analcime to occlude organic matter has been investigated by Barrer and Ibbitson (1944). Thus the occlusion of organic matter by viséite is not surprising, although it apparently escaped detection previously.

It should be emphasized, however, that the dehydration data obtained by Mélon (Fig. 1) probably do not represent equilibrium conditions because the isobaric dehydration data for viséite should not give a simple curve. If as postulated here, viséite is a definite hydrate, it should produce a dehydration curve of the type obtained for natrolite or for scolecite by Milligan and Weiser (1937). These authors were able to show that the erroneous, smooth curve which Kelley, Jenny, and Brown (1936) obtained for scolecite can be attributed to failure to maintain a constant aqueous vapor pressure or to allowance of insufficient time to permit establishment of equilibrium. For some points as many as 1200 hours were required, according to Milligan and Weiser. In the present instance, the quality and quantity of the viséite sample preclude precision measurement of isobaric dehydration.

Analyses for the non-volatile constituents indicated the approximate oxide ratios: $5CaO$, $5Al_2O_3$, $3SiO_2$ and $3P_2O_5$. In addition 1.77 per cent of Na_2O and 0.67 per cent of fluorine were obtained. The latter constituent can substitute for hydroxyl ions in the structure but, since the amount present is not particularly significant, fluorine will be disregarded in all further considerations. The soda, however, will be taken into account.

If a perfect analogy with analcime is assumed, it is possible to formulate the chemical relationships in a series of simple steps, as follows:

The structural unit of analcime is:

$$Na_{16}[(Al_{16}Si_{32})O_{96}]\cdot 16H_2O.$$

This can be written in general form as:

$$X_{16}[(Y_{16}Z_{32})O_{96}]\cdot 16H_2O.$$

Examining the analytical data, one finds for viséite:

$$16X \simeq 2Na + 10Ca + 4 \text{ vacant positions}$$
$$16Y + 32Z \simeq 20Al + 6Si + 10P + 12(H_3).$$

Thus viséite becomes:

$$(Na_2Ca_{10})[(Al_{20}Si_6P_{10}H_{36})O_{96}]\cdot 16H_2O$$

or

$$(Na_2Ca_{10})[(AlO_2)_{20}(SiO_2)_6(PO_2)_{10}(H_3O_2)_{12}] \cdot 16H_2O$$

where the brackets enclose the constituents of the structural framework.

The weight per cents required by this theoretical formula are compared with the average results given by Mélon in Table 1. The ratios of the non-volatile oxides indicate good agreement, particularly if an error in the water determination is assumed and other constituents are recalculated on this basis (Column 6). Thus, it can be concluded that in spite of the complex isomorphic substitutions encountered, the ratios suggested by Mélon are approximately correct, but they are somewhat improved if the sodium is considered. In light of the isomorphic relation

Table 1. Calculation of the Chemical Composition of Viséite According to the Analcime Structure

(1) Oxides	(2) Theoretical oxide ratios	(3) Mol. wts.	(4) Weight percents (theoretical)	(5) Experimental results (average)	(6) Experimental results (re-calculated using theoretical water content)
Na_2O	1	62	1.87	1.77	1.97
CaO	10	561	16.88	14.79	16.50
Al_2O_3	10	1019	30.65	26.15	29.18
SiO_2	6	360	10.83	9.93	11.08
P_2O_5	5	710	21.36	20.49	22.86
H_2O	34	612	18.41	26.11	(18.41)
F	—	—	—	0.67	—
			100.00	99.91	100.00

$AlO_4 \rightarrow SiO_4 \rightarrow PO_4$, the slight excesses of SiO_2 and P_2O_5 and the slight deficiency of Al_2O_3 are quite understandable.

Thus by assuming a structural analogy with analcime, it is possible to account for the chemical composition of viséite. It remains to examine the validity of this structural analogy.

Physical Properties

Before proceeding to a detailed consideration of the contents of the unit cell, discussion of the physical and optical properties of viséite and analcime might be advantageous. Comparative data follow.

	Analcime	*Viséite*
Optical character	isotropic or nearly so	isotropic
Refractive index	1.48–1.49	1.53
Specific gravity	2.22–2.29	2.2
Fusibility	$2\frac{1}{2}$	$2\frac{1}{2}$
Hardness	$5–5\frac{1}{2}$	3–4
Behavior with HCl	gelatinizes	gelatinizes

In comparing analcime and viséite it is noteworthy that the refractive index of the latter mineral is greater whereas the density is less. Unless the ionic refractivity of $(H_3O_2)^-$ is unexpectedly large, no explanation of this phenomenon is forthcoming. In part, the higher refractive index of viséite is probably explainable in view of the significantly greater ionic refractivity of Ca as compared with Na. The hardness would be expected to decline with the introduction of hydrogen in place of silicon.

The similarities of these physical properties deserve attention because they offer important clues to structural relationships. The ability to gelatinize with HCl is a property typical of tectosilicates in which Al substitutes for Si and Al:Si>2:3 (Murata, 1943). Evidently the phosphate ions do not significantly decrease the ability to gelatinize and there is no theoretical reason why they should, except insofar as they would affect the concentration relations.

Structural Data

Powder diffraction patterns of viséite were obtained in precision cameras with a diameter of 114.6 mm. using CuK_α and FeK_α radiation. The patterns were not as sharp and clear as might have been desired but, nevertheless, it soon became apparent that many of the diffraction lines of viséite were similar in both intensity and spacing to those of analcime (Table 2).

Because of the existence of abundant experimental data on analcime (Gruner, 1928; Taylor, 1930; Hartwig, 1931), the interpretation of the pattern of viséite was a simple matter, once these similarities had been discovered. Several important conclusions are permissible from these data:

(*a*) The structure of viséite is probably essentially similar to the open framework of linked AlO_4 and SiO_4 tetrahedra which constitutes analcime according to Taylor (1930) and later workers.

(*b*) The oxygen framework of viséite probably contains 96 oxygens (exclusive of water) and the unit cell probably contains 16 water molecules.

(*c*) Inasmuch as the silica content is completely inadequate to build such a framework with the alumina content, PO_4 and H_xO_4 tetrahedra

TABLE 2. COMPARISON OF POWDER DIFFRACTION DATA FOR ANALCIME AND VISÉITE (Cu K_α RADIATION, $r = 57.3$ mm.)

No.	Indices	Analcime		Viséite		
		d	I	I	d	a_0
1	211	5.57	9	4	5.68	13.91
2	220	4.87	4	1	4.98	14.08
3	321	3.66	2			
4	400	3.42	10	5	3.46	13.84
5	332	2.915	7	10	2.92	13.70
6	422	2.800	2			
7	510, 431	2.690	3			
8	521	2.505	3			
9	440	2.430	2			
10	611, 532	2.222	3	2	2.20	13.56
11	620	2.171	1			
12	541	2.122	1	<1	2.11	13.67
13	631	2.023	1	<1	2.014	13.66
14	640	1.903	4	3	1.886	13.60
15	721, 633, 552	1.870	3			
16	732, 651	1.746	5	6	1.740	13.70
17	800	1.719	2			
18	811, 741, 554	1.692	3			
19	820, 644	1.668	1			
20	822, 660	1.622	1			
21	831, 750, 743	1.598	3			
22	842	1.501	2			
23	921, 761, 655	1.482	2			
24	664	1.465	1	Diffuse		
25	930, 851, 754	1.449	1	band		
26	932, 736	1.417	3			
27	941, 853, 770	1.389	<1	1	1.380	13.66
28	10.00, 860	1.376	1			
29	10.11, 772	1.361	4			
30	950, 943	—	—	1	1.323	13.62
31	10.31, 952, 765	1.307	2			
32	871, 855, 774	1.287	3	1	1.282	13.69
33	10.33, 961	1.264	2			
34*	11.30, 970	—	—	2	1.196	13.64
35*	10.62	—	—	2	1.155	13.67
36*	12.00, 884	—	—	1	1.138	13.66
37*	12.40, 10.64	—	—	1	1.105	13.62

* For lines with $2\theta > 75°$ similarities between the patterns of viséite and analcime apparently do not exist, and lines for analcime with $d < 1.264$ consequently are not tabulated here.

must occur in this framework with essentially the same linkages as the AlO_4 and SiO_4 tetrahedra.

If these premises are acceptable, it becomes possible to reconstruct the atomic constituents of the unit cell from a knowledge of the analysis, as follows:

96 O	20 Al	10 Ca	2 Na	6 Si	10 P	36 H	16 H_2O
1536	540	400	46	168	310	36	288/3324

A further test of these premises can be applied. If 13.65 Å is taken as the edge of the unit cube, then

$$\rho = \frac{1.66 \times 3324}{(13.65)^3} = 2.17$$

and this calculated density shows good agreement with the specific gravity determination of 2.2, which Mélon made with a pycnometer.

The structure of viséite is highly defective, as indicated by the broad diffuse nature of the low-order diffraction lines as well as the disappearance of many of the low intensity reflections. Therefore, although there are marked similarities between the structures of viséite and analcime, one can not conclude that viséite is truly cubic. However, it seems reasonable to conclude that the framework structure of tetrahedral groups obtains in both instances, and the disorder of viséite arises largely from non-systematic substitution of phosphorus and hydrogen for silicon, as well as vacancies in the sodium positions.

In all of the above considerations the structure of analcime has been assumed to be in accord with the proposal of Taylor (1930) rather than the proposal of Náray-Szabó (1938*a*). Taylor (1938) has presented certain objections to the structure described by Náray-Szabó (1938*a*), which seem to be valid. Admitting that such a highly defective structure as viséite cannot furnish critical evidence concerning the relative merits of these structures for analcime, nevertheless, it is interesting to assume the structure of Náray-Szabó in order to make certain comparisons, as follows:

	Structure of Taylor	*Structure of Naray-Szabo*
Theoretical Na positions (analcime)	24	16
Number occupied in viséite	12	12
Number occupied in analcime	16	16
Number of H_2O positions (analcime)	16	24
Number of H_2O positions (viséite)	16	24
Calculated density (viséite)	2.17	2.26
Weight per cent of H_2O (viséite)	18.41	21.80

Although the experimental data for viséite, show better agreement with

the water content of 24 molecules, the agreement is still far from satisfactory.

Still another possible structure for viséite can be obtained by assuming that half of Taylor's 24 positions for large cations are occupied by Ca and Na while the other half are occupied by water molecules. Under these circumstances the calculated density becomes 2.31 and the calculated water content 23.39 per cent, the oxide ratios then being: Na_2O, $10CaO$, $10Al_2O_3$, $6SiO_2$, $5P_2O_5$ and $46H_2O$. Still another possibility would be the placement of water molecules in the vacant positions for large cations in the structure of Náray-Szabó, in which case the number of water molecules would be the same, i.e. 46. The analytical data will not permit selection of one probable structure amongst the several possibilities.

Previous studies of structures related to nesosilicates and nesophosphates have indicated the existence of separated H_4O_4 groups. The present calculations are consistent with the postulate of adjacent H_3O_4 groups in which the tetrahedrally arranged oxygen atoms are shared between neighboring similar groups, thus giving an over-all composition for this part of the structure of $(H_3O_2)^-$. Because of uncertainty arising from the non-critical nature of the analytical data for viséite, it seems best to regard these tetrahedral groups merely as H_xO_4 and thus avoid a premature conclusion concerning the number of hydrogens associated with 4 oxygens. Certainly the geometrical concept of H_4O_4 is not as disturbing as H_3O_4, unless it is assumed that the tetrahedra are significantly distorted.

Summary

Viséite has a highly defective structure which is essentially pseudocubic. The chemical, physical, optical, and x-ray diffraction data indicate analogies between the structures of analcime and viséite. Inasmuch as the Si, P and Al contents of viséite are completely inadequate to build a structural framework similar to that of analcime, oxygen tetrahedra containing hydrogen ions are called upon to complete the framework. The tetrahedral group, H_xO_4, is tetrahedrally linked and x appears to be 3, giving rise to $(H_3O_2)^-$. The structural formula suggested for the average unit cell of viséite is: $(Na_2Ca_{10})[(AlO_2)_{20}(SiO_2)_6(PO_2)_{10}(H_3O_2)_{12}] \cdot 16H_2O$. Half of Taylor's 24 positions for sodium appear to be vacant in viséite. The edge of the unit cell is 13.65 Å which permits calculation of the density as 2.17. By pycnometer measurement Mélon obtained 2.2.

References

Barrer, R. M., and Ibbitson, D. A. (1944), Occlusion of hydrocarbons by chabazite and analcime: *Trans. Faraday Soc.*, **40**, 195–206.

Flint, E. P., McMurdie, H. F., and Wells, L. S. (1941), Hydrothermal and x-ray

studies of the garnet-hydrogarnet series and the relationship of the series to hydration products of portland cement: *Nat. Bur. Standards, Jour. Research,* **26,** 13–33.

GRUNER, J. W. (1928), Die Struktur des Analcims. I. Die Raumgruppe: *Zeits. Krist.,* **68,** 363–378.

HARTWIG, W. (1931), Strukturbestimmung des Analcims: *Zeits. Krist.,* **78,** 173–207.

HUTTON, C. O. (1943), Hydrogrossular, a new mineral of the garnet-hydrogarnet series: *Trans. Royal Soc. New Zealand,* **73,** 174–183.

KELLEY, W. P., JENNY, H., and BROWN, S. M. (1936), Hydration of minerals and soil colloids in relation to crystal structure: *Soil Sci.,* **41,** 259–274.

MCCONNELL, DUNCAN (1942), Griphite, a hydrophosphate garnetoid: *Am. Mineral.,* **27,** 452–461.

——— (1950), The crystal chemistry of montmorillonite: *Am. Mineral.,* **35,** 166–172.

MÉLON, J. (1942), La Viséite, nouvelle espèce minérale: *Ann. Soc. Géol. Belg.,* **66,** *B*53–*B*56.

MILLIGAN, W. O., AND WEISER, H. B. (1937), The mechanism of the dehydration of zeolites: *Jour. Phys. Chem.,* **41,** 1029–1040.

MURATA, K. J. (1943), Internal structure of silicate minerals that gelatinize with acid: *Am. Mineral.,* **28,** 545–562. (Also: *U. S. Geol. Survey, Bull.,* **950,** 25–33 (1946).

NÁRAY-SZABÓ, ST. v. (1938*a*), Die Struktur des Pollucits Cs $AlSi_2O_6 \cdot xH_2O$: *Zeits. Krist.,* **99,** 277–282.

——— (1938*b*), Note on the structure of analcime: *Zeits. Krist.* **99,** 291.

PABST, ADOLF (1937), The crystal structure of plazolite: *Am. Mineral.,* **22,** 861–868.

STRUNZ, H. (1936), Die chemische Zusammensetzung von Pollucit: *Zeits. Krist.,* **95,** 1–8.

TAYLOR, W. H. (1930), The structure of analcime ($NaAlSi_2O_6 \cdot H_2O$): *Zeits. Krist.,* **74,** 1–19.

——— (1938), Note on the structures of analcime and pollucite: *Zeits. Krist.,* **99,** 283–290.

Manuscript received Oct. 20, 1951

HISINGERITE FROM JAPAN

Toshio Sudô and Takeshi Nakamura, *Geological Institute, Faculty of Science, Tôkyô University.*

Abstract

The mineralogical properties of hisingerite from the Kawayama Mine, Yamaguchi Prefecture, Japan, are described and discussed. The specimen is dark brown in color, massive, and intimately associated with the ore body—a bedded deposit in graphite-sericite-quartz schist. Under the microscope, it is apparently isotropic but shows tension polarization. The chemical analysis shows it to be a more highly hydrated variety than specimens previously reported in the literature. The differential thermal analysis curve resembles allophane, that is, a very strong endothermic peak between 100° and 200° C. and a weak exothermic peak between 900° and 1000° C. The *x*-ray powder pattern shows three broad bands which agree with some of the strong lines of nontronite, however, a line of 12~15 Å was not detected. The occurrence indicates that hisingerite is an alteration product derived from pyrrhotite and other iron minerals that were attacked by hot spring water of hypogene origin.

Hisingerite is found associated with certain metallic ore deposits of Japan, for example, with tin, copper and pyrrhotite deposits. One of the typical examples is at the Kawayama Mine, Yamaguchi Prefecture. The mineralogical properties of the hisingerite are recorded here and discussed.

The ore deposit of the Kawayama Mine is a bedded deposit formed along the thrust zones in graphite-sericite-quartz schist and is partly a replacement deposit in limestone. The ore is largely composed of pyrrhotite, chalcopyrite, sphalerite, pyrite, and marcasite with small amounts of cubanite, arsenopyrite, and galena. The gangue minerals are hedenbergite, actinolite, garnet, calcite, and quartz. The mineralization took place in four stages: (1) pyrrhotite, sphalerite (marmatite), cubanite, and chalcopyrite, (2) pyrrhotite, (3) chalcopyrite, (4) pyrite. A fault movement was recognized between stages (3) and (4). The deposits are pyrometasomatic.

Hisingerite is found in the ore body and in the surrounding country rock. In the ore body, it is intimately associated with pyrrhotite, chalcopyrite, and pyrite and is found as small patches included in the ore, or as a filling in small fissures or fault zones in the ore body, and also in the country rock near the ore body. There is no relationship between the amount of hisingerite and the depth from the present earth surface, that is there are no indications that most of the hisingerite is the result of a weathering process.

Hisingerite is commonly dark brown in color when massive with a somewhat vitreous luster. Also dark green masses were observed which may turn brown in daylight.

Under the microscope hisingerite is commonly brown or golden-yellow in color and isotropic. Some portions of the hisingerite show polarization tints, the isotropic areas show a mottled appearance and a gradation can be seen between an isotropic and an anisotropic area. However, as shown in the differential thermal analysis curves mentioned below, no differences were recognized between the curves of the isotropic and the anisotropic grains. From this it is inferred that the birefringence is due to "tension polarization" commonly recognized in gel materials.

The chemical analysis of the hisingerite which was concentrated and carefully selected for purity is shown in Table 1. It contained very small amounts (less than 1%) of pyrite and calcite. It is noteworthy that this analysis shows more adsorptive water than has been reported in other analyses (1) (2) (3).

Table 1. Chemical Analysis of Hisingerite

	(1)	(2)	(3)	(4)
SiO_2	27.99%	35.57%	38.14%	32.85%
Al_2O_3	none	0.38	—	2.64
Fe_2O_3	34.25	39.20	36.66	40.70
FeO	0.54	4.80	0.84	—
CaO	2.33	0.85	none	1.50
MgO	none	1.60	2.45	2.05
$H_2O(-)$	27.89(<110° C.)	6.00(<110° C.)	13.20	11.40(<110° C.)
Ig. Loss	7.11*	11.60(>110° C.)	8.53	7.90(>110° C.)
Total	100.11	100.12	99.82	100.04
SiO_2/Fe_2O_3	2.16	2.40	2.80	2.14

(1) Hisingerite from the Kawayama Mine.
(2) After G. M. Schwartz (3). TiO_2, 0.12%.
(3) After D. F. Hewett and W. T. Schaller. MnO tr.; P_2O_5, SO_4, and CO_2 absent.
(4) After A. C. Hawkins and E. V. Shannon (1): (canbyite) MnO 0.74%, TiO_2, 0.26%.
* Ignition loss above 110° C.

The x-ray powder pattern of the specimen analyzed chemically shows three broad bands between 1 Å and 15 Å, as shown in Table 2. The powder lines of pyrite and calcite are not present because of their small amounts. The diffuseness of each band is symmetrical with no indications of two dimensional imperfection. Although it is very difficult to evaluate the powder pattern because of the presence of only three broad bands, reference to the summarized data of the x-ray powder patterns of clay minerals prepared in the writer's laboratory shows that the three bands are in approximate correspondence to a few strong lines of nontronite.

TABLE 2. *X*-RAY POWDER DIFFRACTION DATA FOR HISINGERITE

I	*d*
ss	4.4_4 Å
ss	2.6_1
ss	1.5_0

Three broad bands of the hisingerite from the Kawayama Mine.

The spacing (*d*) is calculated from the measurement of the middle part of each broad band. The radius of the camera used is 56.8 mm. Filtered Cr radiation.

However, it is noteworthy that the strong line of nontronite occurring at 12∼15 Å is not present. This is one of the important lines of nontronite.

The differential thermal analysis curve of the specimen analyzed chemically is shown in Fig. 1. The curve shows a strong sharp endothermic reaction at 134° C. and a weak exothermic peak at 907° C., with a trace of an exothermic peak at 463° C.∼483° C. caused by pyrite. The endothermic reaction of calcite was not observed because it is eliminated by the exothermic reaction of hisingerite. The type of the curve is quite similar to that of allophane, heated at the same rate, although the exothermic peak is shifted slightly downward from that of allophane (commonly at 957° C.). The differential thermal curves are the same for both the isotropic grains and the anisotropic flakes.

Thus the mineralogical properties of hisingerite show that it is largely a gel mineral like allophane and contains submicroscopic nuclei of a

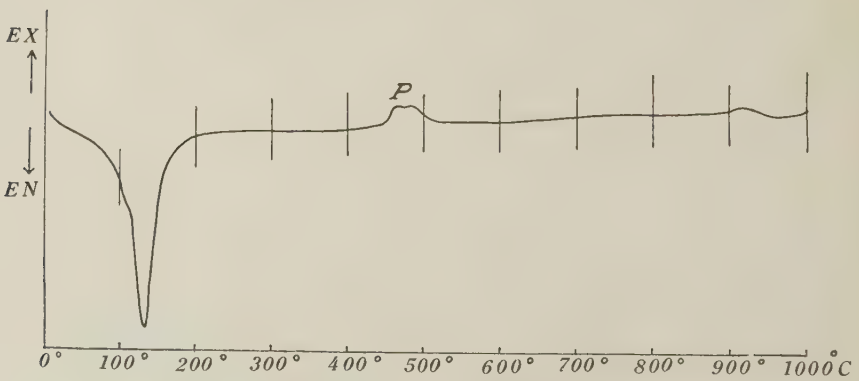

FIG. 1. Differential thermal analysis curve of hisingerite from the Kawayama Mine, Yamaguchi Prefecture, Japan. A mixture of 25 per cent hisingerite and 75 per cent of alumina was used. Pure hisingerite produced such a violent reaction during its dissociation that the cover of the sample holder was blown off. The specimen is composed chiefly of apparently isotropic grains. The rate of heating is 10° C. per minute. P=pyrite.

crystalline phase which shows three broad x-ray bands. It is difficult to identify the crystalline phase, however, the ratio of silica to ferric oxide near 2, as shown in the chemical analysis, strongly suggests that hisingerite may crystallize to a phase with the ideal chemical formula of $2SiO_2 \cdot Fe_2O_3 \cdot nH_2O$. This has already been reported as canbyite by A. C. Hawkins and E. V. Shannon (1).

The occurrence of hisingerite shows that it is not the result of weathering but is clearly an alteration product from pyrrhotite and other iron minerals which were attacked by hot spring waters of hypogene origin.

In Japan, hisingerite is also found in other metallic ore deposits, for example, the epithermal copper-quartz vein of the Sano Mine, Wakayama Prefecture and the tin deposit of the Suzuyama Mine, Kagoshima Prefecture. The mineralogical properties of the hisingerite from the Sano Mine agree well with the Kawayama material.

The writers are greatly indebted to Dr. G. T. Faust, U. S. Geological Survey for valuable criticism, to Professor Takeo Watanabe, Tokyo University, for guidance to the ore deposit, and also to Mr. S. Iwai, Tokyo Institute of Technology, for help in taking the x-ray powder photographs.

References

(1) Hawkins, A. C., and Shannon, E. V.: *Am. Mineral.*, **9**, 1 (1924).
(2) Hewett, D. E., and Schaller, W. T.: *Am. Jour. Sci.*, Fifth Series, **10**, 29 (1925).
(3) Schwartz, G. M.: *Am. Mineral.*, **9**, 141 (1924).

Manuscript received July 12, 1951

STRUCTURAL IMPERFECTIONS IN QUARTZ CRYSTALS

W. L. Bond and J. Andrus, *Bell Telephone Laboratories, Murray Hill, New Jersey.*

Abstract

A method for examining the topography of atomic planes is developed and applied to quartz crystals. It is thought to have higher resolution than the method of Wooster and Wooster (*Nature*, **155**, 786 (1945)), or that of Ramachandran (*Proc. Ind. Acad. Sci.*, **19A**, 280 (1944)). Because of the higher resolution it gives more detailed information. A fair percentage of ostensibly perfect quartz is shown to have slight irregularities.

Quartz crystals that seem to be perfect by the ordinary tests such as etching and single crystal x-ray double reflection, can be shown to be imperfect by x-ray double reflection. The apparatus for examining crystals in this way is shown in Fig. 1. X-rays from the target T are reflected at the Bragg angle from the reference crystal R onto the work crystal W.

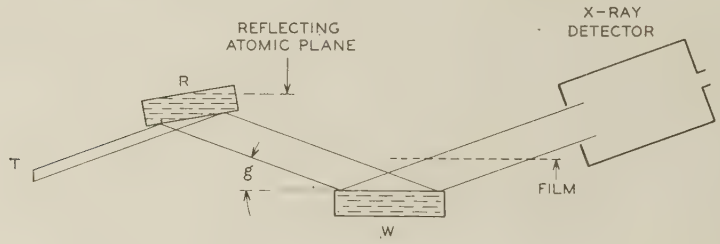

Fig. 1

If the reflecting planes of W are parallel to those of R and the Bragg angles are the same, the rays can also reflect from W into the x-ray detector or can be intercepted by a photographic film to give a picture of the reflecting area of W. If the reflecting planes of the two crystals are not parallel, no ray can be reflected from both crystals. With nearly perfect crystals, if the planes are a few seconds out of parallel the energy received by the x-ray detector (ionization chamber or Geiger counter) is noticeably below maximum as shown by the rocking curve, Fig. 2 where the intensity of reflection is plotted against the grazing angle g.

As shown in Fig. 1 the reflecting surface of crystal R is cut several degrees from the atomic plane in order to expand the beam width. This enables larger W crystals to be examined. The reflecting face of R is optically polished, otherwise shadows of grinding pits show on the film. A number of quartz crystals were cut and polished $6\frac{1}{2}$ degrees from an $(01\cdot1)$ plane and slightly etched. The one showing the cleanest reflection

was chosen as R. A slight etch after polishing narrows the width of the rocking curve. Rough ground crystals may have a peak width at half max. of 3 minutes. Polished and etched crystals may have a width of less than 10 seconds.

The film is placed as close to W as possible because the copper radiation used has two wave lengths $K\alpha_1$ and $K\alpha_2$ both of which reflect but at slightly different angles. Hence two overlapping pictures are given, but if the film is close to W the offset can be kept to a few thousandths of an inch. The (d) spacing of quartz for the (01·1) plane is 3.3432 Å at 26° C.

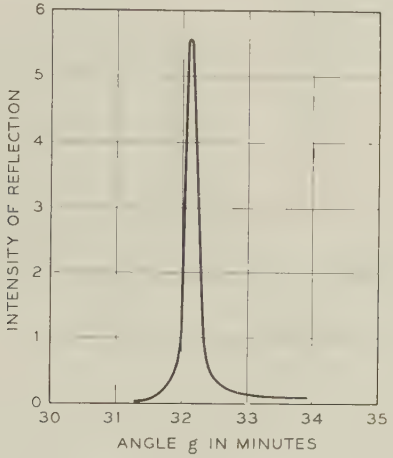

FIG. 2

$K\alpha_1$ (which is twice as strong as $K\alpha_2$) has a wave length 1.54050 Å. Hence, from Bragg's law: $\lambda = 2d \sin \theta$ we see that the θ's for α_1 and α_2 differ by 2.03 minutes.

If a minor part of crystal W is slightly misoriented, this part will not reflect most strongly at the same angle setting as does the major part of the crystal. If W is rotated to make the minor part reflect most strongly, then the major part reflects less strongly. The photographic film will show in each case from where the strong reflection came. Figure 3 illustrates such a case. The two pictures are of a natural (01·$\bar{1}$) face of a small quartz crystal found in Herkimer County, New York —a so called Herkimer County Diamond. The crystal was turned through 50 seconds between pictures a and b. The rocking curve indicates where interesting features may be found. Picture a was made with the crystal set at the peak as indicated by the letter (a) over the taller peak of the rocking curve. Picture b was made at the crystal setting indicated by the letter

b on the lower peak of the rocking curve. The bright area of picture *a* shows that about a third of the face was reflecting at this setting. Picture *b* shows that the larger part of this face is about 50 seconds in orientation away from the smaller part, but is curved so that only a small part reflects at any one setting. The sketch above the rocking curve shows the direction in which the *x*-rays approach and leave the crystal. This is important because the resolving power is highest if the plane containing the incident beam direction and the reflected beam direction is perpendicular to the line in which the atomic planes of the two crystal parts intersect. For this reason in investigating a surface, rocking curves are made for

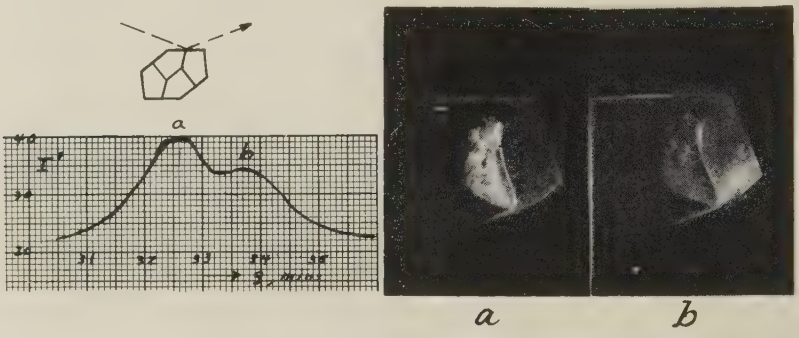

FIG. 3

two directions at 90° to each other. The poorer reflection is then investigated photographically.

The intensity axis of the rocking curve, Fig. 3, is marked I'. In this figure and subsequent ones meter readings are plotted and $I=0$ corresponds to a reading of 20. The meter is non-linear so that if Fig. 3 were corrected for this, as was done in Fig. 2, the peaks would appear somewhat sharper.

Figure 4 shows a crystal from Hot Springs, Arkansas. The crystal was cut in two in a plane parallel to $(01\cdot\bar{1})$. It is seen that the crystal is quite imperfect. The fine parallel lines along two nearly perpendicular edges are probably "growth lines." Picture *b* shows that below the major part is a smaller region turned about 50 seconds from the major part about a vertical axis. The small peak at the left of the rocking curve was photographed but not included here. It is due to a very small area of the face below *b* and also reflection from the prism face which does not lie in the plane of the cut face. Since the largest part of this reflection is from an area not parallel to the photographic plate it appears as a long streak going to the right of the film. The pictures are without distortion only when the film is parallel to the reflecting face.

Figure 5 shows six pictures from a plate made by the W. E. Co. at Kearny to be used as a reference crystal *R*. Although it is unsuitable for a reference crystal it should make a perfectly good oscillator plate. The diagonal stripes are parallel to a rhombohedral edge, the vertical stripes are parallel to an *a* axis. The six pictures were made to determine

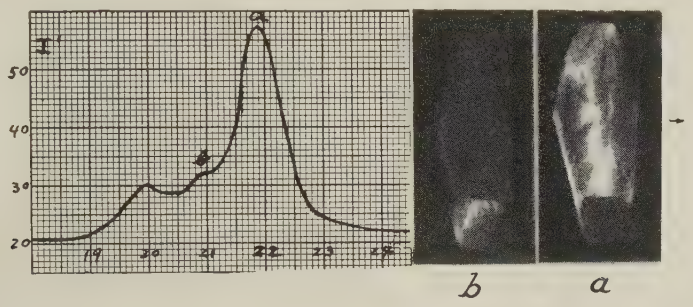

Fig. 4

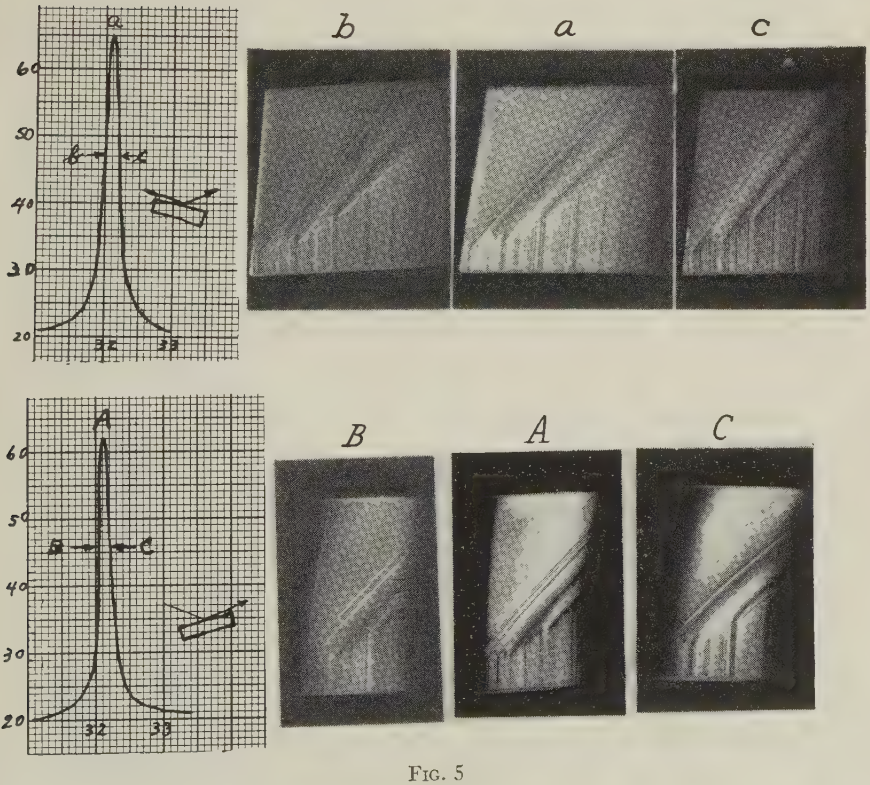

Fig. 5

whether the stripes were due to different orientations, or could possibly be interpreted as showing regions of different atomic spacing d (which would necessitate different θ's). If a plate has a small part in which the d constant is slightly larger than that of the major part but whose atomic planes are parallel to those of the major part, the best reflection for the minor part occurs at a slightly smaller angle regardless of direction of x-ray beam. Hence turning the plate 180° in its plane does not reverse the positions of the reflection, that is, the minor part always appears at a lower angle than does the major. On the other hand, if the minor part has the same d constant but its atomic planes are not quite parallel to those of the major part, turning the plate 180° does reverse the order of occurrence of reflection. By choosing a point on the crystal that can be identified, for instance the tip of an inverted V that terminates a group of lines one can study the relative intensities of adjacent lines throughout the six pictures. Two lines thus checked showed that the line order does reverse on reversing the crystal. Hence it is concluded that it is primarily an orientation difference (of about 5 seconds), not a d spacing difference. If impurities can change the d spacing by, say, one part in 10^6, then roughly every half millimeter the fit of the old material on the new is out by one cell. We may be able to find here a mechanism whereby a slight d spacing difference caused by changing impurity content can, by an accumulative effect, cause regions to be misoriented by amounts such as are observed even if the d spacing difference is too small to detect by this method.

The narrowness of the pictures of the second series, Fig. 5, is caused by the plate in this reversed position being more nearly perpendicular to the x-ray beam, hence the beam covers less of the crystal width. The curved edges of the pictures A, B, C show the conical nature of a reflection. The locus of all lines from a point (on the x-ray target) making a constant angle θ with a plane is a cone. The slight curvature of some of the diagonal lines is caused by the film not lying perfectly flat. With the x-ray beam coming onto the film at only 13°20′ a slight curvature of the film gives an exaggerated curve to what would otherwise be a straight line.

The large quartz piece Fig. 6A was seen to be clear to the left of the line 1-1 but smoky to the right. This boundary proved to be (10·1) plane. The piece was sawed on the lines 1-1 and 2-2, the piece between these lines proved to be also part clear and part smoky with a (11·1) plane boundary as shown in Fig. 6B. The surface 2-2 of this piece was investigated. A pair of light scratches were made on the surface to mark the ends of the clear-smoky boundary (see arrows, Fig. 6b). At maximum reflection, picture a shows only the edges of the piece are reflecting. If we turn to smaller angles, picture b shows that we have poorer reflections

everywhere. Going to larger grazing angles, picture *c* shows two zones of reflection separated by a narrow dark band. Picture *d*, which is 24 seconds away from picture *a*, has only a narrow band of reflection. This indicates that the atomic layers at the surface are warped into an (*s*) curve, Fig. 6*E*. With the atomic planes warped in this way regions such as *m* and *n* have the same orientation and give a picture such as Fig. 6*c*. A maximum slope occurs at *p*, which gives Fig. 6*d*. If we turn the crystal further we get no picture.

If the unit cell of smoky quartz is larger than the nuit cell of clear

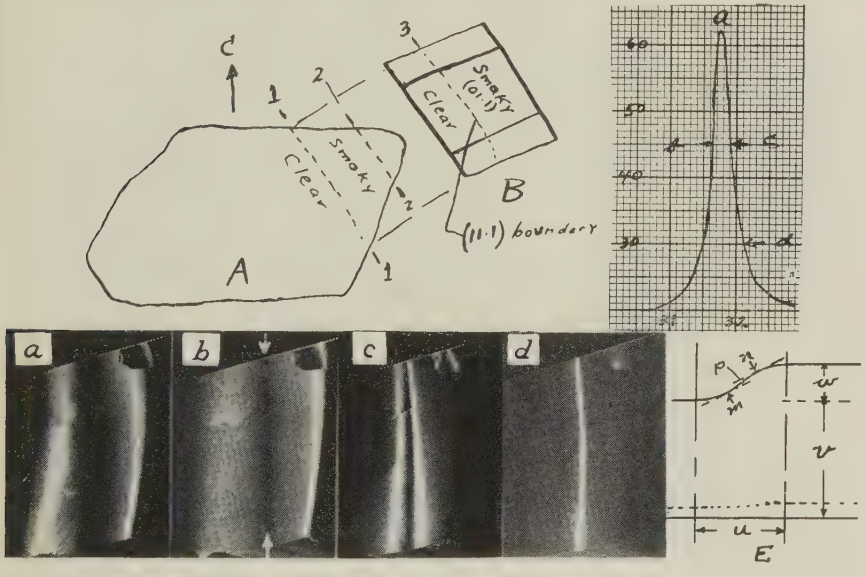

Fig. 6

quartz and the atomic layers are continuous (i.e. no dislocations), the layers would warp to such a continuous curve. In laying on a thickness *v* (Fig. 6*E*) the accumulated difference is *w*. If we assume the transition is a sine curve of length *u* height *w* and with a maximum slope of 24 seconds it is easily shown that $(\pi w\sqrt{2}/4u) \doteq 116\times10^{-6}$. On picture *a*, *u* was found to be about 1.5 cms.

Whence $$w \doteq 70 \times 10^{-6}$$

If the difference *w* is accumulated in a thickness 0.9 cm. (the thickness of the plate, since the lower face borders on clear material) then the cell dimensions of clear and smoky quartz would differ by one part in *v*/*w* or 1 part in 13,000 which seems not unreasonable. H. D. Keith (*Proc. Phys.*

Soc., **B63,** 208) says "Quartz parameters vary from sample to sample by amounts as large as .01% according to impurity content."

The "smoke" was cleared by heating the specimen to 300° C. Pictures taken after cooling were the same as before.

Figure 7 is a study of vicinal faces on a quartz crystal found at "Crystal Hill," Pennsylvania (near Stroudsburg). The obvious vertical line in the pictures divides the face into two nearly equal areas. These areas

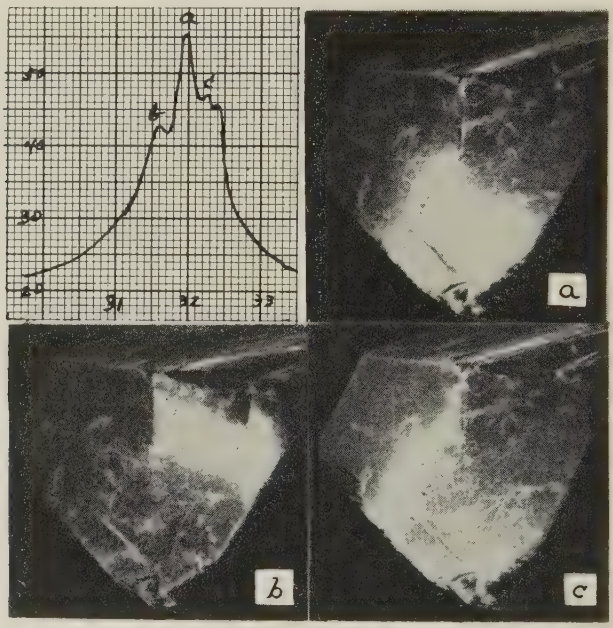

FIG. 7

form a low "roof" of angle eleven minutes as determined by optical reflection (two very sharp images are seen in the optical goniometer). The x-ray rocking curve shows a quadruple peak with a total spread of less than a minute—and no other reflections within 30 minutes to either side. The eleven minute roof angle does not appear in the x-ray data. Hence we conclude that the apparent faces are ones of very high indices, not two crystals joined at eleven minutes. A hint of the cause of vicinal faces is given by this crystal and a few others examined. A thin sheet of flawed material comes up from the base of the crystal and points directly at the ridge of the roof. This probably puts the material in a state of stress, the stress reversing sense at the end of the flawed sheet. If the speed of growth is altered by stress this might cause the growing face to have

indices $h+\Delta_1$, $k+\Delta_2$, $l+\Delta_3$ on one side of the flawed region and $h-\Delta_1$, $k-\Delta_2$, $l-\Delta_3$ on the other side—the Δ's being very much smaller than unity.

The pictures, Fig. 7, show many scratches. The crystal (from the private collection of Mr. George Shoemaker of Summit, New Jersey) was in a box with many other quartz crystals. They probably scratched one another slightly but it is not apparent to the naked eye. Experiments with ammonium dihydrogen phosphate show that when a metal point is pressed against a polished face there is a misoriented region much larger than the obviously damaged region. Probably minute fissures are

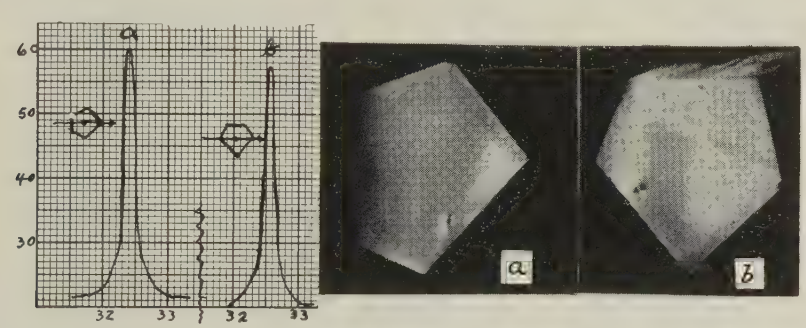

FIG. 8

made, and broken off material is forced into these, wedging them open thus causing strain over an extended area. This is possibly the main mechanism of disorientation of ground surfaces of non-plastic crystals. The material actually broken off and trapped in the fissures is of very small amount and is probably misoriented to a much greater extent. If it were randomly oriented the probability that any one particle would have a plane (01·1) within a minute of the reflecting position is one chance in four million. Hence it seems probable that the slight misorientations are in the still attached material put under strain by the impacted material.

Figure 8 shows the best face of a Bell Laboratories synthetic quartz crystal. The crystal, which is 32 millimeters long is shown in Fig. 9*c*, the face pictured in Fig. 8 being the lower right major rhombohedral face of Fig. 9*c*. There is a low pimple shaped mound near an edge of this face. There is local strain around this pimple but the rest of the face is nearly perfect.

Figures 9*a* and *b* show the upper rhombohedral face of Fig. 9*c*. This face is far from perfect. There is a central mound much more prominent than the mound of Fig. 8, no inclusions can be seen under either mound

at 360 magnification. Fifty minutes away from the main peak is a secondary peak that is due to ring shaped regions, picture 9*b*. It would be interesting to put this crystal back in the bomb and grow more quartz onto it to see if the face would become more perfect.

Figure 10 shows several views of a slice of a synthetic quartz crystal grown at the Bell Laboratories. A seed plate about $\frac{1}{8}$ inch thick and $1\frac{1}{2}$ inches square parallel to $(01\cdot1)$, was grown to about $\frac{3}{8}$ inches thick. A slice was cut out of the center and since it was too long to cover in one picture it was sawed in two. In cutting the slice the cuts were made along

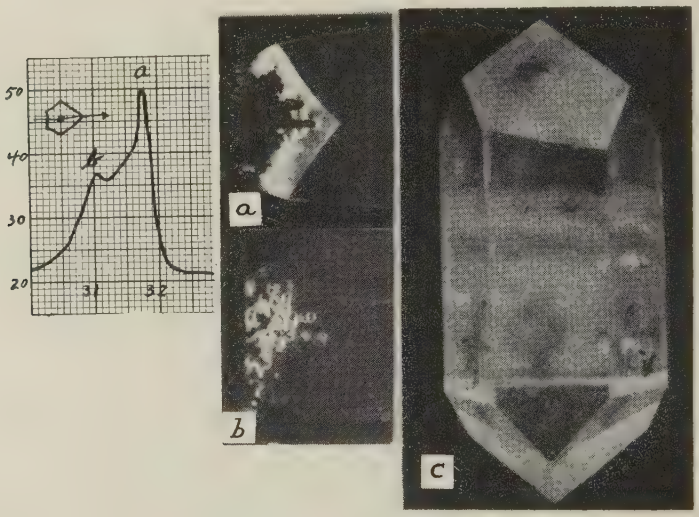

FIG. 9

$r(0\bar{1}\cdot1)$ planes which are 76°26′ from $z(01\cdot1)$, giving a surface nearly perpendicular to the growing face (see Fig. 10*a*) so the process of growth could be studied. The original seed was Brazilian quartz and shows diagonal stripes which are growth lines on prism faces. The new material shows stripes over the large face edges, growth on $(01\cdot1)$ faces. The joint between the old and new quartz shows a fair amount of misorientation. Under the microscope, one sees many fine radial crystal aggregates in the new material near the boundary with the old material. The aggregates are about 10 microns in diameter. They are much more numerous on one side of the seed than on the other. The side with the greatest number was probably uppermost during growth. They may be recrystallized material from the bomb wall. If, as is likely, the upper side of the seed was least dissolved back at the beginning of the growth run, it may

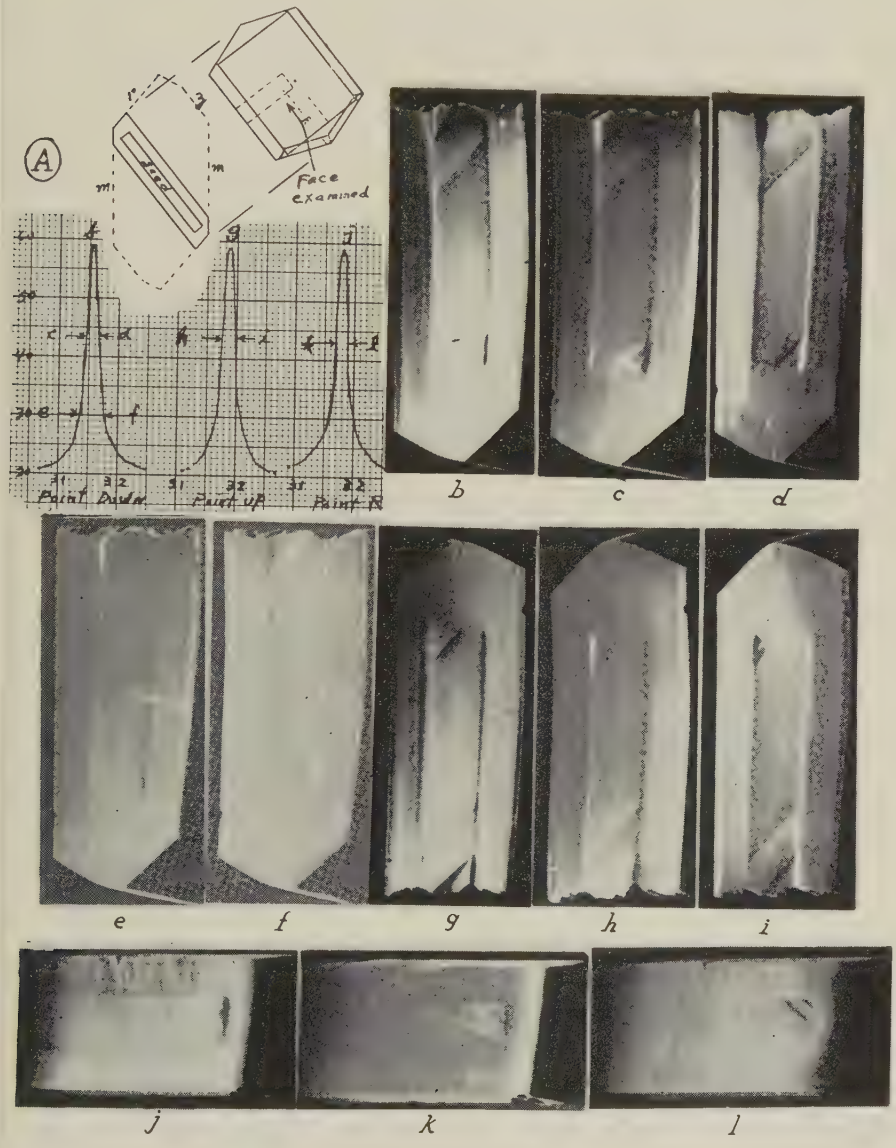

FIG. 10

have kept a region strained from grinding. This region could cause a pimple.

In the *old* material near the boundary there were three small voids, about 20μ in diameter, 60μ long, perhaps 40μ apart and parallel to each

other. Exactly opposite, near the other boundary were three more quite similar, also in the old material. Each was full of liquid except for a gas bubble. Probably there were three submicroscopic holes through the seed or three submicroscopic rutile needles. These etched out a short distance at the beginning of the growth run, then sealed over. No line connecting each with its opposite could be seen at 100 magnification of the microscope. Pictures, *j*, *k*, *l* taken with the *x*-ray beam traveling along the length of the slice shows a slight rumpling in the new material above the seed. Better "joins" of old to new material are now being made, at least better by the criterion of joint visibility but these newer crystals have not been tested by this *x*-ray test.

H. D. Keith (*op. cit.*) finds that the cell size of synthetic quartz varies with the temperature at which it was grown. Crystals grown at 390° C. have smaller cells than crystals grown at 280° C., smaller by 1 part in 10,000 along the (*a*) axes, by 1 part in 17,000 along the (*c*) axis. This is probably due to the effect of temperature on impurity content. The growth lines could be due to such a temperature effect.

Five *AT* quartz blanks were examined. One was found to have a *V* shaped twinned portion. This twinned portion showed perfect alinement with the rest of the plate. There was no strain at the boundary. Since $(0\bar{1}\cdot 0)$ reflects more strongly than $(01\cdot 1)$ this part merely reflected more strongly than the rest of the plate at all orientations near the peak. One of the five blanks showed stripes like those of Fig. 5 across a corner of the plate.

Manuscript received Oct. 24, 1951

OCCURRENCE OF METASOMATIC HYPERSTHENE, AND ITS PETROGENETIC SIGNIFICANCE

Allan F. Wilson, *University of Western Australia, Nedlands, Western Australia.*

Abstract

Hystersthene pseudomorphs augite where a dolerite is cut by an alumina-rich granitic rheomorphic vein. The control of alumina in the formation of hypersthene is not confined to basic melts, but is also effective in the solid state.

Introduction

A zone of intense metamorphism extends for six feet on both sides of an olivine dolerite dyke (nearly vertical and fifteen feet thick). The emplacement of the dolerites is the last manifestation of igneous activity which affected an Archaean complex in the Kulgera Hills about 160 miles S.S.W. of Alice Springs in Central Australia.

Granitic rocks have been converted in situ to rocks resembling quartz porphyries, and a case of mobilization of cordierite gneiss was found. A description of these unusual contact effects is given elsewhere (Wilson 1952). Metasomatic hypersthene occurs pseudomorphing augite where the rheomorphic vein (the result of mobilization on the metamorphism of the cordierite gneiss) cuts the dolerite. The dolerite is normally devoid of hypersthene.

Petrography

The rheomorphic vein

No. 30104* is representative of the vein resulting from the mobilization of granitic cordierite-bearing gneisses which comprise the bulk of the oldest rocks of the Kulgera Hills.

The dark gray vein is straight, several yards long and nearly one inch thick. It has clean walls, and transgresses both the dolerite and the gneisses in which it appears to arise. Microxenoliths are roughly parallel to the walls of the vein.

The vein consists of a fine-grained groundmass of plagioclase, strongly zoned from andesine to albite, and potash feldspar-quartz microgranophyre, abundant flakes of pale green sericite, numerous granules of dull

* Catalogue number in the collection of University of Western Australia, but duplicates are housed in the University of Adelaide. Field work was in part financed by a Commonwealth Research Grant administered by the University of Adelaide, and this assistance is here acknowledged.

black iron ore, wisps of graphite, and ragged plates of biotite (X = colorless, Y = Z = khaki green). The average grain size of the groundmass minerals is 0.04 mm.

There are no true phenocrysts, but xenocrysts and microxenoliths of all sizes are so abundant that it is difficult to decide the nature and origin of many mineral clusters in the groundmass. The most conspicuous foreign bodies are large, very deeply embayed masses of quartz, many of which are 3 or 4 mm. long. Several microxenoliths were noted comprising large bundles of sillimanite needles (largest observed is 8 mm. × 2 mm.). A few strongly pinitized cordierite anhedra (some enclosing sillimanite needles) are present, and are in several places associated with irregular patches of dull black octahedra of magnetite (or some other ferriferous spinellid). Also observed were some irregular kaolinized xenocrysts of plagioclase. Occasional zircon and (?) monazite occur. Relict ophitic texture is readily seen in a "hydrated" xenolith of dolerite (2.5 mm. × 2 mm.). Pyroxene is pseudomorphed by yellowish-green serpentine which is studded with tiny octahedra of magnetite. Plagioclase is almost completely kaolinized and carbonated.

Contact Phenomena

The walls of the rheomorphic vein are well defined, and augite is pseudomorphed by hypersthene in a zone extending up to 0.4 mm. from both contacts (see Fig. 1).

Owing to the granular nature of the hypersthene its identity is not obvious. Indeed, it was suspected that the metasomatic masses may well be microintergrowths of clino- and ortho-pyroxene. Grains were removed from an uncovered slide, and it was found that the masses are monomineralic. Some of the properties of this mineral are: $\gamma = 1.698$ (approx.); $2V = (-)$ 70° to 75°; weakly pleochroic with X = very pale pinkish gray, Z = very pale greenish gray; good {110} cleavages (nearly at right angles), good {010} parting, and poor {100} parting; optic plane parallel to {010} with Z parallel to *c*. These properties indicate the mineral to be hypersthene (approx. 25 mol. % Of).

Within the contact zone plagioclase shows no alteration. But olivine (perfectly fresh elsewhere in the normal dolerite) is completely serpentinized near the vein, and it was the writer's first impression that the formation of the hypersthene and serpentine took place at the same time. More careful study, however, shows that in almost every case a tiny serpentinized crack can be found emanating, apparently, from the vein and traversing the normal olivine dolerite for a few mm., and serpentinizing any olivine with which it comes in contact.

Discussion

Although the serpentinization of the olivine may only indicate the activity of "late magmatic waters" from the rheomorphic vein, it seems strange that the "dry" mineral hypersthene should form under the influence of a magma (or crystal mush) in which the "wet" mineral biotite

Fig. 1. *Metasomatic hypersthene* at the junction of rheomorphic vein (right) and olivine dolerite (left).

The rheomorphic vein is made up of xenocrysts of quartz (white) and antiperthitic andesine (poorly cleaved mass with irregular patches of potash feldspar), and a xenolith of sillimanite needles set in a groundmass of plagioclase, potash feldspar-quartz microgranophyre, and ragged flakes of biotite (cleaved). The dolerite is made up of large ophitic flakes of augite and late pigeonite (cleaved and lightly stippled), and plagioclase (white). A little end-phase alkali feldspar, magnetite, and biotite is shown in the upper left portion of the field. Hypersthene (heavily stippled) replaces all clinopyroxene within about $\frac{1}{3}$ mm. from the contact.

was stable. Further, there seems to be no dearth of alkali in the vein, and under such conditions one could reasonably expect to find either an amphibole or biotite in the contact zone.

A remarkable feature is that the hypersthene is *metasomatic* (see Fig. 1). The formation of hypersthene in a basic *magma* which has assimilated

aluminous material is a well known process (Read (1935), Kuno (1950), etc.). In a crystallizing basic magma so much CaO is needed to combine with xenolithic Al_2O_3 to form anorthite that hypersthene (a calcium-free pyroxene) takes the place of the clinopyroxene, diopsidic augite. In the case of the metasomatic hypersthene here described, however, it seems that this process, known to take place in basic melts, can also take place in the solid state.

The formation of the hypersthene seems to have been conditioned by the high Al_2O_3 content of the vein (as shown by xenolithic sillimanite schist). CaO was taken from augite in the wall rocks and formed plagioclase with excess Al_2O_3, Na_2O, and SiO_2 in the vein. The CaO of the augite seems to have been replaced by FeO from the vein to form hypersthene. (Small quantities of FeO are to be expected in the vein in view of the tendency for conversion of Fe_2O_3 to FeO, and expulsion of some FeO during the metamorphism which culminated in the formation of the rheomorphic vein (Wilson, 1952).)

Petrogenetic applications of these phenomena are, doubtless, very limited, otherwise they would have been described before. However, one is tempted to speculate whether mobilization of certain lime-deficient pelitic sediments during intense metamorphism, and subsequent lit-par-lit injection into basic rocks, may be factors in the formation of certain diopside-hypersthene-biotite-bearing migmatites with charnockitic affinities. This may preclude the necessity felt by some to postulate an assimilation of alumina by basic magma to give hypersthene-diopside-bearing rocks prior to their injection by granitic liquors and formation of biotite at the expense of the pyroxenes.

Whether this be true, or not, there are at least three features which are clear, viz.,

(1) Hypersthene may form metasomatically.
(2) Although a "dry" mineral, hypersthene can form under "wet" conditions.
(3) Contamination of magma by alumina may give rise to hypersthene in either the magma, or the wall rocks.

References

Kuno, H. (1950), Petrology of Hakone Volcano and the adjacent areas, Japan: *Bull. Geol. Soc. Am.*, **LXI,** 957–1020.

Read, H. H. (1935), The gabbros and associated xenolithic complexes of the Haddo House district, Aberdeenshire: *Quart. Journ. Geol. Soc. London*, **XCI,** 591–638.

Wilson, A. F. (1952), Metamorphism of granitic rocks by olivine dolerite in Central Australia: *Geol. Mag.*, London, **LXXXIX,** 73–86.

Manuscript received Nov. 23, 1951

IONIC DIFFUSION AND ELECTRICAL CONDUCTIVITY IN QUARTZ

J. VERHOOGEN, *University of California, Berkeley, California.*

ABSTRACT

The diffusion coefficients of Li^+, Na^+, K^+ parallel to the *c*-axis of natural quartz crystals in the range 300–500° C. are given by the following expressions:

$$D_{Li} = 6.9 \times 10^{-3} \times e^{-20,500/RT} \text{ cm.}^2/\text{sec.}$$
$$D_{Na} = 3.6 \times 10^{-3} \times e^{-24,000/RT} \text{ cm.}^2/\text{sec.}$$
$$D_{K} = 0.18 \times e^{-31,700/RT} \text{ cm.}^2/\text{sec.}$$

In the same temperature range the diffusion coefficients of Mg^{++}, Ca^{++}, Fe^{++}, A^{+++} are considerably smaller, below the limit of experimental determination by the present method.

It is suggested that electrical conduction parallel to the *c*-axis of quartz results from motion of Frenkel oxygen defects. On this hypothesis, the coefficient of self-diffusion of oxygen in quartz at 500° C. is found to be approximately 3×10^{-11} cm.^{2}/sec. It is suggested also that diffusion of foreign univalent ions occurs mainly through vacant oxygen lattice positions. Experimental values are compared with those predicted by the theory of absolute reaction rates.

TABLE OF CONTENTS

INTRODUCTION

The minerals and fabric of a rock, either igneous or metamorphic, depend to a large extent on the kinetics of the processes by which the rock is formed. Glassy rocks, for instance, form when the rate of cooling is rapid compared with that of crystallization. Oscillatory zoning in plagioclase presumably testifies to processes that were rapid in comparison with the rate of the exchange reaction between crystal and melt. If minerals A and B in a thermally metamorphosed rock react to produce mineral C, occurrence of C not only indicates that the rock was heated to the equilibrium temperature for the reaction $A + B = C$; it indicates also that the rock was subjected to conditions under which the rate of this reaction

became appreciable as compared to the length of time during which the rock was held under those conditions. This may point to a temperature much higher than the equilibrium temperature, or to operation of other catalytic factors. It is possible, also, that C might form as a metastable phase below the equilibrium temperature, as when cristobalite forms well below its own range of stability. Some knowledge of reaction rates, and of factors which may affect them, is thus essential to correct understanding of the sequence of events recorded in igneous or metamorphic rocks.

The over-all rate of a heterogeneous reaction involving several successive steps is determined essentially by the rate of the slowest step. There is little doubt that in processes involving solids, the rate-determining step, or "bottleneck," is the rate of diffusion of reactants and products in the various solid phases. For instance, the rate of the reaction by which a crystal of quartz is converted to orthoclase, or andalusite is replaced by muscovite, depends mostly on the rate at which the alkali aluminates diffuse through the pre-existing crystal lattice. Knowledge of diffusion rates in solid silicates is thus of fundamental importance. The object of the present paper is to report on some experiments to determine the order of magnitude of the diffusion coefficients of common ions (K^+, Na^+, Li^+, Mg^{++}, Ca^{++}, Al^{+++}) in quartz.

Acknowledgments

This work was made possible by grants from the Institute of Geophysics and the Board of Research of the University of California, which are gratefully acknowledged. B. C. Morrisson, W. F. Burke, J. B. Farr, and P. I. Eimon assisted in the experiments, numerical calculations, and drafting of figures.

Definition of Diffusion Coefficient

It is customary to define a diffusion coefficient in the following manner: Let a particle with mass m be subjected to a force F arising from a concentration gradient or, as in the case of the present experiments, from an electrical field. Let it be assumed that this particle moves through a solid medium in which it encounters frictional resistance proportional to its velocity v. The equation of motion is then

$$m\frac{dv}{dt} = F - \frac{1}{B}v$$

where the coefficient B is the "mobility" of the particle. If $v=0$ at time $t=0$, the solution of this equation is

$$v = FB[1 - e^{-t/Bm}]. \qquad (1)$$

The numerical values of m and B are always such that the velocity

reaches an approximately constant value $v = FB$ within a very small fraction of a second. The mobility B may thus be interpreted as the velocity of a particle under unit force.

Now if c is the concentration of diffusing particles (number of particles per unit volume), the flux, or number S of particles flowing across a unit surface in unit time is

$$S = vc = FBc \tag{2}$$

so that B may be found if F, S, and c are known. Where diffusion results from a concentration gradient, it is convenient to use, instead of B, a "diffusion coefficient" D defined as

$$D = BkT \tag{3}$$

when k is Boltzmann's constant, and T is (absolute) temperature. With this definition we have, very simply, that the flux S_x in any arbitrary direction x under a concentration gradient dc/dx is

$$S_x = -D\frac{dc}{dx} \tag{4}$$

(Turner and Verhoogen, 1951, p. 41). D has dimensions $cm^2 . sec^{-1}$. B, the mobility, has dimensions GM^{-1} sec.

Diffusion coefficients are known to increase rapidly with temperature, following in general a law of the type

$$D = D_0 e^{-E/RT} \tag{5}$$

where D_0 is independent (or nearly independent) of temperature. E is an experimental "activation energy" for the process of diffusion.

Experimental Procedure

Equation (4) shows that D may be computed if we can measure the flow of particles under a given concentration gradient. The diffusion coefficient of sodium in quartz at 500° C. is, however, of the order of 10^{-10} cm.^{2}/sec. If we had a plate of quartz one millimeter thick in contact on one side with sodium chloride, say, the average gradient across the plate would be of the order of 2×10^{23} (since the concentration of sodium in sodium chloride is about 2.2×10^{22} particles per cm.^{3}), and the resultant flux across the plate would be $2 \times 10^{23} \times 10^{-10} = 2 \times 10^{+13}$ particles per cm.^{2} per second, or only 0.07 milligram/day. The actual rate would be much less because not all sodium ions in sodium chloride are free to migrate; the factor c which appears in (4) should really be the number of "free" ions, or the "activity" which is considerably smaller than the concentration. Such small diffusion rates have been measured by using radioactive isotopes, but unfortunately the radioactive isotopes of Li, Al and other geologically important elements have very short half-lives and cannot be

employed for this purpose. It is possible, however, to accelerate the ions appreciably by using an electrical field rather than a concentration gradient, and thus obtain a measurable flow.

The experimental technique is simple (Fig. 1). A thin layer of a non-volatile salt of the ion under study (e.g., NaCl, LiCl) is spread on a platinum foil resting on a lower massive copper electrode inside a furnace. A plate of quartz 2 or 3 mm. thick and 4 or 5 cm.^{2} in cross-section rests on this layer of salt and is covered in turn by a second platinum foil. A heavy upper copper electrode weighs down on the assemblage to maintain good contact. The two copper electrodes are connected to a D.C.

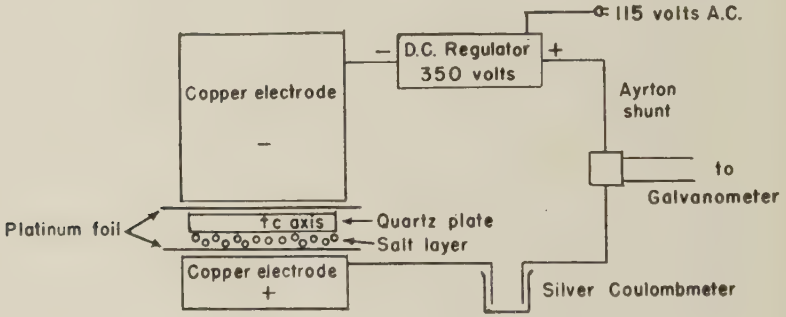

FIG. 1. Schematic drawing of diffusion assembly.

constant voltage supply adjustable in the range 100–350 volts, the upper electrode being the negative one. The metallic positive ions are accelerated towards the upper electrode and move across the quartz plate, carrying a current which is measured by means of a sensitive galvanometer, this current being proportional to the concentration and to the velocity of the diffusing ions, which are collected on the upper platinum foil, usually as a mixture of hydroxide and hydrous carbonates. The total amount transported in a given time may thus be determined by weighing. The total electrical charge which has flowed through the circuit in this same time may be ascertained, if necessary, by inserting a silver coulombmeter in the circuit.

An approximate value of D may be obtained in the following way: Using (3), equation (2) may be written

$$S = D\frac{Fc}{kT}.$$

If an ion carrying a charge ez (z is valency) is placed in a field of intensity dV/dx in the x-direction, the force F in that direction is

$$F = -ez\frac{dV}{dx} \qquad (6)$$

the minus sign indicating that a positive ion diffuses towards the negative electrode. As an approximation let us take $dV/dx = -(\Delta V/h)$ where ΔV is the difference in potential and h the thickness of the quartz plate. Then the total number of ions diffusing in time θ across a plate with cross-section s is

$$Q = Ss\theta \tag{7}$$

and

$$D = \frac{kT}{ez}\,\frac{hQ}{sc\theta\Delta V} \tag{8}$$

from which D may be determined if Q and c are known. Care must be taken to express all quantities in the same units. If e, the electronic charge is expressed in c.g.s.e.u. ($e = 4.8\times10^{-10}$), the potential drop ΔV must be expressed in the same units (1 volt = 1/300 c.g.s.e.u.). The constant k is 1.38×10^{-16} ergs/deg. The time θ in these experiments was usually of the order of 10 days $= 8.64\times10^{5}$ seconds.

Alternatively, D may be determined from the electrical conductivity σ. According to Ohm's law, the current density i (current per unit surface) is

$$i = -\sigma dV/dx. \tag{9}$$

If the current density results from a flux S of particles with charge ez,

$$i = Sez$$

and S, as before, is

$$S = -Bezc\frac{dV}{dx} \tag{10}$$

so that

$$B = \frac{\sigma}{e^2z^2c} \qquad D = \frac{\sigma kT}{e^2z^2c}. \tag{11}$$

The conductivity σ is usually expressed in ohm^{-1} cm.$^{-1}$, so that, after conversion to electrostatic units

$$D = 5.55\times10^{14}\,\frac{\sigma T}{z^2c}. \tag{12}$$

The conductivity σ is easily determined for simple geometric shapes from the potential drop ΔV and the total current I flowing through the circuit

$$\sigma = Ih/s\Delta V$$

where σ will be given in ohm^{-1} cm.$^{-1}$ if I is expressed in amps. and ΔV in volts.

Equation (12), of course, is only applicable if it can be ascertained that the conductivity is due entirely to the diffusing ion. This, however, is

rarely the case, for part of the current may be carried by electrons, or by ions of opposite sign diffusing in the opposite direction. Occurrence of such negative carriers appears indeed to be a necessity, for if only positive ions were to diffuse into and through the quartz plate, the plate would soon acquire a very high electrostatic charge. This could be checked by comparing the intensity of the current as it enters or leaves the crystal. The equation of continuity

$$\text{div } i = -\frac{\partial \rho}{\partial t}$$

where ρ is the density of electrical charges shows indeed that the current must decrease in the x-direction if positive space charges are being built up. No differences in current could be detected that could not be traced to leakage through faulty insulation.* Hence, it appears that the crystal plate as a whole maintains electric neutrality during the process of diffusion, which requires a motion of negative charges to balance advancing positive charges. A comparison of the values of Q and of the integral $\int_0^\theta I dt$ (measured with a coulombmeter or by graphical integration) shows that usually no more than about 50% of the current is carried by the diffusing ion. The exact proportion, however, is uncertain because of difficulty in determining exactly the quantity Q. What is collected on the negative electrode is indeed usually found to consist of a mixture of hygroscopic hydroxides and carbonates in various states of hydration (in the case of lithium, for instance, at least three constituents were recognized optically in the deposit); and it is difficult to determine the exact proportion of each of these in a deposit weighing a few milligrams or less. This uncertainty on Q appears to be the main source of error in these experiments.

The question also arises as to whether diffusion occurs through the body of the crystal or through mechanical defects such as invisible cracks, or grain boundaries, or twin planes. The quartz crystals used in these experiments were natural crystals and were certainly not free from defects, as shown by the scatter in observed values of the conductivity of the quartz itself. In general, quartz plates used for diffusion experiments were selected on the basis of their low conductivity, which was interpreted to indicate few mechanical defects. In spite of this, diffusion along cracks could be shown in the case of experiments with silver. Silver ap-

* Since the resistance of a quartz plate 2 mm. thick and 5 cm.^{2} in cross-section is about 4×10^8 ohms at 500° C., careful insulation is necessary, particularly where the wires enter the furnace. Also, on account of the extreme resistivity of quartz, it was not found practicable to place guard rings around the quartz plate, as the insulating material between rings and main electrodes could probably be a better conductor than quartz itself.

parently diffuses with extreme rapidity through such cracks which are later found to be lined with a thin deposit of metallic silver. This produces a rapid and very marked increase in conductivity, which soon reaches values typical of conduction in metals. Such, however, was not the case with the other ions, such as K, Li, Na, Mg, etc. The crystal remains perfectly clear after the experiment and the cathodic deposit is usually evenly distributed on the negative electrode, reproducing the outline of the plate. It is thus likely that transport of ions occurred mainly through the lattice itself. In any event, since the measurements were carried out on natural crystals, present results should be applicable to processes of diffusion in real crystals in nature.

Experimental Results

Using for c, the average concentration of the diffusing ion, a value the determination of which will be discussed later, the following results were obtained for the diffusion coefficient at 500° C., for diffusion parallel to the c-axis of quartz.

$$D_{Li} = 1.1 \times 10^{-8} \text{ cm.}^2 \text{ sec.}^{-1}$$
$$D_{Na} = 5.8 \times 10^{-10} \text{ cm.}^2 \text{ sec.}^{-1}$$
$$D_{K} = 2.0 \times 10^{-10} \text{ cm.}^2 \text{ sec.}^{-1}$$

These values are not believed to represent more than the order of magnitude of the diffusion coefficients; numerical values may be in error by a factor of 2 or 3.

To obtain the temperature coefficient of diffusion rates, it was assumed that since c changes only very slowly (due to the small value of the diffusion coefficient), any rapid change in σ with temperature would be due essentially to changes in D itself (see equation 12). It was found that by cooling or heating rapidly (i.e., in a matter of an hour) a quartz plate in which diffusion had been going on at a steady rate for some time (of the order of a few days), the conductivity changed exponentially, i.e., could be represented as a function of temperature by the relation

$$\sigma = \sigma_0 e^{-E/RT}.$$

The value of E appearing in this relation was taken to be the same as that appearing in equation (5), and was determined by measuring the ratio of the conductivities at two different temperatures, provided these two measurements could be carried out within a short interval of time. The following values were obtained, by averaging several determinations

$$E_{Li} = 20{,}600 \text{ cal./mole}$$
$$E_{Na} = 24{,}000 \text{ cal./mole}$$
$$E_{K} = 31{,}700 \text{ cal./mole}$$

with a probable error of ± 1000 calories, approximately. Combining these

results with the values of D at 500°, the following values were obtained in the range 300–500° C.

$$D_{Li} = 6.9 \times 10^{-3} \times e^{-20,600/RT}$$
$$D_{Na} = 3.6 \times 10^{-3} \times e^{-24,000/RT}$$
$$D_{K} = 0.18 \times e^{-31,700/RT}.$$

Tests were also made with Mg^{++}, Ca^{++}, Fe^{++} and Al^{+++}. In the case of Mg, a small amount of magnesium was detected spectroscopically on the negative electrode after a few days, but the amount was too small to be determined with accuracy; hence D_{Mg} is probably less than 10^{-12} at 500° C. The other ions gave completely negative results, and probably hardly diffuse at all. The anomalous case of silver, using silver foil as a source, has been mentioned earlier. Similar tests with gold, platinum, aluminum and copper foils gave no result at all.

Electrical Conductivity of Quartz

In order to throw light on the mechanism of diffusion, experiments were made on the conductivity of quartz in the absence of diffusing ions from an external source. The conductivity of quartz has been investigated by many writers apparently because of its peculiar behavior (for a summary of earlier work see Sosman, 1927, pp. 525–554). It is well known, for instance, that the conductivity parallel to the c-axis is considerably greater than the conductivity along any direction normal to this axis. The c-conductivity at 500° C. was found in our experiments to range from about 5×10^{-10} to 5×10^{-9} ohm^{-1} cm.$^{-1}$, depending on the specimen, whereas Rochow (1938) reports an equatorial conductivity of 2.1×10^{-12} at this same temperature. Rochow states that the equatorial conductivity is essentially electronic, whereas current in the c-direction is carried mainly by ions. Reasons for this difference are not known.

An interesting feature of the c-conductivity is its dependence on time. If a plate of quartz is placed between electrodes and a field applied in the direction of the c-axis, the current flowing through the circuit decreases at first very rapidly, then more slowly. Although the actual rate of decay varies somewhat from one sample to the next, the current after 10 or 15 minutes is commonly less than 1/10 of the current after 1 minute; indeed, the initial rate of decay (that is, during the first minute) is so great that it is difficult to determine experimentally the value of the initial conductivity. Conductivity may be observed to decrease continuously, although more slowly, over periods of many days. [This is in sharp contrast to the behavior observed when foreign ions are made to diffuse through the plate, in which case the conductivity increases slowly with time as more and more ions move into the crystal.] (Fig. 2). If the electric field is removed after a certain time, the quartz slowly regains its initial

conductivity, but if the field is actually reversed, the conductivity reverts almost instantaneously to its initial value or a higher value. Apparently, this is why the conductivity for alternating current is considerably higher than for direct current. If the circuit containing the quartz plate is short-circuited after removal of the field a "recovery," or "relaxation," or "inverse" current is observed to flow, the quartz plate acting somewhat like a storage battery. Joffé (1929) claims that this recovery current equals in magnitude the direct, or charging current; in our own experiments the recovery current was always considerably less than the charging current, although it decays at about the same rate.

The conductivity of quartz depends on temperature according to an exponential law

$$\sigma = \sigma_0 e^{-E/RT}$$

where the activation energy is about 23,000 cal. in the range 300–500° C.

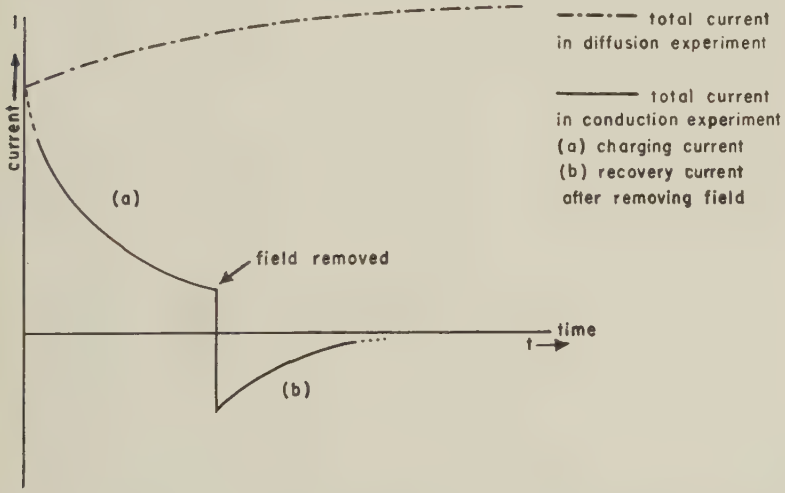

FIG. 2. Current-time curves for conduction and for diffusion in quartz.

There is no sudden change in the conductivity at the α-β transition point, although the activation energy seems to increase somewhat above this point. If a specimen is heated slowly to 500° and allowed to cool, the conductivity measured during cooling is less (by a factor of 2 to 3) than the conductivity measured during heating; but this may be due partly to the time dependence of conductivity since the cooling curve is determined after the heating curve. Curie (1889) observed however, that the conductivity may be greatly reduced by preheating the specimen. This effect is presumably similar to annealing, insofar as preheating re-

moves lattice defects due to strain or acquired otherwise during the previous history of the crystal, and which contribute to the conductivity.

Several explanations have been suggested for the time-dependence of axial conductivity. Curie (1889) suggested that it results from water filling channels of molecular size parallel to the *c*-axis; the conductivity of this water would gradually decrease as more and more of the salts dissolved in it are removed by electrolysis. Warburg and Tegetmeier (1888) suggested that the conductivity is due to ions (mostly Na) present initially as impurities in the quartz lattice; again these foreign ions would be gradually eliminated. There is little doubt that part of the initial con-

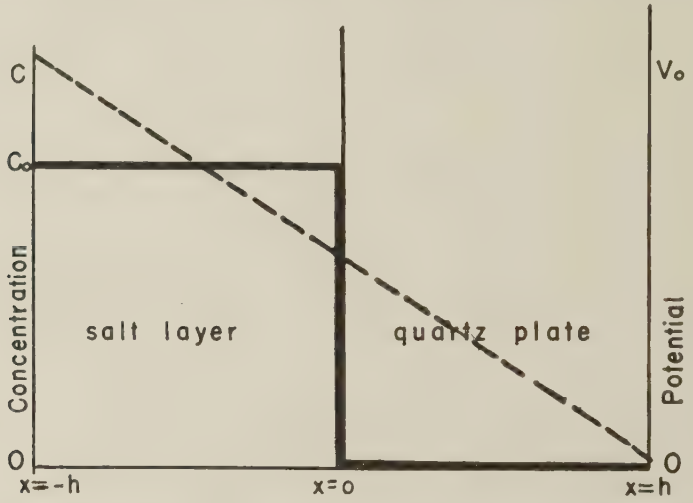

FIG. 3. Initial distribution of potential and concentration in diffusion experiments.

ductivity of quartz may be due to such impurities, for in one of our experiments with a quartz crystal from Arizona, noticeable amounts of boron were collected on the cathode. But such "impurity" theories fail to explain why quartz may regain its initial conductivity merely by standing for a few days.

The same time-dependence of conductivity has been observed for other ionic crystals, such as NaCl, and Beran and Quittner (1930) pointed out that both the rate of decay of the recovery current and the absence of any measurable change in dielectric constant of a crystal during an experiment indicate that the time-dependence of conductivity, or the existence of a recovery current cannot be due only to displacement currents and dielectric polarization. Joffé (1929) and von Seelen (1924) have succeeded in measuring the potential distribution across crystals of quartz and halite respectively, and from the curvature of the potential

curve showed the existence of space charges. In NaCl these are mostly positive charges accumulated on the anode-side of the crystal, whereas in quartz Joffé found practically equivalent amounts of positive and negative charges, the positive charges residing on the half of the crystal plate in contact with negative electrode. It is apparently the gradual building up of these space charges which produces the decrease in the charging current, whereas a redistribution and gradual disappearance of these same charges explains the recovery current. Joffé explained the occurrence of these space charges by assuming dissociation of quartz into units of opposite sign which migrate in opposite directions in the electric field. He was vague as to the nature of these units, although he mentioned briefly (p. 92) that "a deposit of silicon and liberations of oxygen from a normal crystal lattice may be observed." He succeeded in measuring the average density of these positive and negative space charges and found them to be roughly equal, with a value of 2×10^9 electronic charges per cm.^{3} at 17° C.

Mechanism of Conduction and Self-Diffusion Rate of Oxygen

It is now well known that electrical conduction in ionic, or nearly ionic, crystals results essentially from the motion of lattice defects, although electronic conduction may also be present in some cases (e.g., Ag_2S, FeO). The lattice defects usually considered in this connection are either of the Frenkel or Schottky type. In the former type, ions are assumed to move from a lattice to an interstitial position, leaving "holes" behind them; other lattice ions may then be expected to move into these holes, which therefore migrate in a direction opposite to that of the ions themselves. In the Schottky type of defect it is assumed that ions of both signs migrate out of the lattice towards its surface, leaving equivalent numbers of holes of both signs which migrate in opposite directions when an electrical field is applied. If ϵ_F is the energy per ion to form a Frenkel defect, i.e., to move an ion from a lattice to an interstitial position, the number n_F of such interstitial ions in a crystal in equilibrium at temperature T is (Mott, 1948, p. 21)

$$n_F = \gamma\sqrt{NN^1}\, e^{-\epsilon_F/2kT}$$

where N is the total number of lattice positions and N^1 is the number of possible interstitial positions. The factor $\frac{1}{2}$ in the exponential arises from the fact that displacement of *one* ion creates *two* defects (an interstitial ion and a hole). The factor γ arises from the change in vibrational frequencies, and hence in free energy, of the atoms and ions surrounding the interstitial ion or the hole; it may be greater or less than 1. The number n_S of Schottky defects, on the other hand, is

$$n_S = \gamma N e^{-\epsilon_S/kT}$$

being the energy to produce such a defect. The factor γ in this case may be of the order of $10^3 - 10^4$ (see also Barrer, 1941, p. 294). Thus if electrical conduction results from motion of Frenkel defects, its temperature coefficient would be of the type $exp[-(\epsilon_F + 2\epsilon_F')/2kT]$ where ϵ_F' is the activation energy for migration of a defect, whereas for conduction by Schottky defects the corresponding term would be $exp[-(\epsilon_S + \epsilon_S')/kT]$ ϵ_S' being the activation energy for migration of a Schottky defect.

As mentioned above, Joffé finds that the average density of charges of one sign in quartz at 17° is 2×10^9 electronic charges per cm.^{3} If this corresponds to the density of Frenkel defects for oxygen ions, the corresponding number of interstitial oxygen ions is 1×10^9/cm^3. The total number N of oxygen lattice position in one cm.^{3} of quartz is approximately 5.2×10^{22}, so that assuming $\gamma = 1$, $N = N^1$, we find $\epsilon_F = 36{,}400$ cal./mol. [The same value would obtain if we considered silicon defects.] The activation energy for conduction in quartz is about 23,000 cal. Hence

$$(36{,}400 + 2\epsilon'_F)/2 = 23{,}000$$

and $\epsilon_F' \cong 5{,}000$ cal./mole. On the other hand, if conduction occurs by Schottky defects we find, for $\gamma = 10^4$, $\epsilon_S = 23{,}800$ cal., $\epsilon_S' = -800$ cal., which is impossible. These figures are, of course, quite approximate, since an exact calculation would require evaluation of γ for the quartz lattice, which is not available. The suggestion is, however, that conduction occurs by Frenkel defects, which is what one would expect in a lattice with high evaporation energy (hence high ϵ_S) and relatively high compressibility (hence low ϵ_F).

It is impossible to decide from Joffé's experiments whether oxygen, or silicon, or both, move into interstitial positions, but it seems likely that it is oxygen. Removing an oxygen requires breaking 2 O—Si bonds, whereas removing a silicon requires breaking 4. In other cases it is usually the ion with the lesser charge (in this case O^{--}) which moves most readily.

If the hypothesis is accepted that conduction of electricity parallel to the c-axis in quartz results from motion of oxygen ions in one direction and simultaneous displacement of holes (bearing an effective positive change) in the opposite direction, it becomes possible to compute the self-diffusion coefficient of oxygen from the conductivity itself by using equation (12). Joffé's measurements show that the mobility of oxygen ions and oxygen holes is about the same; hence it may be assumed that either one carries half the total current. From the number of defects at 17°, measured by Joffé, the number of such defects at 500° C. is found to be 3.6×10^{18}/cm^3. Then

$$D_0 = 5.55 \times 10^{14} \times \frac{\sigma}{2} \times \frac{773}{4 \times 3.6 \times 10^{18}}.$$

Thus for a crystal with an initial conductivity (obtained by extrapolation of the readings after 1 minute) of 2×10^{-9}, the diffusion coefficient of oxygen is 3×10^{-11} cm.^{2}/sec.

Mechanism of Diffusion

Very simple experiments with a scale model of the quartz lattice and marbles of various sizes indicate that the maximum radius of a rigid sphere capable of moving freely through the lattice is about 0.57 Å; larger ions cannot diffuse without making room for themselves by distortion of the lattice, or availing themselves of preexisting holes. If the diffusing ion makes room for itself by crowding the lattice ions aside, the energy requirements, and hence the diffusion rates, would be very sensitive to ionic size. While this is true to some extent, the fact remains that the large K^+ ion diffuses more rapidly than smaller bivalent or trivalent ones. Hence, foreign ions may diffuse mainly through preexisting holes, such as vacant oxygen lattice positions. Once a foreign ion, say sodium, has occupied a hole, it moves farther under the influence of the electric field or of a concentration gradient by exchanging position with neighboring oxygens which migrate in the opposite direction, thus accounting for the fact that the diffusing ion apparently carries only a fraction of the total current.

Since the oxygen holes are originally distributed uniformly through the crystal, they cannot all become occupied at once. The number of admitted ions and occupied holes will thus increase gradually with time, leading to a gradual increase in conductivity, as observed. (See Fig. 2.) When all the holes are occupied, the conductivity reaches a steady value, which is usually found to occur after a few days. The concentration of diffusing ions then presumably reaches a maximum value of 3.6×10^{18}/cm.^{3} at 500° C. The values of the diffusion coefficients listed above were obtained by substituting this value and the corresponding value of the steady-state conductivity in equation (12), checking the result by means of (8) to determine the fraction of the total conductivity due to migration of the diffusing ions.

An oxygen hole, formed by removing a negative oxygen ion to an interstitial position, carries an effective positive charge; it would then tend to repel an invading positive ion. This repulsion would increase with increasing charge of the diffusing ion. This may explain why bivalent ions, even of relatively small size (e.g., Mg^{++}) diffuse more slowly than larger univalent ones (e.g., Na^+, K^+).

How the crystal manages to maintain electric neutrality during the process of diffusion is difficult to understand. The charge corresponding with a concentration of 3.6×10^{18} foreign univalent ions per cm.^{3} would be

sufficient to raise the potential of the capacitance formed by the quartz plate and its metallic electrodes to a value of about 10^{10} volts, which obviously does not happen. It is thus necessary to assume that additional negative charges are also present. These might consist, for instance, of negative oxygen ions in excess over the stoichiometric proportion. Such is the case, for instance, for cuprous oxide which shows a marked increase in conductivity when heated under high partial pressure of oxygen. Electric neutrality in quartz could also be restored by electrons from the external source which become trapped in the crystal structure.

It is interesting to compare experimental values of the diffusion coefficients with values predicted from the theory of absolute reaction rates. According to Eyring's theory [Glasstone, Laidler and Eyring, 1941] the constant D_0 in equation (5) should be given by the relation

$$D_0 = e\lambda^2 \frac{kT}{h} e^{\Delta S/R}$$

where k and h are the Boltzman's and Planck constants, respectively, λ is the average length of a jump, i.e., the distance between successive equilibrium positions of the diffusing particles, and ΔS is the entropy of activation. λ is not likely to be less than the distance between two oxygen sites, which is about 2.6 Å. Substituting this value and the experimental value of D_0 at 500° C., the following values of the entropy of activation are found:

$$\text{for Li } \Delta S = -1.45R$$
$$\text{for Na } \Delta S = -2.1R$$
$$\text{for K } \Delta S = +1.8R.$$

As we have chosen a minimum value for λ, the above values of ΔS are the maxima that are consistent with the experimental values of D_0. It is interesting to notice that the value for Na is such as could have been predicted on the simplest possible hypothesis, namely, that the entropy of activation corresponds merely to a redistribution of degrees of freedom, the diffusing sodium ion exchanging its three vibrational degrees of freedom in the NaCl lattice for one translational degree of freedom in the direction of diffusion. This would correspond to a negative entropy change of about $2R$ at 500° C. This negative value of the entropy of activation indicates also that diffusion of sodium and lithium does not involve any considerable distortion or disordering of the quartz lattice, in agreement with our hypothesis that diffusion occurs through preexisting holes. This, however, is no longer true for potassium: the positive value of the entropy of activation indicates in this case that some disordering does occur, presumably because of the larger size of the potassium ion. This disordering may well occur when oxygen and potassium

ions exchange position, and is consistent with the higher value of the activation energy observed in this case.

Geologic Implications

To give a more pictorial representation of diffusion rates in quartz, let us assume that potassium ions diffuse from a plane boundary into a quartz crystal under the influence of a concentration gradient. The average distance $\bar{x}$ from the boundary reached by potassium ions after time t is then given by the relation

$$\bar{x}^2 = 2Dt$$

so that, at 500° C., the average distance reached in one million years (3×10^{13} sec.) is

$$\bar{x} = (2 \times 2 \times 10^{-10} \times 3 \times 10^{13})^{1/2} \cong 110 \text{ cm.}$$

which is very small compared to the dimensions of a batholith, say. It should be remembered also that these diffusion coefficients apply to diffusion parallel to the c-axis; diffusion normal to this axis is apparently much slower. Admittedly, in large masses of rocks, diffusion will occur preferentially along crystal boundaries rather than through crystals; yet metasomatic replacement does involve at times penetration into the grains themselves. Present results would indicate very slow rates of metasomatic replacement.

Are the present results at all applicable to processes of metasomatic replacement? The popular view of "clouds of ions" diffusing into rocks and replacing them is, of course, completely inadequate unless these "clouds" happen to be of such composition as to remain electrically neutral; otherwise the diffusion cloud, if it has any appreciable concentration, would involve impossibly large electric potentials. Thus the "cloud" which allegedly transforms great masses of quartz into great masses of orthoclase must contain, in addition to potassium and aluminum ions, a proper number of oxygen ions, as shown already by the simple fact that the chemical formula $3\ SiO_2+K^+ + Al^{+++}$ does not add up to orthoclase $KAlSi_3O_8$. The problem of the source of this oxygen does not seem to have been given proper attention. It might be solved by assuming removal of some of the silicon, i.e., $4SiO_2+K^+ + Al^{+++} = KAlSi_3O_8 + Si^{++++}$; but once again the problem of electric potential in the cloud would present itself. Furthermore, since diffusion rates in quartz seem to be more sensitive to electric charge than to ionic size, diffusion of Si^{++++}, which would be the rate-determining step of the reaction, must be extremely slow. Obviously, diffusion in the solid state does not have the answer to all our problems.

APPENDIX

Equations of Diffusion in an Electrical Field

Let us suppose that a positive ion with valence z diffuses from a layer of salt of thickness h into a quartz plate of equal thickness under the influence of an electrical field (Fig. 3). At time $t=0$, the concentration satisfies the conditions

$$c = c_0 \quad \text{for} \quad -h < x < 0$$
$$c = 0 \quad \text{for} \quad 0 < x < h$$

and may thus be represented by the function

$$c = \frac{c_0}{2} - \frac{2c_0}{\pi}\left[\sin\frac{\pi x}{h} + \frac{1}{3}\sin\frac{3\pi x}{h} + \frac{1}{5}\sin\frac{5\pi x}{h} + \cdots\right]. \tag{1}$$

At time $t=0$, we apply a potential $+V_0$ at $x=-h$, the potential at $x=+h$ being taken as zero. Hence, at $t=0$, $\partial V/\partial x = -(Vo/2h)$; and $V=V_0$ for $x=-h$, $V=0$ for $x=h$ at all times.

1. Let us assume first that only the positive ion moves (no negative carriers). The equations to be satisfied for $o<x<h$ are

(a) The equation of continuity

$$\operatorname{div} S = -\frac{\partial c}{\partial t} \tag{2}$$

where S, the flux in the x-direction, is

$$S = vc \tag{3}$$

the velocity v being given by the relation

$$v = -ezB\frac{\partial V}{\partial x}. \tag{4}$$

(b) Poisson's equation

$$\frac{\partial^2 V}{\partial x^2} = -\frac{4\pi}{\epsilon}ezc \tag{5}$$

where ϵ is the dielectric constant of quartz.

Eliminating S, V, and v leads to the equation

$$c^2 + \frac{\partial c}{\partial x}\left[\int_0^z c\,dx - A\right] = -\beta\frac{\partial c}{\partial t} \tag{6}$$

where

$$A = \frac{\epsilon}{4\pi ez}\left(\frac{\partial V}{\partial x}\right)_{x=0}, \qquad \beta = \frac{\epsilon}{4\pi e^2 z^2 B}.$$

It appears simpler to eliminate c rather than V. The differential equation for the potential V is then

$$\frac{\partial V}{\partial x}\frac{\partial^3 V}{\partial x^3} + \left(\frac{\partial^2 V}{\partial x^2}\right)^2 = \frac{1}{ezB}\frac{\partial^3 V}{\partial x^2 \partial t}. \tag{7}$$

Substituting $y = \partial V/\partial x$, $ezB = 1/\alpha$ the general solution of (7) is found to be

$$F\left[\left(y + \frac{\phi}{\alpha}\right), \left(x + \frac{\psi}{\alpha} + \frac{ty}{c^2} + \frac{t\phi}{\alpha^2}\right)\right] = 0 \tag{8}$$

where F is any arbitrary function of the variables indicated in parentheses, ϕ is an arbitrary function of t only, and $\psi = \int \phi dt$. This function F must satisfy the boundary conditions for V given above, and in addition,

$$-\frac{\epsilon}{4\pi ze}\left(\frac{\partial^2 V}{\partial x^2}\right)_{t=0} \text{ must satisfy (1).}$$

2. It seems hardly worth looking for a suitable form of (8), since condition (5) is not likely to represent conditions accurately. Equation (5) implies indeed an unbalanced concentration of space charges, the crystal acquiring a total charge $\int_0^h ezc_h dx$ which would raise its potential to a very high value. We will certainly be closer to experimental facts if we assume a simultaneous motion of negative charges in the opposite direction at a rate sufficient to maintain electric neutrality. Let us then assume first that there is a detailed balancing of charges everywhere, so that $\partial^2 V/\partial x^2 = 0$ and

$$\frac{\partial V}{\partial x} = -\frac{V_0}{2h}$$

at all times. The equations to be satisfied (2, 3, 4) become very simply

$$\mu \frac{\partial c}{\partial x} = -\frac{\partial c}{\partial t} \tag{9}$$

where

$$\mu = (ezBV_0)/2h. \tag{10}$$

The solution of (9), subject to boundary condition (1), is

$$c = \frac{c_0}{2} - \frac{2c_0}{\pi}\left[\sin\frac{\pi}{h}(x - \mu t) + \frac{1}{3}\sin\frac{3\pi}{h}(x - \mu t) + \cdots\right].$$

To determine B, or D, we consider what happens at $x = h$. The concentration there is

$$c_h = \frac{c_0}{2} - \frac{2c_0}{\pi}\left[\sin\frac{\pi\mu t}{h} + \frac{1}{3}\sin\frac{3\pi\mu t}{h} + \cdots\right] \tag{11}$$

and the total number Q of particles flowing across the plate boundary with cross-section s in time θ is

$$Q = \int_0^\theta s\mu c_h dt. \tag{12}$$

Set $n = \mu\theta/h$, $v = sh$, v being the volume of the crystal. Substituting (11) into (12) and integrating, we obtain

$$\frac{Q}{c_0 v} = \frac{n}{2} - \frac{2}{\pi^2}\left[1 + \frac{1}{3} + \frac{1}{9} + \cdots - \left(\cos n\pi + \frac{1}{9}\cos 3n\pi + \cdots\right)\right].$$

The right-hand member of this equation is given approximately, for large values of n, by the expression $\frac{1}{2}(n-1)$, so that

$$n = \frac{2Q}{c_0 v} + 1.$$

Hence, if Q, c_0 and v are known, n may be computed. Since $n = \mu\theta/h$, $\mu = ezBV_0/2h$, we obtain finally

$$D = \frac{2nkT}{ezV_0\theta} \tag{13}$$

from which D may be calculated. A difficulty arises, however, in the determination of c_0. c_0 is not necessarily the total initial concentration of positive ions in the salt; it is the concentration of free ions, i.e., of ions which are not so tightly held in the lattice that they cannot move. c_0 might be taken, for instance, as the number of metallic ions which would participate in electrical conduction in the salt itself. As this number cannot be evaluated accurately at 500° C. for any of the salts used in these experiments, there is nothing to gain by using the exact relation (13) rather than the approximate method (also assuming $\partial V/\partial x = \text{constant}$) outlined previously.

3. Finally, we might attempt a more exact solution by considering that there is not necessarily a detailed balancing of charges at every point in the crystal although its total charge should remain zero. This implies two different carriers (the positive diffusing ion and a negative one) with valencies z_1, z_2 and concentrations c_1, c_2, respectively. Poisson's equation is then

$$\frac{\partial^2 V}{\partial x^2} = -\frac{4\pi}{\epsilon} e(z_1 c_1 - z_2 c_2) \tag{14}$$

subject to the condition

$$\int_0^h \frac{\partial^2 V}{\partial x^2}\, dx = 0 \tag{15}$$

expressing neutrality as a whole. The equations of continuity for each carrier are

$$\left.\begin{aligned} ez_1 B_1 \frac{\partial V}{\partial x}\frac{\partial c_1}{\partial x} + c_1 ez_1 B_1 \frac{\partial^2 V}{\partial x^2} &= \frac{\partial c_1}{\partial t} \\ ez_2 B_2 \frac{\partial V}{\partial x}\frac{\partial c_2}{\partial x} + c_2 ez_2 B_2 \frac{\partial^2 V}{\partial x^2} &= \frac{\partial c_2}{\partial t} \end{aligned}\right\}. \tag{16}$$

Let us consider the steady state in which the current remains constant, and in which presumably

$$\frac{\partial c_1}{\partial t} = \frac{\partial c_2}{\partial t} = 0.$$

This state is usually reached after a few days. Eliminating $\partial V/\partial x$ in equations (16), we get

$$-c_1 \frac{\partial c_2/\partial x}{\partial c_1/\partial x} \frac{\partial^2 V}{\partial x^2} + c_2 \frac{\partial^2 V}{\partial x^2} = 0$$

and since we assume $\partial^2 V/\partial x^2 \neq 0$ locally

$$\frac{1}{c_2} \frac{\partial c_2}{\partial x} = \frac{1}{c_1} \frac{\partial c_1}{\partial x}$$

which together with (14) and (15) leads to $z_1 c_1 = z_2 c_2$, $\partial^2 V/\partial x^2 = 0$ everywhere. This is contrary to our assumption, and we must conclude therefrom that either there is detailed balancing everywhere, or that a steady state cannot be reached. As it appears experimentally that a very close approach to a steady state may be reached after a few days, $\partial^2 V/\partial x^2$ can never be very large, and may therefore be neglected. We revert thus to the previous case.

References

Barrer, R. M. (1941), Diffusion in and through solids. Cambridge University Press.

Beran, O., and Quittner, F. (1930), Die Feldstärkeabhängigkeit von Gegenspannung und wahren Leitvermögen in Ionenkristallen: *Zeits. für Physik*, **64**, 760–776.

Curie, P. (1889), Recherches sur la conductibilité des corps cristallisés: *Ann. Chimie Phys.*, ser. 6, **18**, 202–255.

Glasstone, S., Laidler, K. J., and Eyring, H. (1941), The theory of rate processes. McGraw-Hill, New York.

Joffé, A. F. (1928), The Physics of Crystals, McGraw-Hill Book Co., New York.

Mott, N. F., and Gurney, R. W. (1948), Electronic Processes in Ionic Crystals, Oxford, Clarendon Press.

Rochow, E. G. (1938), Electrical conduction in quartz, periclase and corundum at low field strengths: *Journ. Appl. Physics*, **9**, 664–669.

Sosman, R. B. (1927), The Properties of Silica, Chemical Catalog Co., New York.

Turner, F. J., and Verhoogen, J. (1951), Igneous and Metamorphic Petrology, McGraw-Hill, New York.

von Seelen, D. (1924), Ueber die elektrische Leitfähigkeit des Steinsalzkristalles: *Zeits. für Physik*, **29**, 125–140.

Warburg, E., and Tegetmeier, F. (1888), Ueber die elektrolytische Leitung der Bergkrystalls: *Ann. d. Physik u. Chemie*, **35**, 455–467.

Manuscript received Nov. 30, 1951

STRONTIAN APATITE[1]

ESPER S. LARSEN, JR., MARY H. FLETCHER, AND EVELYN A. CISNEY,
U. S. Geological Survey, Washington, D. C.

ABSTRACT

An apatite from a syenite dike near Libby, Mont., has 11.6 per cent SrO, a specific gravity of 3.35, and indices of refraction of $\omega = 1.638$ and $\epsilon = 1.634$. It is believed to be deuteric in origin.

OCCURRENCE

The apatite described in this report came from a dike on the upper part of the ridge between Kearney and Rainy Creeks in the Rainy Creek district near Libby, Mont., and near the Vermiculite mine (Larsen and Pardee, 1929, p. 108). The dike, which cuts apatite pyroxenite, is a syenite with streaks and patches of darker-colored rock rich in pyroxene, sphene, and apatite. Apatite makes up as much as 10 per cent of some of these streaks and yellow sphene even more. The apatite here described came from one of these streaks. The form of the streaks and the way in which the pyroxene and sphene penetrate the large feldspar crystals strongly indicate that the minerals are deuteric in origin. Most apatite in igneous rocks has a specific gravity a little below 3.20, but in attempting to separate the apatite and sphene of this rock the apatite was found to have a much higher specific gravity; most of it was suspended in or just sank in methylene iodide (sp. gr. 3.33).

The indices of refraction and other optical properties of this apatite are within the range of those of apatite commonly found in igneous rocks. When strontium replaces calcium in minerals the indices of refraction are not greatly changed but there is a large change in the specific gravity. The apatite here described, therefore, was tested spectrographically for strontium and was found to be high in that element. Apatite from other parts of the dike that contained the strontian apatite had normal specific gravities and contained little strontium. The sphene associated with the strontian apatite contained little strontium.

DESCRIPTION

Analytical data on strontian apatite from Montana and on a similar apatite from Kola Peninsula, Russia, are shown in Table 1.

The strontian apatite from Libby, Mont., is very much like the apatite from Kola Peninsula called saamite by Volkova and Melentev (1939),

[1] Publication authorized by the Director, U. S. Geological Survey.

Table 1. Analyses and Properties of Strontian Apatite

	From Montana[1]			From Kola Peninsula, Russia[2]
	Weight per cent	Molecular proportion		Weight per cent
SiO_2	0.14	2		1.55
Al_2O_3	0.38	4		0.34
Fe_2O_3	0.27	2		0.12
TiO_2	0.04	1		0.00
MnO	0.02	—		0.05
CaO	46.3	825		42.38
SrO	11.6	112		11.42
BaO	0.06	—	10×94.5	0.00
MgO	0.25	6		0.05
Na_2O	0.10	2		0.13
K_2O	0.02	—		0.07
P_2O_5	39.2	272	3×91	38.33
As_2O_3	<0.001	—		0.00007
F	2.57	135	2×67	3.73
Ignition loss	0.14			0.10
	101.09			101.67
O=F	−1.08			−1.57
Total	100.01			100.10
Specific gravity	3.35 (by pycnometer)			3.355
ω	1.638			
ϵ	=1.634			

[1] Strontian apatite from vicinity of Libby, Mont. (R.C. 158). Analysis by Mary H. Fletcher made on sample dried at 110°C. Alkalies determined by flame photometer by Charles A. Kinser. MgO determined spectrographically by Claude Waring. Sample had more than 99 per cent apatite and checks very closely with the theoretical composition of apatite—$10(Ca_{0.88}Sr_{0.12})O \cdot 3P_2O_5 \cdot 2F$.

[2] Strontian apatite or saamite, Mt. Poachvrimchorr, Kola Peninsula, Russia. Analysis by E. K. Vacharov (Volkova and Melentev, 1939). V_2O_5 not determined. As_2O_3, 0.00007; ZrO_2, 0.001; ΣTR_2O_3, 3.22; and H_2O, 0.28.

except that the Kola mineral has more than 3 per cent of rare earths. It seems better to eliminate the name saamite and to call the Libby and Kola minerals strontian apatites (Schaller, 1930).

Strontian hydroxylapatite has been prepared artificially by Klement (1939) and strontian chlorapatite by Carobbi (1950). Carobbi gives the indices of refraction of the artificial strontian chlorapatite as: $\omega = 1.658$, $\epsilon = 1.664$ (these data indicate crystals that are optically positive). Natural

chlorapatite has $\omega = 1.667$, $\epsilon = 1.664$, and sp. gr. = 3.20. Here, too, strontium has little effect on the indices of refraction of apatite.

An x-ray powder pattern of strontian fluorapatite was taken with CuK_α radiation (1.5418 Å). This pattern is identical with that of fluorapatite except for a slight difference in spacing. The lattice constants of strontian fluorapatite were calculated by Evelyn Cisney from measurements of the powder pattern. A comparison of these lattice constants with those of fluorapatite (Winchell, 1951) is as follows:

	a_0 (*in Å units*)	c_0 (*in Å units*)
Fluorapatite	9.38[2]	6.89[2]
Strontian fluorapatite	9.41±0.01	6.91±0.01

The lattice constants of hydroxylapatite and 100 per cent strontium hydroxylapatite (Klement, 1939) are given below to show the magnitude of change in lattice constants when the calcium is completely replaced:

	a_0 (*in Å units*)	c_0 (*in Å units*)
Hydroxylapatite	9.42[2]	6.94[2]
Strontium hydroxylapatite	9.76[2]	7.21[2]

The specific gravity of strontian fluorapatite, calculated from the above parameters, is 3.34. This is larger than the specific gravity of calcium fluorapatite, but it is appreciably smaller than that of pure strontium hydroxylapatite (sp.gr. = 4.17) calculated from its lattice parameters (Klement, 1939).

The differences between the lattice constants of fluorapatite and strontian fluorapatite, though small, are greater than the error of measurement and therefore real, and they could be used to distinguish between the two. However, the high specific gravity of strontian apatite is probably the best property for its identification.

References

Carobbi, Guido (1950), Celestina e apatite di stronzio sintetiche contente piccole quantita di mercurio: *R. accad. Lincei, Cl. sci. fis., mat. e nat., Atti*, serie 8, **8**, fasc. 2, 87–93.

Klement, R. (1939), Basische Phosphate zweiwertigen Metalle. IV. Strontium-Hydroxylapatite: *Zeits. Anorg. Chemie*, **242**, 215–221.

Larsen, Esper S., Jr., and Pardee, J. F. (1929), The stock of alkaline rocks near Libby, Montana: *Jour. Geology*, **37**, 97–112.

Schaller, W. T. (1930), Adjectival endings of chemical elements used as modifiers to mineral names: *Am. Mineral.*, **15**, 566–574.

Volkova, M. I., and Melentev, B. N. (1939), Chemical composition of the Khibiny apatites: *Acad. sci. U.R.S.S., C. R.*, **25**, 120–122.

Winchell, Alexander N. (1951), Elements of Optical Mineralogy, part II, 4th ed., John Wiley and Sons.

Manuscript received Oct. 24, 1951

[2] Recalculated to Å units from the formula 1 Å = 1.00202 kX.

HYDROTHERMAL URANOTHORITE IN FLUORITE BRECCIAS FROM THE BLUE JAY MINE, JAMESTOWN, BOULDER COUNTY, COLORADO[1]

GEORGE PHAIR AND KIYOKO ONODA SHIMAMOTO,
U. S. Geological Survey, Washington, D. C.

ABSTRACT

In the course of thin-section and heavy-mineral studies of fluorite breccias from Jamestown, Colorado, the mineral thorite, variety uranothorite, was identified on the basis of chemical, spectrographic, optical, and *x*-ray data. This uranothorite is compared with uranothorite from South Westland, New Zealand, that was described by Hutton in 1950, and with similar material from an Alaskan placer sample studied by the writers. These uranothorites are in turn contrasted with the uranothorites described in the older literature, all of which represent hydrated material. Thorium halos in fluorite are described, probably for the first time. The uranothorite associated with the fluorite breccias is clearly of hydrothermal origin—unlike all previously described thorites and uranothorites, with one very doubtful exception.

INTRODUCTION

The Blue Jay mine is one of the larger fluorite producers in the Jamestown district, Boulder County, Colorado. George Phair visited the second level of this mine in September 1949, guided by R. U. King and H. C. Granger of the U. S. Geological Survey's Denver office, and collected some 30 pounds of the breccia ore for mineralogic and chemical studies of the radioactive constituents. A preliminary binocular study of the heavy-mineral contents of this ore revealed scattered grains of an unknown glassy green mineral. Qualitative chemical and spectrographic tests showed that the mineral resembled uranothorite in chemical composition. Although the uranothorite (?) accounted for only a small part of the total radioactivity of this ore, its occurrence in a mineral assemblage which is definitely of hydrothermal origin seemed unique. Largely for this reason the mineral was considered of sufficient interest to justify the numerous separations and the tedious hand-picking of grains for its positive identification. Moreover, the fact that a similar-appearing green mineral had been found in a placer sample from the Ruby district, Alaska, emphasized the need for the specific determination. This mineral was identified tentatively as thorite, variety uranothorite, by Kiyoko Shimamoto; its physical properties, however, depart widely from those of the dozen or so thorites described in the literature prior to 1950.

This investigation is part of the program on radioactive raw material undertaken by the U. S. Geological Survey on behalf of the U. S. Atomic

[1] Publication authorized by the Director, U. S. Geological Survey.

Energy Commission. We are indebted to F. E. Ingerson, J. C. Rabbitt, E. S. Larsen, Jr., and T. Botinelly, all of the Geological Survey, for critical review of the manuscript, and to other members of the staff, particularly to J. Berman and E. Dwornik, for helpful discussions of phases of the "thorite" problem of mutual interest. The many chemists and spectrographers of the Survey who obtained the analytical data upon which this report is largely based are cited in the text. We should like also to thank Max White of the Geological Survey for the use of mineralogic material and Professor Clifford Frondel of Harvard University for the reference to Gordon's description of doubtful uranothorite from Llallagua, Bolivia.

Methods of Separation

To obtain enough uranothorite for analyses, the parts of the fluorite breccia selected for high radioactivity were crushed to -120, $+200$ mesh and the heavy minerals separated in methylene iodide. These heavy minerals consisted chiefly of deep-purple fluorite containing heavy impurities; these were impure carbonates, pyrite, galena, sphalerite, iron oxides, uraninite, and uranothorite. The light fractions consisted chiefly of light-purple fluorite, quartz, carbonate, clay minerals, and altered feldspar; in bulk samples the light fractions showed negligible radioactivity. Some slight additional concentration of the heavy-mineral fractions was obtained by passing them through the Frantz isodynamic separator; the uranothorite tended to accumulate in the moderately magnetic fraction. The desired material was hand-picked from these concentrates under the binocular microscope, and this sample, in turn, was hand-picked a second time for the reasons described later.

Identification of the Uranothorite

Preliminary optical studies had shown that the green mineral in the fluorite breccias, like that in the Alaskan placer sample, was completely metamict (isotropic) with $n=1.84$. The specific gravity of several crystals of the Alaskan mineral determined on the Berman microbalance was found to be 6.5 ± 0.2. It was impossible to reconcile the green color, the high refractive index, and the high density of these minerals with the properties of thorite and uranothorite reported in the literature prior to 1950 ($n=1.68$ to 1.72, sp. gr. 4.1 to 5.2). Nevertheless both unknown minerals had the typical thorite form, tetragonal with the prism {110} terminated by the pyramid {111}. Like most completely metamict minerals, prior to ignition they gave the x-ray pattern of an amorphous solid. Unlike many completely metamict minerals, the isotropic thorites do not revert to their original crystalline condition after being heated. Instead, as noted by Robinson (1950), uranothorites after ignition at 800° C. for

half an hour in an inert atmosphere give an anomalous face-centered cubic powder pattern; neither the unknown green mineral from Jamestown, Colorado, nor that from the Ruby district, Alaska, was an exception to this rule. According to J. Berman of the Geological Survey, who is at present engaged in x-ray diffraction studies of the different members of the thorite group, our uranothorites after ignition gave powder patterns nearly identical with the pattern of a thorianite having $a_0 = 5.60$ Å and similar to that given by synthetic ThO_2 prepared by igniting $Th(NO_3)_4$ in a stream of nitrogen. The patterns of heated thorianite and of our heated uranothorites are nearly identical with respect to the relative intensities and spacings of the major lines; they differ in only one particular, namely, several weak lines present in the thorianite pattern are absent from the less intense uranothorite pattern.

Preliminary qualitative spectrographic analyses were made on a few nearly pure grains of each of the two green minerals. Additional separations yielded, after a single hand-picking, a sample of the Jamestown mineral large enough for the semiquantitative work planned, but because of mineral intergrowths, its over-all purity was lower than was thought desirable. In contrast to the Alaskan mineral, pure samples of which could be obtained with little difficulty, the hand-picked Jamestown material consisted largely of grains of the green mineral more or less intergrown with a brown alteration product of much lower refractive index. Grains containing other mineral intergrowths were less abundant but common. The bulk sample was subdivided by a second hand-picking as follows:

1. Mixed green and brown phases free of other impurities, about 30 mg.
2. Green mineral alone plus impurities, about 5 mg.
3. Brown mineral alone plus impurities, about 5 mg.

All mixed green and brown grains containing other impurities were discarded.

The small size of the samples of the separate brown and green phases (2 and 3 above) permitted only a qualitative spectrographic analysis of each plus a quantitative chemical analysis for uranium. The results of these analyses showed that both the green mineral and its brown alteration product were thorium minerals of similar composition (Table 1). The presence of much intergrown sphalerite in both samples accounts for: (1) the high zinc content, (2) the high refractive index (over 2.00) of some of the intergrown material, and (3) the weak sphalerite powder pattern given by the less pure grains of the green and of the brown minerals before ignition. The brown alteration product contained much less uranium (4.2 per cent) than the green (20.0 per cent). It was weakly birefringent, with a mean index of refraction close to 1.64 in white light. After ignition for half an hour in the flame of a blast lamp, it showed a large increase in

TABLE 1. CHEMICAL COMPOSITION, IN WEIGHT PER CENT, OF URANOTHORITES

	Ranges of 4 earlier anal.[1]	South Westland, N.Z. (Hutton 1950)[1]	Placer, Ruby, Alaska. Phair and Shimamoto[2]	Green and brown minerals in fluorite from Blue Jay mine, Colo. Phair and Shimamoto[2]
Th	40.6 –56.6 *c*[3]	55.1 *c*	56.6 *c*	≫10.0 *s*[4]
U	6.7 –14.6 *c*	10.1 *c*	8.2 *c*	11.8 *c*
Si	6.1 – 9.1 *c*	9.1 *c*	>10.0 *s*	>10.0 *s*
Fe	0.9 – 5.3 *c*	1.6 *c*	0.1–1 *s*	1–10 *s*
Ce	0.07– 1.18 *c*	0.9 *c*	Close to 0.1 *s*	<0.1 *s*
Ca	0.7 – 3.1 *c*	0.2 *c*	Close to 0.1 *s*	1–10 *s*
Pb	0.4 – 1.5 *c*	0.5 *c*	Not detected *s*	0.1–1 *s*
H_2O+ } H_2O- }	9.24–11.31 *c*	1.93 *c*	Very low by qual. test	Very low by qual. test
				Green mineral plus inclusions U 20.0 *c* Th, Zn major *s* (qual.) *Brown mineral plus inclusions* U 4.2 *c* Th, Si, Zn major *s* (qual.)

[1] Analyses listed by Hutton (1950, p. 679) converted to percentages of elements.

[2] Analyses by following members of U. S. Geological Survey: chemical analyses by F. S. Grimaldi, Mary H. Fletcher, Irving May, and Harry Levine; semiquantitative spectrographic analyses by C. L. Waring; qualitative spectrographic analyses by Jules Stich.

[3] *c* indicates data obtained by chemical analysis.

[4] *s* indicates data obtained by semiquantitative spectrographic analysis except where followed by (qual.), which indicates that constituents were determined only as major, minor, or trace.

mean refractive index ($\Delta n = +0.14$), which was probably caused by a loss of water, and it turned greenish brown. In its mean index, color, high thorium and silicon contents, low uranium content, probable high water content, and its association with other thorium minerals the brown mineral fits the descriptions of the simple hydrated species (?), hydrothorite, $ThSiO_4 \cdot 4H_2O$(?).

The analytical data obtained on the sample of mixed brown and green thorium minerals free of other impurities are shown in Table 1, last column. Also shown are the corresponding data for (1) the Alaskan green mineral, column 4; (2) definite uranothorite of similar composition described by Hutton (1950) column 3; (3) the ranges in composition shown by four analyses of other uranothorites listed in the older literature column 2. The results of the analyses indicated that the green Alaskan

mineral and the green Jamestown mineral (together with its hydrated brown alteration product) were chemically very similar. Each contained only the constituents typical of uranothorite in amounts within the ranges shown by chemical analyses of uranothorites from other localities. As might be expected, the uranium content of the bulk sample of the Jamestown material (11.8 per cent) was intermediate between the uranium contents of its separate green and brown mineral constituents. The percentage of uranium (20.0 per cent) is high even for the uranium-rich variety, uranothorite, but not excessive. Uranothorites containing as much as 17 per cent uranium (20.0 per cent U_3O_8) are listed in a table of Canadian radioactive minerals compiled by Lang (1950).

Hutton's description (1950, p. 677) of a definite nonmetamict placer uranothorite from South Westland, New Zealand, which had a maximum index of refraction, color, and specific gravity similar to those shown by the Alaskan and Jamestown thorium minerals, provided a useful standard of comparison and explained the differences in physical properties between these and the uranothorites previously described. Hutton pointed out that the earlier descriptions of thorite and uranothorite were based on hydrated metamict material that contained on the average about 10 per cent water. It is not surprising that such material had low indices (generally in the range 1.68 to 1.72) and low specific gravities (generally in the range 5.19 to 5.40). Larsen (1921, p. 144) reported that several thorites from Norway showed a marked increase in index of refraction after ignition for half an hour over a blast lamp, with resulting indices as high as 1.85. Neither the green uranothorite from the Alaskan placer nor that from the Blue Jay mine in Colorado showed an increase in refractive index after ignition for half an hour over a blast lamp; the Alaskan mineral actually showed a slight but probably real decrease in index. Presumably these uranothorites, like Hutton's, are relatively anhydrous; but unlike Hutton's, they are metamict. Recently George (1951, p. 129) described a green uranothorite from several California placers that has physical properties (color, refractive indices, and specific gravity) almost identical with those of the two uranothorites described in this paper; moreover, like these, it is completely metamict and is intergrown with a brown alteration product of lower mean index. The physical properties of the four comparable uranothorites are summarized in Table 2.

Of 18 thin sections of parts of the fluorite breccia from the Blue Jay mine selected for high radioactivity, 6 showed one or more euhedra of green uranothorite, partly replaced by pseudomorphs of yellow-brown hydrothorite. Nearly all of these uranothorite euhedra form inclusions in fluorite. The square basal sections range in length from 0.02 to 0.10 mm., and the prismatic sections are only slightly longer. Within large grains

of fluorite, halos that have maximum widths of 41 microns corresponding to the calculated range in fluorite of high-energy alpha particles emitted by Po^{212} (Th C′) serve as conspicuous indicators of uranothorite (Fig. 1). Alpha-sensitive nuclear emulsions applied to uncovered thin sections and developed in the manner described by Stieff and Stern (1950, p. 9) showed, under suitably high magnification, swarms of alpha tracks di-

Table 2. Comparison of Physical Properties of Four Uranothorites

	S. Westland, N. Z. (Hutton 1950)	California (George 1951)	Ruby, Alaska (Phair, Shimamoto)	Blue Jay mine, Colo. (Phair, Shimamoto)
System	Tetragonal	Tetragonal	Tetragonal	Tetragonal
Specific gravity	6.7±0.05	6.36	6.5±0.2	—
Color in oils	Green (dichroic)	Blue green	Greenish	Green
Optical characteristics	Uniaxial +	Isotropic (metamict)	Isotropic (metamict)	Isotropic (metamict)
Refractive indices	$nX=1.815$ $nY(\max)=1.850$	$n=1.82$–1.87	$n=1.86\pm0.01$	$n=1.86\pm0.01$
X-ray diffraction patterns	—	—	Anom. f-c cubic $a=5.60$ Å	Anom. f-c cubic $a=5.60$ Å

rected radially outward from the uranothorite cores of the halos. Thorium halos in fluorite, unlike uranium halos, have not been previously reported. These halos, together with the more abundant uranium halos (maximum widths of 31 microns) were found to be especially numerous in parts of the fluorite darkened by radioactivity.

Discussion

In thin section most of the uranothorite is associated with relatively unsheared fluorite and is almost completely unsheared, retaining its sharp euhedral outlines (Fig. 1). The lack of visible crushing indicates that the uranothorite crystals were not introduced into the fluorite mechanically in the course of the brecciation. The close association of the uranothorite with a fluorite-carbonate-sulfide assemblage, and in particular the tendency of the uranothorite to form inclusions in the fluorite, is strong evidence of a hydrothermal origin. Apparently all thorites and uranothorites previously described in the literature have been found either as residual concentrates in placers or in situ in granitic igneous

rocks, especially pegmatites. The one exception to this rule is a very doubtful occurrence of a single microscopic crystal of thorite (?) noted by Gordon (1944, p. 329) in a sample from the high-temperature tin veins of Llallagua, Bolivia. Its tentative identification as thorite was based on morphological measurements; its interfacial angles were intermediate between thorite and xenotime but closer to thorite.

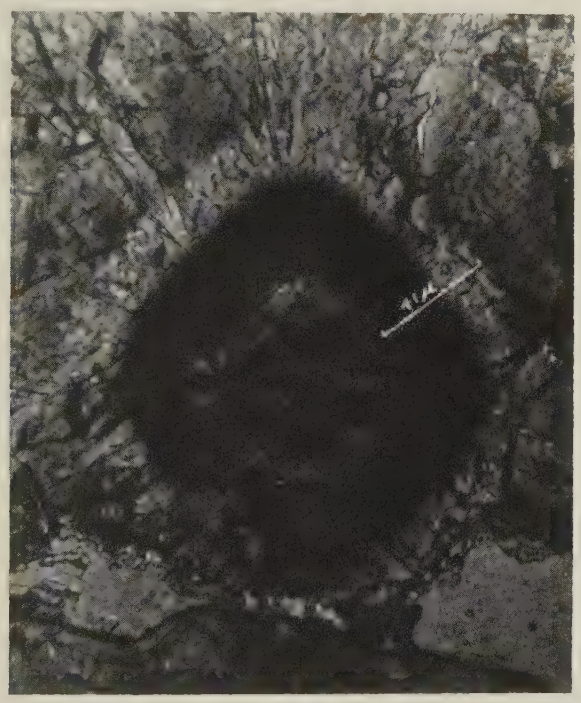

FIG. 1. Thorium halo surrounding euhedral uranothorite inclusion in fluorite. A basal section of uranothorite forms the center of a thorium halo consisting of a semiopaque inner "ring" and an outer bleached "ring." The width of the halo is 41 microns as measured from the inner boundary of the darkened zone to the outer boundary of the bleached zone. (Uncrossed nicols.)

The temperatures at which the Jamestown uranothorite was deposited may have reached the mesothermal range but were certainly no higher. The Jamestown fluorite deposits are at the northern end of the Front Range mineral belt—a region wherein the ore deposits assume many epithermal characteristics in contrast to the characteristics of deposits at the southern end of the belt, where mesothermal conditions prevailed (Lindgren, 1933, p. 635). Lindgren lists the Jamestown fluorite deposits with mesothermal ores, and Goddard (1946, p. 19) noted that enargite and tennantite were among the early sulfides in many of the ores. However, the brecciation that accompanied the latest stages of fluorite min-

eralization left open spaces and could have taken place only under relatively near-surface conditions.

Previously thorite has been considered a rare mineral, but it seems likely that, once the properties of the unaltered mineral become more widely known, it will be found rather widely distributed not only in "high-temperature" granitic pegmatites and in placers but also in many hydrothermal veins.

The rare-earth content of many fluorites is relatively high; samarium, neodymium, and cerium contents in a fluorite described by Chang (1945) ranges from 0.1 to 1.0 per cent. Heinrich (1948, p. 64) found that "fluorite and rare-earth minerals are associated in 19 of the 22 pegmatite districts in North America from which fluorite has been reported." Th^{4+} has many chemical properties in common with the rare earths, and its ionic radius is in the same range. The oxides UO_2, ThO_2, and CeO_2 and the fluoride CaF_2 all have the face-centered cubic "fluorite" lattice with the unit cell close to 5.50 Å. The preference of the uranothorite and fluorite for the same geochemical environment is, therefore, readily explained by the Goldschmidt rule. It seems probable that thorium minerals as well as rare-earth minerals will prove to be of widespread, but scattered, distribution not only in fluorite-bearing pegmatites but also in many fluorite-rich hydrothermal deposits.

References

Chang, Ting-Chao (1945), Chemical studies on Chinese fluorites III. *Shanghai Sci. Inst. Jour.*, new ser., **2**, no. 5, 223–230.

George, D. R. (1951), Thorite from California, a new occurrence and variety: *Am. Mineral.*, **36**, 129–132.

Goddard, E. N. (1946), Fluorspar deposits of the Jamestown district, Boulder County, Colo.: *Colorado Sci. Soc. Proc.*, **15**, no. 1, 47 pp.

Gordon, S. G. (1944), The mineralogy of the tin mines of Cerro de Llallagua, Bolivia: *Acad. Nat. Sci. Philadelphia Proc.*, **96**, 279–359.

Heinrich, E. W. (1948), Fluorite-rare earth mineral pegmatites of Chaffee and Fremont Counties, Colo.: *Am. Mineral.*, **33**, 64–75.

Hutton, C. O. (1950), Studies of heavy detrital minerals: *Geol. Soc. America, Bull.* **61**, no. 7, 677–682.

Lang, A. H. (1950), Summary account of Canadian uranium deposits, Table I: *Canada Geol. Survey.*

Larsen, E. S., Jr. (1921), The microscopic determination of the nonopaque minerals: *U. S. Geol. Survey, Bull.* **679**, 294 pp.

Lindgren, W. (1933), Mineral Deposits, 4th ed., McGraw-Hill Book Co., 930 pp.

Robinson, S. C. (1950), *Canada Geol. Survey Memorandum.*

Stieff, L. R., and Stern, T. W. (1950), The preparation of nuclear-track plates and stripping films for the study of radioactive minerals: *U. S. Geol. Survey Trace Elements Investigations, Rept.* **127**, 16 pp.

Manuscript received Sept. 24, 1951

TEMPERATURE AND HEAT OF REACTION CALIBRATION OF THE DIFFERENTIAL THERMAL ANALYSIS APPARATUS

Isaac Barshad, *University of California, Berkeley, California.*

Abstract

Differential thermal curves representing one or several substances of known melting or inversion points, and of known heats of fusion or decomposition are proposed as a means for a direct temperature and heat of reaction calibration of the differential thermal analysis apparatus. Excellent agreement between determined and calculated heats of reaction of several substances attested to the validity of the derivation relating peak area of a thermal break to the heat of reaction causing the break. The proposed calibration imparts to *d.t.a.* curves constant parameters and consequently curves obtained with different instruments become comparable. The heat of reaction calibration enables a direct determination of the heat quantities involved in desorption or sorption of liquids on clay minerals—namely *the integral heat of desorption and the integral net heat of desorption.*

It is widely recognized that due to several factors inherent in the instrumentation of the *d.t.a.* apparatus (1, 5), the *d.t.a.* curves of minerals are not strictly constants. The deviation from constancy appears to be in all the parameters defining the thermal breaks in a *d.t.a.* curve—namely, initial temperature, peak temperature, peak height, peak range, and peak area. Of these parameters, the initial temperature—the lowest temperature at which the reaction could occur—and the peak area—which is proportional to the heat involved in the reaction causing the thermal break—(6, 10) are the most important. A simple calibration, therefore, of the *d.t.a.* apparatus which would yield constants for these two parameters would enhance greatly the usefulness of *d.t.a.*

The methods in use for recording the temperature scale on a *d.t.a.* curve involve generally a temperature thermocouple in circuit with a temperature recorder which are entirely separated from the differential thermal recording circuit.

Only a limited amount of work has appeared suggesting methods for calibrating the *d.t.a.* apparatus for evaluating heats of reaction. Wittels' method (11, 12) of using the decomposition of $CaCO_3$ as a means for calibration is so far the most useful, but it is limited to a narrow range of temperature and small amounts of material.

The purpose of the present paper is to suggest methods whereby the differential thermal circuit itself may be utilized to obtain calibrated temperature and heat of reaction scales. The methods consist in obtaining *d.t.a.* curves of organic and inorganic substances of known melting and/or inversion points and of known heats of fusion and heats of decomposition. The usefulness of such *d.t.a.* curves lies in that at the instant of melting, inversion, or decomposition, an endothermic break ap-

pears the initial point of which marks the temperature of fusion, inversion, or decomposition and the area of which is proportional to the heat of fusion, inversion or decomposition. In the present paper substances used for the heat of reaction calibration are termed temperature indicators.

Experimental

Temperature Calibration

The equipment used was as follows: the sample holder consisted of a rectangular nickel block with dimensions 23×23×15 mm. and with two holes—7 mm. in diameter and 13 mm. in depth—capable of holding 0.55 gm. of tightly packed Al_2O_3. A cover for the block was not used. Platinum —platinum (90%) rhodium (10%) thermocouples were employed and the recorder consisted of a reflecting galvanometer on photographic paper. All of the experiments were conducted with the galvanometer adjusted to a sensitivity so that at 100° C. a temperature difference of 10° C. produced a deflection of 10 cm.

The base line on which to record the temperature scale is obtained while the galvanometer is resting at the null position and the furnace turned off. The spot of light marking the photographic paper, through its reflection in the galvanometer mirror, is turned on while the drum holding the photographic paper is rotated. A short pause at two or three positions leaves points through which the base line may be drawn.

For a given thermal reaction the galvanometer may be made to deflect the spot of light either upward or downward from the base line depending on the position of the reacting sample with respect to the two thermocouples. In general practice in *d.t.a.*, the deflection due to an endothermic reaction is directed downward and that due to an exothermic reaction upward from the base line. However, in the experiments reported herein, the deflection for a given thermal reaction was made in either direction of the base line depending solely on the position of the sample with respect to the two thermocouples.

For a thermal reaction to be of value as a fixed temperature reference point, it should impress on a *d.t.a.* curve an abrupt break.

To find a method whereby the whole temperature scale could be established with one *d.t.a.* curve having several temperature reference points, several of the factors which may affect the position of a fixed temperature-reference-point on a *d.t.a.* curve were investigated. These were: (1) The rate of heating, (2) The initial temperature, and (3) The existence of temperature differences within the sample holes due to position with respect to the thermocouples.

(1) In most *d.t.a.* apparatus the rate of heating determines directly

the linear dimensions of the temperature scale. A change, therefore, in the rate of heating would alter the temperature scale. Maintenance of a characteristic rate of heating will insure usually a constant temperature scale. Occasionally, however, due to variation in line voltage, the rate of heating alters somewhat, and consequently the scale also alters. If such a situation persists a method will be suggested whereby the temperature scale may be recorded directly on the *d.t.a.* curve of a test sample.

(2) Variations in the initial temperature of the furnace would affect the time of occurrence of a reaction which marks a temperature reference point. Consequently, the position of the point on a scale would vary with the initial temperature. This difficulty may be eliminated by starting the temperature scale from a fixed temperature reference point. Such a reference point is found in the first inversion reaction of NH_4NO_3 occurring at 32° C. Where summer temperatures exceed 32° C. the second inversion point of NH_4NO_3 occurring at 85° C. may be chosen as the initial reference point of the scale. By this method any desired portion of the temperature scale may be delineated by a judicious choice of reference points.

(3) To ascertain the existence of temperature differences in the sample holes due to position with reference to the thermocouple a *d.t.a.* was made of small amounts of an indicator placed at two positions in the sample hole. The appearance of only one reference point in the *d.t.a.* curve as in the curve of $AgNO_3$ (Curve *A*, Fig. 1) indicates that at any given moment the temperature is uniform throughout the sample hole. The same method was utilized to ascertain whether the two differential thermocouples are being heated at the same rate. In this case, however, the same indicator was placed in both sample holes but with one of the holes containing a slightly larger amount of the indicator than the other. The appearance of only one reference point for each reaction as in the curve for NH_4NO_3 (Curve *B*, Fig. 1) indicates that the rise in temperature is identical for the two holes.

The uniform rise in temperature within the sample holes during *d.t.a.* enabled the development of a method for ascertaining the whole of the temperature scale with a single *d.t.a.* curve. The method consists in making a *d.t.a.* simultaneously of several indicators which are placed either around one or both of the differential thermocouples in narrow layers separated by Al_2O_3 as shown in Figs. 3 and 4. The resulting *d.t.a.* curve possesses several thermal breaks which mark the fixed temperature reference points characteristic of each indicator.

The amount of each indicator to be used for such an analysis was found to depend upon the sensitivity of the *d.t.a.* apparatus, the magnitude of

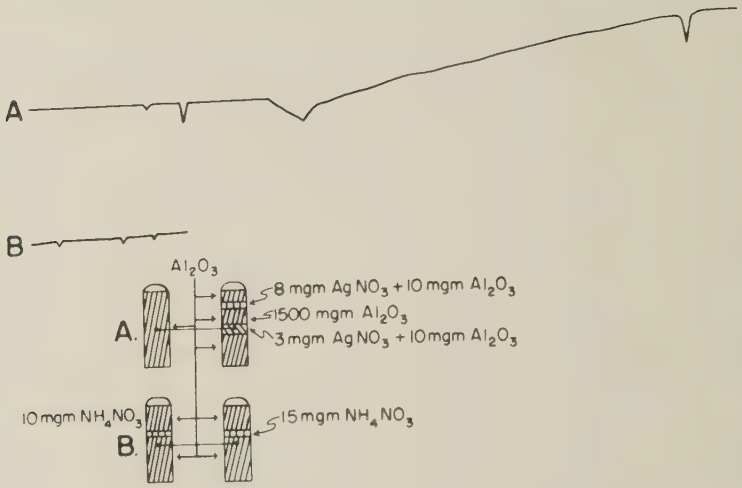

FIG. 1. *D.t.a.* curves of $AgNO_3$ placed at two positions in the same sample hole and of NH_4NO_3 placed at the two thermocouples.

the heat of fusion or inversion of the indicator, and upon the position of the indicator in the sample hole with respect to the thermocouple junction. For example, it was found that an instrument having a sensitivity of a 10 cm. deflection for a 10° C. difference in temperature will register a large enough thermal break to mark a temperature reference point with an amount of 2 mgm. of an indicator having a heat of fusion or inversion of 20 to 30 calories per gram when placed right around the thermocouple junction. However, placing the indicator at a distance of about 4 to 5 mm. from the junction increased the required amount of indicator from 2 to 10 mgm. The indicators should be powdered before use and when placed in direct contact with the thermocouples they should be mixed with about 10 mgm. of Al_2O_3 to prevent them from sticking to the junction and wires upon fusion.

TABLE 1. PEAK AREA OF THE ENDOTHERMIC BREAK IN *d.t.a.* CURVES OF 50 MGM. OF KAOLINITE PLACED AT DIFFERENT POSITIONS* WITH RESPECT TO THE THERMOCOUPLE

Position of sample	Peak area
	$cm.^2$
5.5 mm. above thermocouple	0.68
3.0 mm. above thermocouple	1.80
0.0 mm. from thermocouple	3.24
3.5 mm. below thermocouple	1.21
6.0 mm. below thermocouple	0.40

* To place sample in desired position proper amounts of Al_2O_3 were used as the "filler" for the bottom and top portions of the sample hole.

The dependence of the magnitude of the thermal break of a given amount of indicator upon its distance from the thermocouple junction is shown in Fig. 5 and Table 1. It is seen that the magnitude of the deflection or the peak area are smaller the greater the distance of the reacting substance from the thermocouple junction. With the size holes used in the present experiments, the endothermic reaction occurring in the indicators placed in the bottom of the hole or near its top hardly induced a thermographic response. An exception, however, to this observation are the large exothermic breaks in the *d.t.a.* curves of all of the NH_4NO_3 samples placed below the thermocouple junction. The cause for this exception appears to be in the nature of the exothermic reaction responsible for this exothermic break. The reaction involves a platinum catalyzed oxidation of NH_3 liberated during the decomposition of NH_4NO_3. The presence of larger exothermic breaks in the curves of the samples placed below the thermocouple than in those placed above the thermocouple, results from the larger amounts of NH_3 which must diffuse upwards past the thermocouple from the former than from the latter samples.

It would appear, therefore, that in using NH_4NO_3 as an indicator, either with other indicators or with unknown subtances, to mark the beginning of the temperature scale it would be advisable to limit the exothermic reaction to a minimum so as not to mask any other reaction which might occur in that temperature range. This can be accomplished by placing the NH_4NO_3 about 2 to 3 mm. above the thermocouple junction and limit its amount to about 2 or 3 mgm. For marking the temperature scale in the *d.t.a.* curves of test samples it was found more desirable to place the NH_4NO_3 with the reference sample rather than with the test sample.

The substances found useful for the temperature and the heat of reaction calibration are listed in Table 2, together with their melting and/or inversion temperature points, their heats of fusion or inversion, and the amounts needed in calibration. The individual *d.t.a.* curves of some of these substances are shown in Fig. 2. Among the substances tested, NH_4NO_3 and $AgNO_3$ are among the most useful. The usefulness of NH_4NO_3 lies in the temperature range below 170° C.; it is particularly valuable as an indicator for marking the beginning of the temperature scale. The usefulness of $AgNO_3$ lies in its ability to mark three temperature points, namely 160° C., 212° C., and 960.5° C., from which the whole temperature scale above 160° C. may be constructed if the rate of heating is constant throughout this temperature range. AgI and Ag_2SO_4 are also among the more useful indicators, for they too mark more than one temperature point. AgI marks points at 147° C. and 554° C., and Ag_2SO_4 marks points at 432° C., 652° C., and 960.5° C.

Table 2. Melting and Inversion Temperatures and Heats of Fusion of Substances Useful for Temperature and Heat of Reaction Calibration of the *d.t.a.* Apparatus (3, 7)

Substance	Point*	Temperature	Heat of fusion	Amount for temperature calibration	Amount for heat reaction calibration
		°C.	cal./gm.	mgm.	mgm.
NH_4NO_3	I	32		2–10	
NH_4NO_3	I	85			
NH_4NO_3	I	125			
NH_4NO_3	M	170			
KNO_3	I	128		2–10	
m-Dinitrobenzene	M	90	24.7	2–10	50–100
o-Dinitrobenzene	M	117	32.3	2–10	50–100
Benzoic Acid	M	122	33.9	2–10	50–100
$AgNO_3$	I	160		2–10	
$AgNO_3$	M	212	16.7	2–10	50–100
Ag (from $AgNO_3$)	M	961	25.0	2–10	50–100
AgI	I	147		20–40	
AgI	M	552		20–40	
Ag_2SO_4	I	432		20–40	
Ag_2SO_4	M	652		20–40	
Ag (from Ag_2SO_4)	M	961		20–40	
AgCl	M	307		1–10	50–100
$NaNO_3$	M	314	45.3	1– 5	50–100
$NaMo_2O_4$	I	642		5–10	
	M	687		5–10	
NaCl	M	804		2– 5	20– 50
K_2SO_4	I	583		5–10	
Quartz	I	573		10–50	

* Inversion = I, Melting = M.

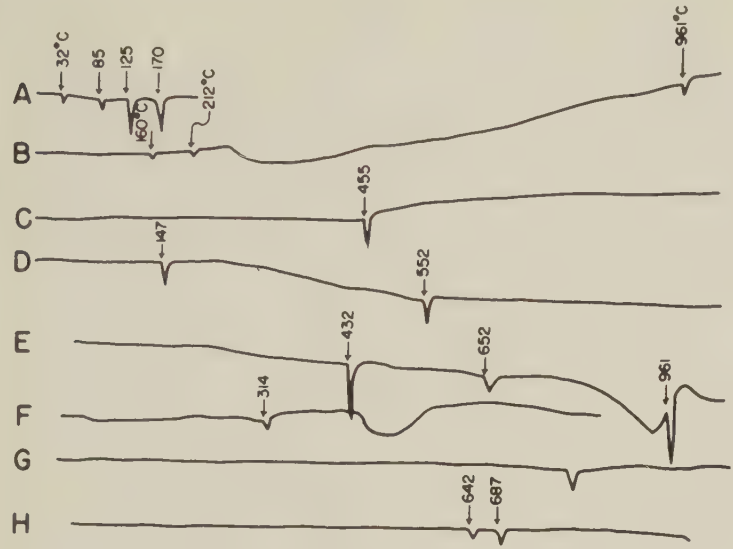

FIG. 2. *D.t.a.* curves of salts useful for temperature calibration. The salts were dispersed in 10 mgm. of Al_2O_3 and centered around the thermocouple.

A. 10 mg. NH_4NO_3
B. 3 mg. $AgNO_3$
C. 2 mg. AgCl
D. 15 mg. AgI
E. 20 mg. Ag_2SO_4
F. 2 mg. $NaNO_3$
G. 2 mg. NaCl
H. 3 mg. $Na_2Mo_2O_4$

When the indicators are mixed prior to *d.t.a.* some retain their identity whereas others do not—the latter assume forms which are the result of interaction of the indicators or their reference points may disappear completely. Thus, when $AgNO_3$, AgCl, AgI, Ag, and quartz are mixed, the identity of each is retained but when NH_4NO_3, AgCl, $AgNO_3$, and $Na_2Mo_2O_4$ are mixed, the former two retain their identity, whereas the latter two do not. It would appear, therefore, that those indicators which do not interact may be mixed prior to anlaysis but those which do should be placed in the sample holes as single layers separated by Al_2O_3. Some of the mixed indicators tested are shown in Figs. 3 and 4.

The method of placing the temperature indicators in narrow layers has its greatest utility in making it possible to register on a *d.t.a.* curve of a test sample the whole or any desired part of the temperature scale. By this means it becomes possible to define a thermal break of a test sample very accurately regardless of inconsistencies which may occur in the *d.t.a.* apparatus. Several such marked curves were obtained of various minerals and with various rates of heating (Figs. 6*a*, 6*b*, 6*c*, and 6*d*). These curves show that the rate of heating had no effect on the temperature defining the initial thermal breaks.

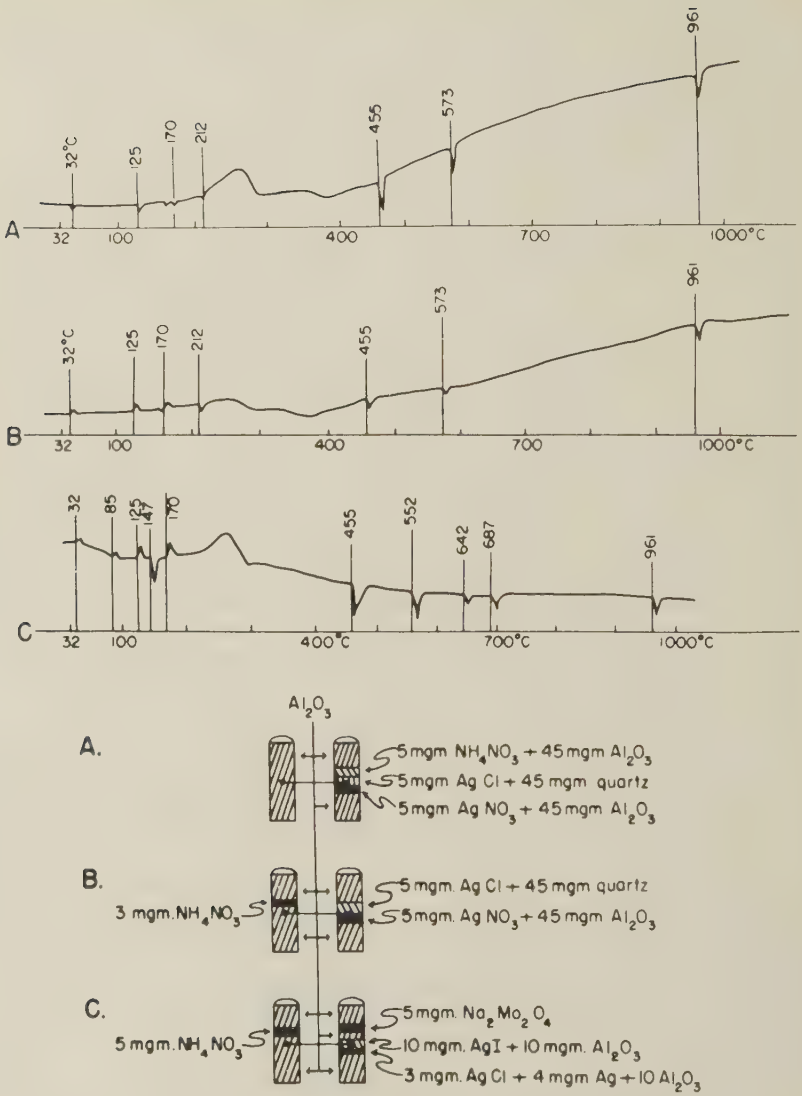

FIG. 3. Curves resulting from simultaneous *d.t.a.* of several substances placed in layers in the sample holes.

The temperature indicators were also found useful in evaluating the sensitivity of the *d.t.a.* apparatus. The method consists in placing in one of the sample holes a material which produces a large endothermic break, in the center of which, right around the thermocouple, is embedded an indicator which registers a temperature reference point near the peak of the endothermic break of the surrounding sample. At the same time one or two indicators are embedded in the reference material which

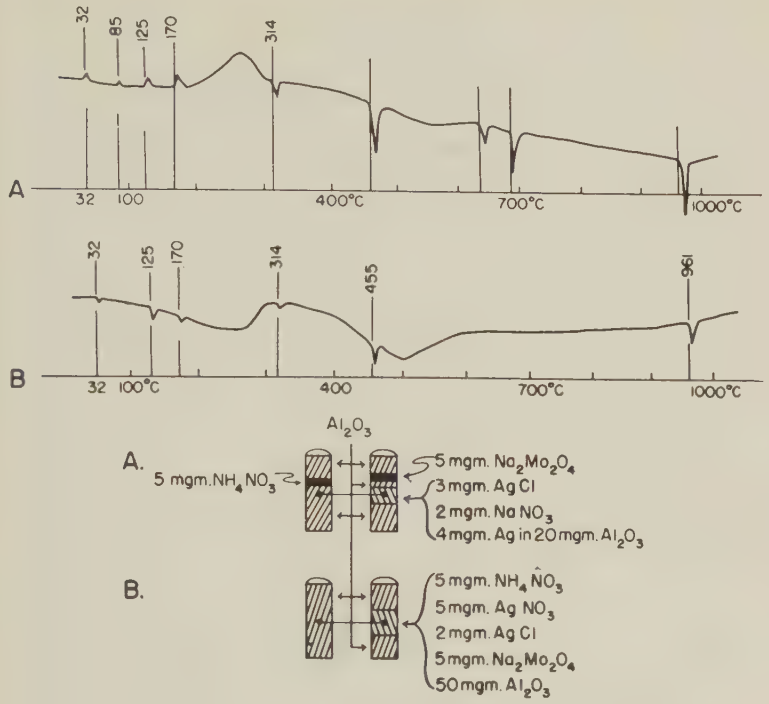

FIG. 4. Curves resulting from simultaneous *d.t.a.* of several substances mixed prior to analysis.

register one reference point preceding and one following the reference point registered by the indicator embedded in the test sample. From the former two points, the temperature in the inert sample at the time the latter point is registered may be ascertained. This determination yields the temperature difference between the thermocouples caused by the endothermic reaction in the test sample. The sensitivity is then obtained by dividing this temperature difference to the peak height at that point in the curve. Ca-montmorillonite was found useful as the test sample at the low temperatures and kaolinite at the higher temperatures. The two temperature points which AgI registers in the *d.t.a.* curve enables it to act as the indicator to be embedded in both of these test samples. The three temperatures which NH_4NO_3 registers make it the suitable indicator to be embedded in the inert sample that is coupled with the Ca-montmorillonite. AgCl and $Na_2Mo_2O_4$ placed in two layers around the junction in the inert material are the suitable indicators to be coupled with the kaolinite. Figure 7 illustrates the curves obtained with these materials and the calculations involved in the determination of the sensitivity.

The sensitivity at 100° C. may be determined without indicators by

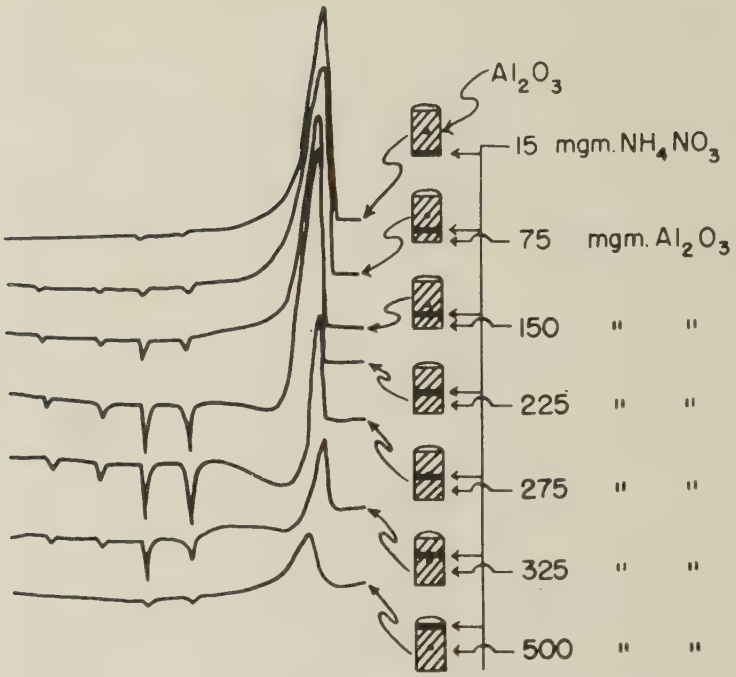

FIG. 5. *D.t.a.* curves of 15 mgm. of NH_4NO_3 placed at different positions with respect to the thermocouples.

the following method which requires two operators. Each of the thermocouples, while in the *d.t.a.* circuit, is placed in a separate beaker of boiling water standing on a small electric hot plate by the *d.t.a.* apparatus. While one operator places a precision mercury thermometer in one of the beakers of boiling water, the other operator observes the galvanometer until it attains a steady state at the null position. A thin sheet of asbestos is then placed under the beaker holding the thermometer. The drop in temperature in the beaker is read off and the change in the position of the light beam is marked on a sheet of paper placed in the position normally occupied by the photographic paper. To measure the sensitivity in the opposite direction of the null point, the foregoing procedure is repeated but with the second beaker being cooled while the first one is kept boiling.

These results are plotted as temperature differences vs. centimeters-deflection curves and converted into e.m.f. vs. centimeters-deflection curves with the aid of the standard calibration tables (4) for the thermocouples in use. These curves together with e.m.f. vs. hot-junction-temperature curves for various temperature differences between the thermo-

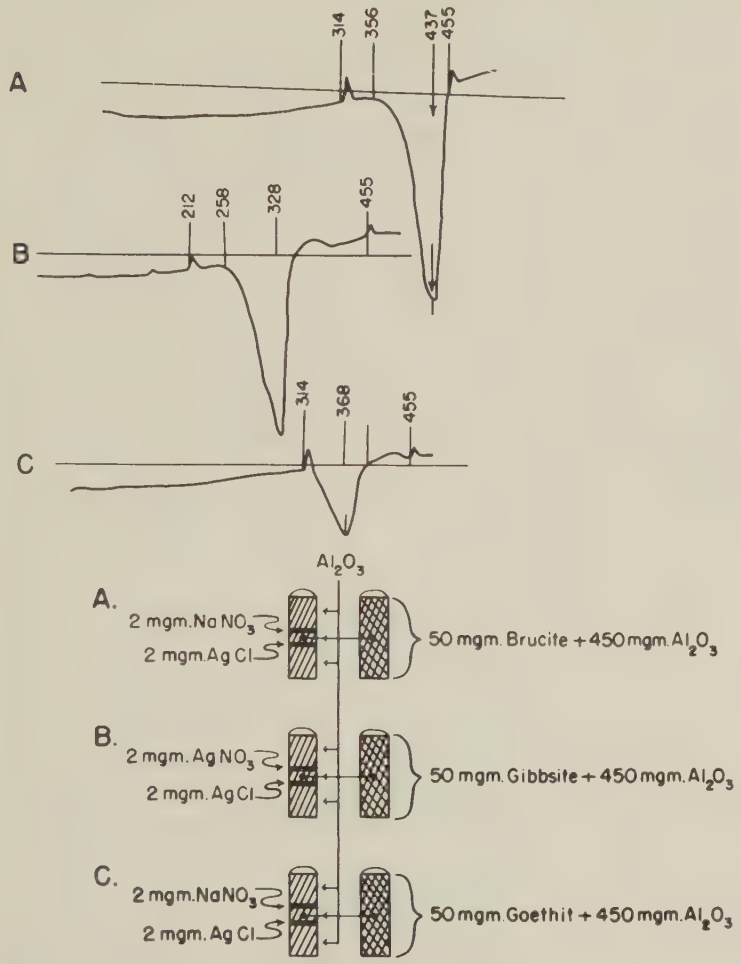

FIG. 6*a*. *D.t.a.* curves of brucite, gibbsite, and goethite with impressed temperature-reference points.

couples (Fig. 8) can be used to determine the sensitivity of the *d.t.a.* instrument at any hot-junction temperature other than 100°C. The determination consists in converting the extent of deflection at a given temperature into e.m.f. values by using the e.m.f. vs. centimeter-deflection curves; the e.m.f. values can then be converted into a temperature difference with the aid of the e.m.f. vs. hot-junction-temperature curves for various temperature differences. The following example illustrates such a determination of the sensititivity at 550° C. from the known sensitivity at 100° C. for a 10 cm. deflection taking place at 550° C. Since a

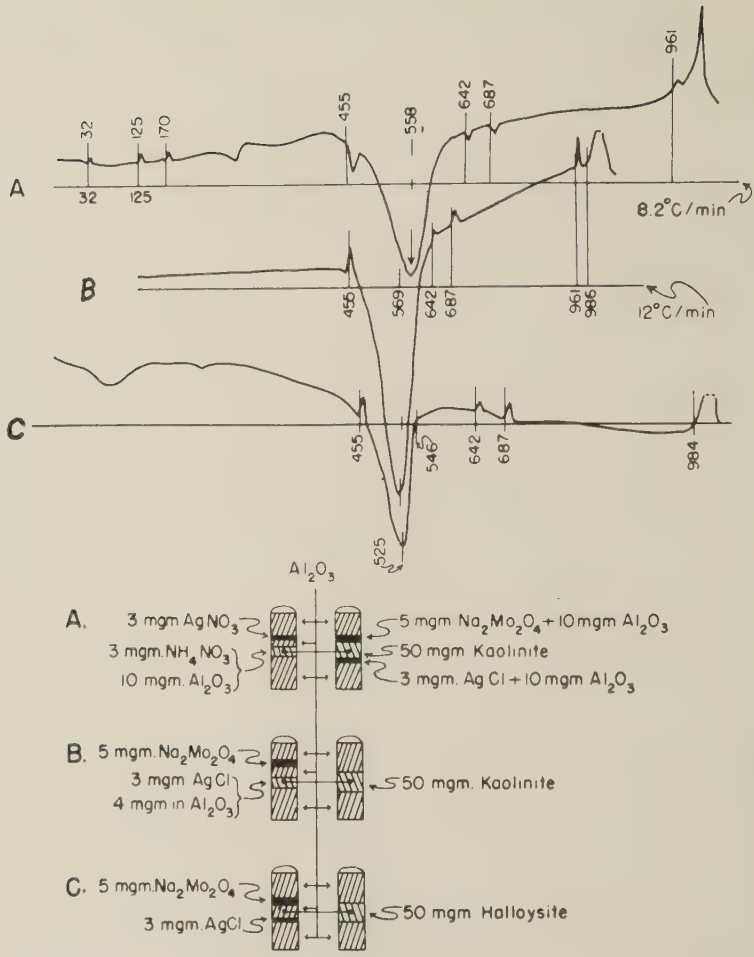

FIG. 6*b*. *D.t.a.* curves of kaolinite and halloysite with impressed temperature-reference points.

given deflection is produced by a given e.m.f. regardless of the temperature at which it takes place, it is found from the calibration curves obtained at 100° C. that the 10 cm. deflection is produced by a e.m.f. of 0.143 millivolt. At a hot-junction temperature of 100° C. such a e.m.f. represents a 10° C. difference in temperature. But at a hot-junction of 550° C., a 10° C. difference in temperature produces an e.m.f. of 0.200 millivolt. Therefore an e.m.f. of 0.143 millivolt at 550° C. is produced by a temperature difference of $10 \times 0.143/0.200$ or 7.2° C. The sensitivity, therefore, at 550° C. is equal to 7.2° C. per 10 cm. deflection.

Two temperatures are associated with the peak of a thermal break in

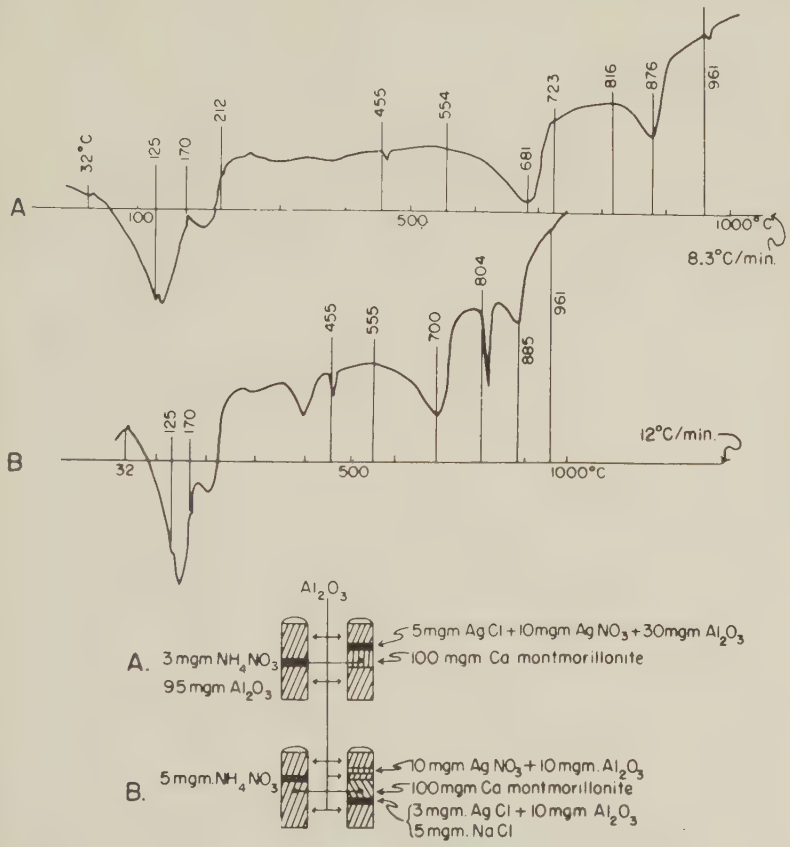

FIG. 6c. *D.t.a.* curves of a Ca-montmorillonite with impressed temperature-reference points.

a *d.t.a.* curve of a test sample—the temperature in the reference sample and the temperature in the test sample. Knowing the sensitivity of the instrument and the temperature scale for the reference material, both of these temperatures may then be determined.

Heat of Reaction Calibration

The dependence of the peak area on the heat of reaction in *d.t.a.* curves was derived theoretically by several investigators (1, 6, 10), therefore, the derivation need not be repeated here. Although the peak area representing a reaction in a definite amount of material is affected by various factors inherent in the *d.t.a.* apparatus (1, 5)—such as rate of heating, nature of sample holder, size of holes in sample holder, nature of thermocouples, and sensitivity of galvanometer—nevertheless a heat of reac-

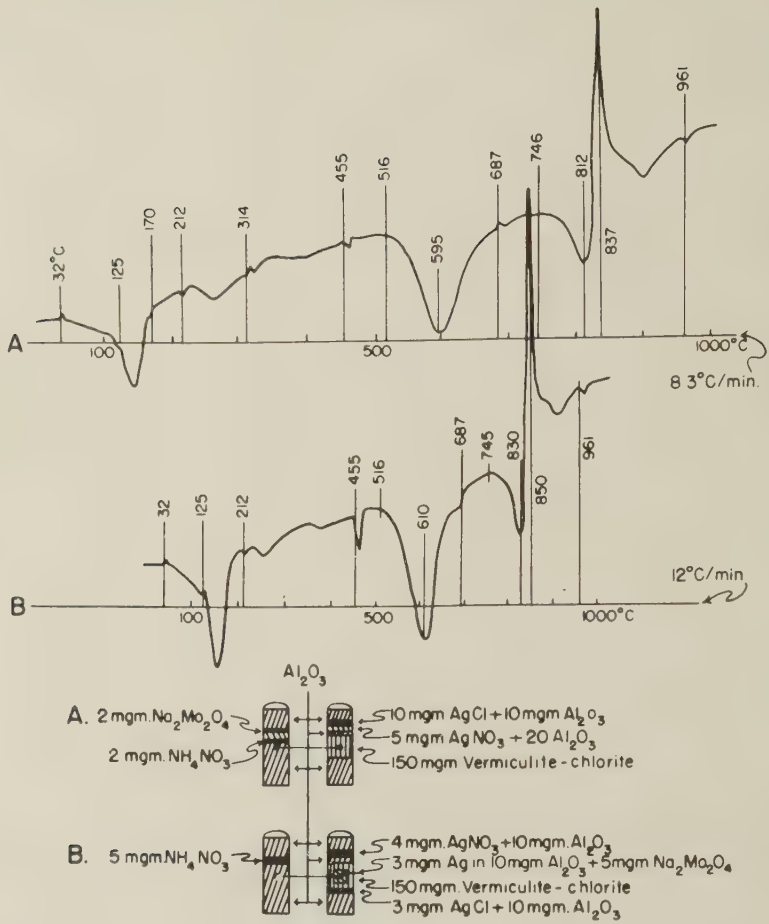

FIG. 6*d*. *D.t.a.* curves of a vermiculite-chlorite with impressed temperature-reference points.

tion determination, may be made possible provided the conditions existing in the *d.t.a.* apparatus at the time of calibration are maintained during analysis of unknown samples.

Some of the indicators found suitable for temperature calibration were found also suitable for the heat of reaction calibration, but to obtain accurately measurable peak areas much larger amounts of the indicators wree needed.

Since the indicators are mixed with an inert material, like Al_2O_3, to prevent them from sticking to the thermocouple junction at time of fusion, an investigation was made of the effect of the proportionality between the indicator and the inert substance on the peak area.

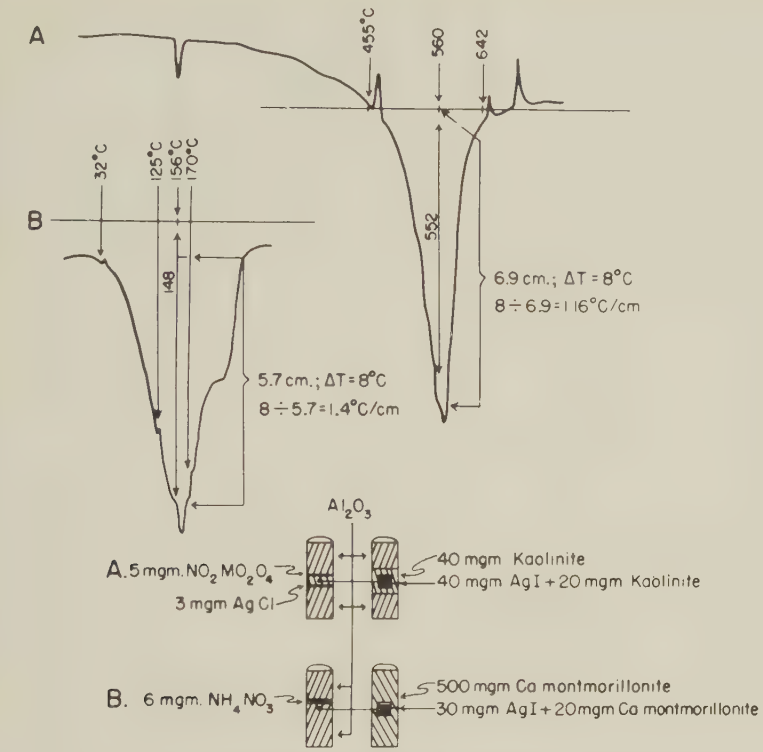

FIG. 7. *D.t.a.* curves of a Ca-montmorillonite and a kaolinite with impressed temperature-reference points suitable for measuring the sensitivity of the *d.t.a.* apparatus.

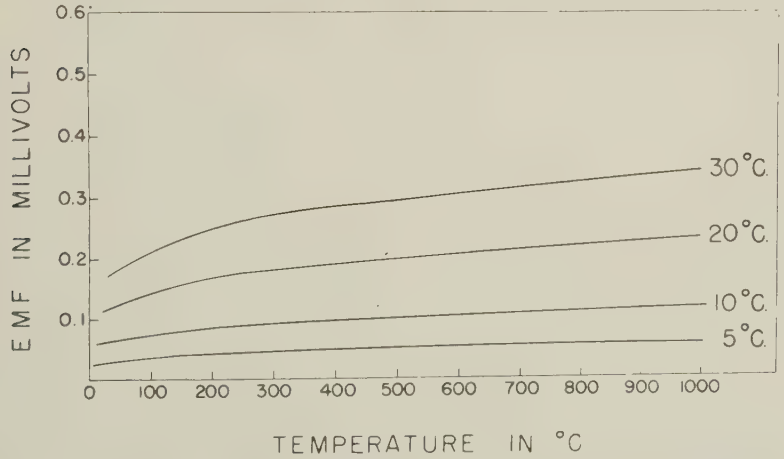

FIG. 8. E.M.F. vs. hot-junction-temperature curves for temperature differences of 5°, 10°, 20°, and 30° C. between the hot and cold thermocouples consisting of Pt-Pt (90%) Rh (10%).

Two methods were employed to obtain various proportions between the indicator and the inert substance. On the one hand a given amount of indicator was dispersed in increasing amounts of Al_2O_3 and consequently the mixture occupied an increasing volume. On the other hand

Table 3. Peak Area of the Endothermic Break in the *d.t.a.* Curves of 50 mgm. of Kaolinite Dispersed in an Increasing Volume and Centered* Around the Thermocouple

Volume of sample	Peak area
cm.^{3}	cm.^{2}
.040	4.06
.130	3.02
.220	2.55
.310	2.23
.400	1.94
.490	1.62

* To center the sample around the thermocouple proper amounts of Al_2O_3 were used as the "filler" for the bottom and the top portions of the sample hole.

increasing amounts of indicator were dispersed in decreasing amounts of Al_2O_3 in such manner that the mixture retained a constant volume. The results of the first method are shown in Table 3 and those of the second

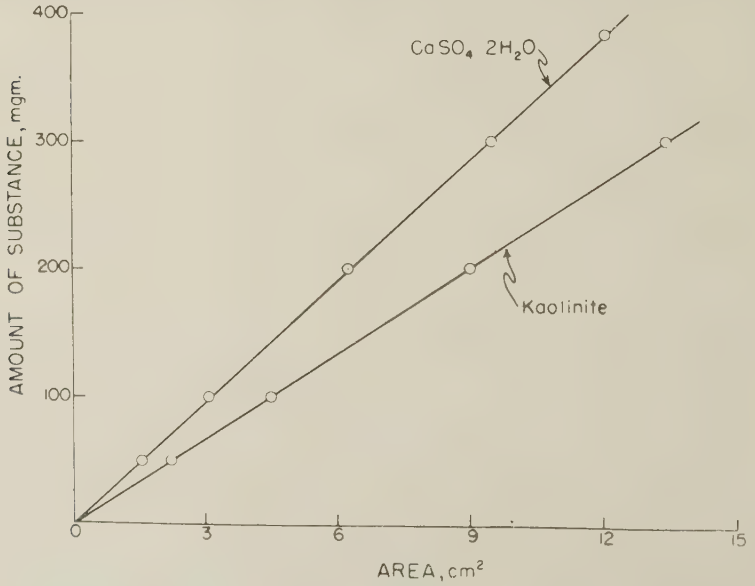

Fig. 9. Peak areas of the endothermic breaks in *d.t.a.* curves of various amounts of kaolinite and $CaSO_4 \cdot 2H_2O$.

method are shown in Figure 9. It is seen that the peak area for a given amount of indicator decreased as the volume which it occupied increased (Table 3), but the peak area for a given amount of indicator remained constant when dispersed in a constant volume. The decrease in the first instance is probably brought about by the increase in distance from the thermocouple of a portion of the indicator as it occupied a larger volume. For, as was shown previously, the peak area and amplitude for a reaction in a given amount of substance is inversely proportional to the distance of the indicator from the thermocouple. Consequently it would appear that the proportionality between the indicator and the inert substance is of little significance as long as the indicator is dispersed in a constant volume; and that in determining a heat of reaction in an unknown sample it should be confined to the same volume and placed in the same position with respect to the thermocouples as the indicator during calibration.

Since the indicators and test samples may vary considerably in their real and apparent densities, the dispersion in a constant volume may be achieved by first placing the desired amount of a substance in a hole of desired volume (made in piece of metal) and filling the remainder of the hole with Al_2O_3 which is packed to the same tightness as for *d.t.a.* The contents are then removed from the hole, mixed thoroughly and placed in the hole of the sample holder of the *d.t.a.* apparatus for analysis.

In using *d.t.a.* to estimate minerals like kaolinite, calcite, or others in unknown samples, the calibration curves of the standard minerals should appear as a plot of the actual quantity of the mineral used vs. the peak area obtained. The peak area in a *d.t.a.* curve of an unknown sample determined from such a calibration curve would correspond, therefore, to a definite quantity of the known mineral. To express this quantity on a percentage weight bases, the amount of the unknown sample used in *d.t.a.* must be known.

The absence of a thermographic response to a thermal reaction in the portion of the sample placed at a large distance from the thermocouple junction, as was shown previously, would suggest that this portion of the hole may be eliminated without affecting the intensity of the thermographic response. Seemingly the hole in the sample holder may be limited to such a size that a reaction in the remotest portion of the sample from the thermocouple would register a fairly strong thermographic response. In other words a small hole would be preferable to a larger one particularly when the recording instrument is of high sensitivity.

Since the sensitivity of thermocouples varies with the temperature, the heat involved in a reaction occurring in a test sample at a specific temperature range, may best be evaluated by using in calibration an indicator registering a thermal reaction at about the same temperature as that of the test sample. Moreover, in order that the calibration with

a given indicator should apply to a fairly wide range of temperature. small amounts of the indicator rather than large ones should be used so that only small differences in temperature between the thermocouples would develop. For, as seen in Fig. 8, the smaller the difference in temperature between the thermocouples the smaller the variation in sensitivity of the thermocouples with temperature.

The following substances with known heats of fusion were found useful for the heat of reaction calibration: *m*-, *o*-dinitrobenzene, or benzoic acid in the temperature range between 25° C. and 150° C.; $AgNO_3$, $NaNO_3$, and AgCl in the temperature range between 150° C. to 500° C., and NaCl and Ag (derived from the decomposition of $AgNO_3$) in the temperature range between 500° C. and 1000° C. Other substances with known heats of fusion which have melting points at desired temperatures may be found just as satisfactory as those listed above.

In practice it is simpler to establish the heat of reaction scale in terms of calories per given weight of paper proportional to the peak area of a thermal reaction than in calories per given area. For it is considerably easier to cut out an area and weigh the paper than measure the area directly. However, the constancy in weight of a given area on a sheet of paper must be ascertained. Transparent millimeter paper of good quality was found satisfactory for this purpose.

The validity of the proposed calibration was tested by evaluating the heats involved in reactions, such as desorption of water from hydrated salts and decomposition of nitrates and carbonates, the values for which

Table 4. Heats of Decomposition of $CaCO_3$, $AgNO_3$, and $NaNO_3$ as Determined by *d.t.a.* and by Calculations* from Heats of Formation (7)

Substance	Decomposition temperature in *d.t.a.*	Determined values	Calculated values	Decomposition temperature (t_2)
	°C.	Cal./gm.	Cal./gm.	°C.
$CaCO_3$	700–830	465	468	787
$AgNO_3$	370–470	212	210	400
$NaNO_3$	600–720	770	776	667

* The calculations were carried out for the following reactions (8)

$$CaCO_3 \rightarrow CaO + CO_2$$
$$AgNO_3 \rightarrow Ag + \tfrac{1}{2}N_2 + 1\tfrac{1}{2}O_2$$
$$NaNO_3 \rightarrow \tfrac{1}{4}Na_2O + \tfrac{1}{4}Na_2O_2 + \tfrac{1}{2}N_2 + 1\tfrac{1}{8}O_2$$

Lewis and Randall's (9) procedure was followed in calculating the temperature effect on these reactions but with the exception that ΔCp—the difference in heat capacities between reactants and products—was equated to the heat capacities of the liberated gases; since by the nature of *d.t.a.* the difference in the heat capacities of the solids is not measurable.

Table 5. Integral Heats of Desorption of Various Hydrated Salts as Determined by *d.t.a.* and by Calculation* from Heats of Formation

Salt	Determined values	Calculated values	Desorption temperature (t_2)
	Cal./gm.	Cal./gm.	°C.
$CaSO_4 \cdot 2H_2O$	164	160	140
$Ca(NO_3)_2 \cdot 4H_2O$	234	230	130
$BaCl_2 \cdot 2H_2O$	120	119	120
$MgSO_4 \cdot 7H_2O$	395	402	130
$SrCl_2 \cdot 6H_2O$	300	311	120
$Na_2S_2O_3 \cdot 5H_2O$	260	269	120

* The calculations were carried out for the following type reaction

$$CaSO_4 \cdot 2H_2O \rightarrow CaSO_4 + 2H_2O \text{ (gas)}.$$

The temperature effect on the reaction was calculated in the same manner as indicated in footnote to Table 4.

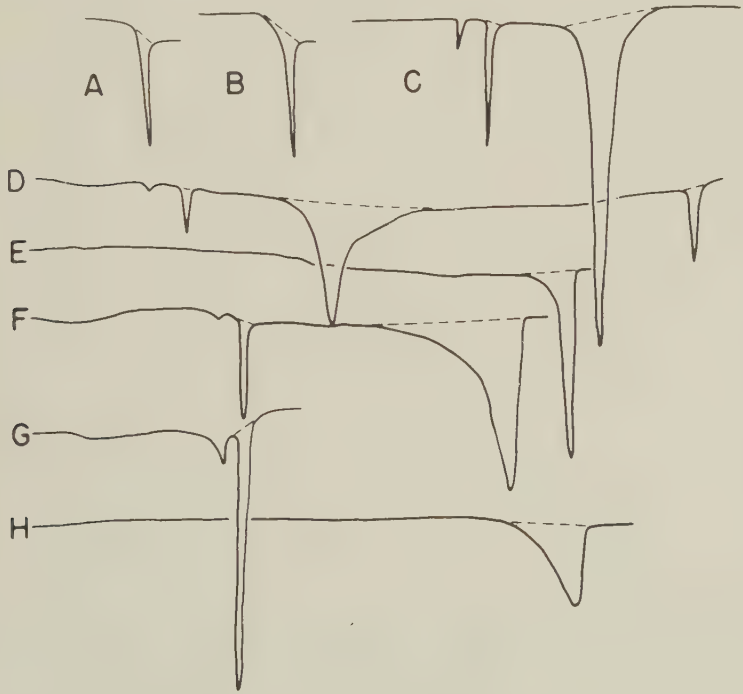

Fig. 10. *D.t.a.* curves of substances useful for the heat of reaction calibration. The substances were dispersed in Al_2O_3 and centered around the thermocouple in a volume of 0.110 c.c. except *B* and *D* which were dispersed in a volume of 0.480 c.c. Rate of heating $=8°$ C. per minute, except $C=12°$ C. per minute.

A. 50 mgm. *m*-dinitrobenzene
B. 100 mgm. benzoic acid
C. 50 mgm. $AgNO_3$
D. 50 mgm. $AgNO_3$
E. 25 mgm. NaCl
F. 15 mgm. $NaNO_3$
G. 50 mgm. $NaNO_3$
H. 10 mgm. $CaCO_3$

can be calculated from heats of formation and heat capacity of the reactants and products (7, 8, 9). The values thus determined are shown in Tables 4 and 5. It is seen that they are in excellent agreement with the calculated values. This excellent agreement verifies not only the accuracy of the scale but also the validity of the derivation relating the proportionality between the peak area of a break in a *d.t.a.* curve and the heat of reaction.

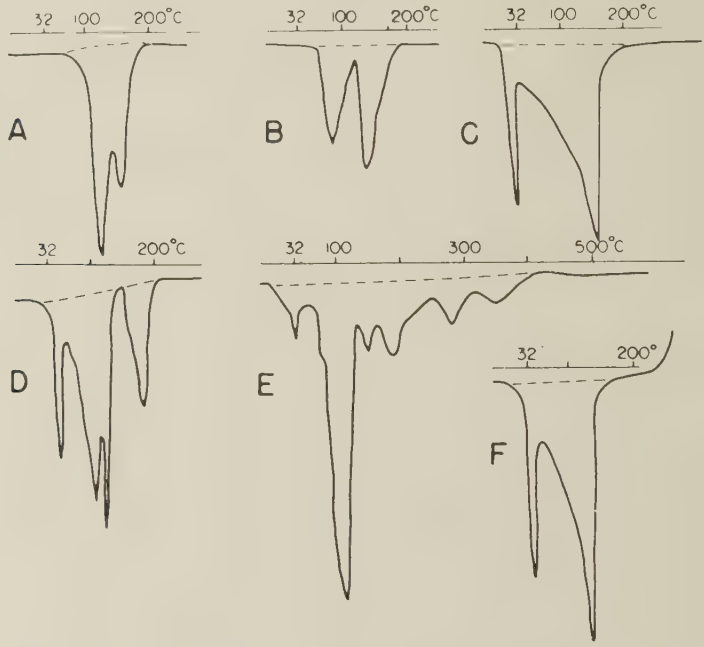

FIG. 11. *D.t.a.* curves of 50 mgm. of various hydrated salts dispersed in Al_2O_3 and centered around the thermocouple in a volume of 0.110 cc.

A. $CaSO_4 \cdot 2H_2O$
B. $BaCl_2 \cdot 2H_2O$
C. $CaNO_3 \cdot 5H_2O$
D. $SrCl_2 \cdot 6H_2O$
E. $MgSO_4 \cdot 7H_2O$
F. $Na_2S_2O_3 \cdot 5H_2O$

A comparison of the shape of the thermal breaks obtained for the various kinds of reactions (Figs. 10, 11) suggests that the desorption of water from gypsum ($CaSO_4 \cdot 2H_2O$), the decomposition of $AgNO_3$ and $CaCO_3$ could be used for a heat of reaction calibration. In fact for the calibration of many instruments, these substances may prove preferable to those previously suggested; for they yield much larger thermal breaks and therefore they are subject to a greater degree of accuracy in measurement. Wittels already suggested for this purpose the use of $CaCO_3$ but the value for the heat of decomposition to which he refers is in error by about

15 per cent. The error appears to be due to failure in correcting the heat of decomposition for the temperature at which it occurs in *d.t.a.*

The method and substances for the heat of reaction calibration for endothermic reactions may also be used for exothermic reactions by merely switching leads to the galvanometer.

Discussion

The value of the suggested method of temperature calibration lies in that the temperature scale reflects all of the heating characteristics inherent in the *d.t.a.* apparatus at the position of the test sample; and that it simplifies the apparatus by eliminating the temperature thermocouple and the associated temperature recording device. Such a simplification would reduce considerably the cost of the apparatus.

The method of registering the temperature scale directly on any *d.t.a.* curve makes possible a precise delineation of the beginning, the peak, and the end of any thermal break. By this method it was shown that the rate of heating apparently has no effect on the initial position of the thermal breaks in *d.t.a* curves of montmorillonite, chlorite, and kaolinite. The differences in position of the breaks in the *d.t.a* curves of these minerals reported in the literature may be due in part to inaccurate temperature scales.

A heat of reaction calibration of the *d.t.a* apparatus in terms of calories per unit peak area would enable the assignment of constant parameter to thermal breaks in *d.t.a* curves of pure minerals. Consequently, it would become possible to compare *d.t.a.* curves of the same mineral or of different minerals obtained with different instruments. Although differences may still appear in *d.t.a.* curves of the same mineral species obtained with different instruments, the difference may reflect differences in the nature of the minerals themselves—such as amount and nature of impurities present, variation in particle size and degree of perfection in crystallization, or other differences.

In reactions involving the liberation of water or CO_2, the heat of reaction may be expressed in calories per unit mass of material being heated and in calories per unit mass of water or CO_2 liberated. The latter expression, however, can be made only when the amount of water or CO_2 liberated during the reaction is known. The magnitude of the heat of reaction as expressed by the first method depends on the purity of the mineral analyzed but by the second method it is independent of the purity. The latter expression for the heat of reaction is, therefore, a better measure for differentiating minerals with overlapping thermal breaks as those of illite and kaolinite in the temperature range between 400° C. and 600° C. In illite the magnitude of the reaction represented by this

thermal break is equal to 1025 calories per gram of water liberated whereas in kaolinite it is equal to 1983 calories per gram of water liberated. Several such measurements for various minerals are given in Table 6.

The heat of reaction calibration was found particularly useful in measuring the heats involved in the desorption of water and other liquids from montmorillonite and vermiculite (2). Examples of such measurements are shown in Table 7.

TABLE 6. HEAT OF DECOMPOSITION OF SEVERAL MINERALS AS DETERMINED BY *d.t.a.*

Minerals	Decomposition temperature in *d.t.a.*	Crystal lattice $H_2O(OH)$	Heat of decomposition	
	°C.	per cent*	Cal./gm. of mineral	Cal./gm. H_2O lost
Brucite	356–455	30.92	332	1075
Gibbsite	258–360	31.10	259	832
Goethite	314–396	11.27	105	932
Kaolinite	455–642	12.76	253	1983
Halloysite	430–550	12.00	166	1385
Ca-Montmorillonite	554–723 816–908	2.43 0.70	67 26	2760 3720
Mg-Illite	400–695 790–950	6.25 1.27	64 15	1025 1180

* Of air dry material.

For a heat of reaction measurement to have thermodynamic significance the temperature at which the measurement is made must be stated. Since the temperature increases continuously in *d.t.a.* a heat of reaction measurement applies to a reaction occurring over a wide range of temperature. However, a single temperature point may be assigned to such a reaction by defining such a temperature point as one at which the heat of reaction is equal to that found in *d.t.a.* For convenience sake such a temperature point is designated as t_2. For the reactions involved in dehydration of crystal lattice water and decomposition of $AgNO_3$ or $CaCO_3$, temperature t_2 may be chosen arbitrarily as the point approximately midway between the beginning and the end temperatures of the

TABLE 7. INTEGRAL HEATS OF DESORPTION OF ADSORBED WATER OF VERMICULITES AND MONTMORILLONITES AS DETERMINED BY *d.t.a.*

Mineral	Adsorbed water	Desorption temperature in *d.t.a.*	Integral heat of desorption	Mean integral heat of desorption
	per cent*	°C.	Cal./gm. of mineral	Cal./gm. H_2O desorption
Mg-Vermiculite	12.7	25–170	130	1026
Mg-Vermiculite	2.7	170–250	38	1415
Ca-Vermiculite	12.4	25–150	113	914
Ca-Vermiculite	3.7	150–210	44	1185
Na-Vermiculite	12.7	25–170	99	779
Mg-Montmorillonite	17.0	25–220	135	794
Ca-Montmorillonite	17.7	25–220	127	718

* Of air dry material.

thermal break representing these reactions. But in reactions involving water desorption, t_2 may be evaluated more accurately by determining the water loss at several of the temperatures at which water loss occurs in *d.t.a.*[1] Subsequently each water loss determination is expressed as a fraction of the total amount of water lost, and multiplied by the rise in temperature to the point of desorption. The sum of these products when added to the initial temperature of the *d.t.a.* apparatus yields temperature t_2 (Table 8). A similar procedure may be followed for evaluating t_2 for the reactions involving loss of crystal lattice water and CO_2 from carbonates.

A clearer concept of the nature of the heat quantities involved in desorption of water from a "wet" mineral may be obtained by picturing the reaction of desorption, namely,

(I) $\text{Mineral}_{\text{(expanded)}} \cdot n\text{H}_2\text{O}_{(l)\,t1} + \Delta\text{H} \rightarrow \text{Mineral}_{\text{(contracted)}\ t2} + n\text{H}_2\text{O}_{(g)\,t2}$ as if it occurs in the following three steps:

1. The rise in temperature of the "wet" mineral from temperature t_1 to temperature t_2 at which desorption takes place:

[1] The most accurate method for determining such water losses would be with a *d.t.a.* apparatus so designed that the water loss may be determined at any point during *d.t.a.* In the absence, however, of such instrumentation, water loss from the test sample must be determined in a regulated furnace under conditions of temperature and heating time simulating those of *d.t.a.*

(II) Mineral $_{(\text{expanded})} \cdot n\text{H}_2\text{O}_{(l)\,t_1} + \Delta\text{H}' \rightarrow \text{Mineral}_{(\text{expanded})} \cdot n\text{H}_2\text{O}_{(l)\,t_2}$

2. The desorption of the water as "liquid" water (l) accompanied by changes in the mineral itself:

(III) Mineral $_{(\text{expanded})} \cdot n\text{H}_2\text{O}_{(l)\,t_2} + \Delta\text{H}'' \rightarrow \text{Mineral}_{(\text{contracted})\ t_2} + n\text{H}_2\text{O}_{(l)\,t_2}$

3. The conversion of the "liquid" water to "gaseous" water at t_2:

(IV) $$n\text{H}_2\text{O}_{(l)\,t_2} + \Delta\text{H}''' \rightarrow n\text{H}_2\text{O}_{(g)\,t_2}$$

The heat quantity involved in reaction (I)—ΔH —is termed here *the integral heat of desorption in d.t.a.*

The sum of the heat quantities involved in reactions (III) and (IV) —$\Delta\text{H}'' + \Delta\text{H}'''$—*is termed here the integral heat of desorption at* t_2.

The heat quantity involved in reaction (III)—$\Delta\text{H}''$—is termed here the *integral net heat of desorption at* t_2.

The evaluation of these three heat quantities is as follows:

The *integral heat of desorption in d.t.a.* is determined directly from the peak area in the *d.t.a.* curves and from the analysis of the total loss in water responsible for the peak area.

The *integral heat of desorption at* t_2 is determined by subtracting from the *integral heat of desorption in d.t.a* the heat quantity involved in reaction (II) $\Delta\text{H}' \cdot \Delta\text{H}'$ is evaluated by accounting for the difference in the specific heat of the "wet" and the "dry" forms of the mineral and by a rise in temperature from t_1 to t_2. If we assume that the difference in specific heat between the "wet" mineral and the reference material is equal to the specific heat of the adsorbed water, which in turn is assumed to be equal to the specific heat of liquid water, $\Delta\text{H}'$ would then be equal to the specific heat of water multiplied by the rise in temperature from t_1 to t_2. It was shown previously how to determine t_2.

The absence of an endothermic break prior to the actual desorption reaction itself as in the *d.t.a.* curves of some minerals and some hydrated salts—would indicate that there is no difference in the specific heat between the reference—inert-material and the test sample. $\Delta\text{H}'$ for such desorption reactions would therefore be equal to zero and consequently the *integral heat of desorption at* t_2 would equal the *integral heat of desorption in d.t.a.* The good agreement between the determined and the calculated *integral heats of desorption at* t_2 for several of the salts studied (Table 5) indicates that equating $\Delta\text{H}'$ to zero is permissible.

The *integral net heat of desorption at* t_2 is evaluated by subtracting from the *integral heat of desorption at* t_2 the heat of vaporization of water at t_2.

The three heat quantities may be expressed as calories per gram of material undergoing desorption and as calories per gram or mole of water being desorpt. The latter expression is obtained by dividing the former one by the amount of water liberated from 1 gram of material and multiplying by 1 or 18.

To evaluate the heat quantities involved in desorption at tempera-

tures other than t_2, the effect of temperature on the reaction of desorption must be estimated. The method of estimating this effect is the same as for any other reaction and the procedure followed is the one given by Lewis and Randall (9). The method mainly accounts for the difference in the heat capacities or specific heats at constant pressure between the reactants and products which is designated as ΔC_p.

Since the *integral heat of desorption at* t_2 is the sum of the heats involved in reactions (III) and (IV), it would be simpler to evaluate separately the effect of temperature on each of these reactions.

In reaction (III), which involves *the integral net heat of desorption*, ΔC_p

TABLE 8. CALCULATION OF THE HEAT QUANTITIES INVOLVED IN VAPORIZATION OF ONE GRAM OF WATER FROM UTAH Ca-MONTMORILLONITE UNDER CONDITIONS SIMILAR TO THOSE EXISTING DURING *d.t.a.*

Column number						
1	2	3	2×3	4	3×4	2×3+3×4
Temperature at point of desorption	Temperature* rise to point of desorption	Fraction of total desorpt† water	Heat absorbed by fraction during rise in temperature	Heat of vaporization	Heat absorbed by fraction during vaporization	Total heat absorbed by fraction
°C.	°C.	gm.	cal.	cal./gm.	cal.	cal.
75	50	0.69	34.5	554.3	382.3	416.8
100	75	0.13	9.8	539.0	70.0	79.8
115	90	0.04	3.6	529.3	21.2	24.8
145	120	0.10	12.0	508.3	50.8	62.8
230	205	0.04	8.2	423.3	17.3	25.5
Totals		1.00	68.1		541.6	609.9

* Temperature rise was computed from an initial temperature of 25° C.

† Total desorpt water = 19.0 gms. per 100 gms. air dry clay.

1. Temperature t_2 is equal to the total of column 2×3—namely, 68.1 plus 25° C., the initial temperature, or 93.1° C.
2. *Integral heat of desorption in d.t.a. was determined* to be equal to 143.5 cal. per gm. air dry clay or 143.5×1/0.19 = 754 cal. per gm. of water desorpt.
3. Integral heat of desorption at t_2—assuming that the difference in the specific heat between "wet" and "dry" clay is equal to that of water—= 143.5 − 68.1×0.19 = 130.5 cal. per gm. air dry clay, or 130.5×1/0.19 = 686 cal. per gm. of water desorpt.
4. Integral heat of desorption at 25° C. = 130.5 + (583 − 542)×0.19 = 137.8 cal. per gm. air dry clay or 137.7×1/0.19 = 726 cal. per gm. of water desorpt (583 = heat of vaporization at 25° C., 542 = heat of vaporization at 93° C.).
5. *Integral net heat of desorption* = 130.5 − 542×0.19 = 27.5 cal./gm. air dry clay or 27.5×1/0.19 = 145 cal. per gm. of water desorpt.

is equal to the difference in the heat capacities of the "wet" mineral and that of the "dry" mineral and liquid water. If we assume that the difference in the heat capacities of the "wet" mineral and the "dry" mineral were equal to that of liquid water, ΔC_p in reaction (III) would then be equal to zero. In consequence the *integral net heat of desorption* would be independent of temperature.

Since reaction (IV) represents the evaporization of liquid water, the effect of temperature on this reaction may be found directly in standard steam tables which list the heat of vaporization at different temperatures. The effect of temperature may also be calculated from the difference in the heat capacity of liquid water and gaseous water and one known heat of vaporization at a known temperature.

It appears, therefore, that the effect of temperature in *d.t.a.* on the *integral heat of desorption* is identical to the effect of temperature on the heat of vaporization of water. The difference in the *integral heat of desorption* at two temperatures is, therefore, equal to the difference in the heat of vaporization of water at the two temperatures.

The data of Table 8 illustrates the method of evaluating temperature t_2, the *integral heat of desorption at* t_2 *and* t_1, and the *integral net heat of desorption* for a Utah Ca-montmorillonite having a water content of 19.0 gm. per 100 g. air dry clay.

The proposed method for evaluating *the integral heat of desorption* and *the integral net heat of desorption* for adsorbed water is also applicable to other adsorbed liquids. Moreover these heat quantities would be equal but opposite in sign to the heat quantities involved in sorption reactions, provided the sorption and the desorption reactions are completely reversible, that is, without hysteresis.

Conclusions and Summary

(1) A uniform rise in temperature in the sample holes containing the differential thermocouples enables a simultaneous *d.t.a.* of several substances each of which marks a fixed temperature reference point in the resulting curve. Such a curve yields directly the temperature scale. To accomplish the analysis small amounts (2 to 10 mgm.) of the desired substances are placed either in one or in both of the sample holes around the thermocouple. To prevent the substances from interacting with each other they are embedded between narrow layers of Al_2O_3. A list of substances found useful for this purpose is given and they are termed "temperature indicators."

(2) By placing small amounts of the desired temperature indicators above and below a test sample or with the reference material, the temperature scale may be registered directly on the *d.t.a.* of the test sample. Several such *d.t.a.* curve are shown.

(3) Two methods are given for determining the sensitivity of the *d.t.a.* apparatus at different temperatures: one involves the use of temperature indicators and the other involves the use of boiling water and the tables of thermocouple characteristics.

(4) The intensity of a thermographic response, as measured by the peak height and peak area, to a thermal reaction in a given mass of material was found to be inversely proportional to the distance of the material from the thermocouple and to the volume which it occupies when centered around the thermocouple.

(5) The relation between the intensity of the thermographic response and the thermal reaction occurring in different amounts of the same material when dispersed in an identical volume and centered around the thermocouple was found to be linear.

(6) Organic substances of known heats of fusion and hydrated salts, particularly gypsum, of known heats of desorption were found useful for the heat of reaction calibration below 200° C., whereas inorganic substances of known heats of fusion or decomposition for the heat of reaction calibration above 200° C. Among the latter substances $AgNO_3$, $NaNO_3$ and $CaCO_3$ proved particularly useful.

(7) In determining in an unknown sample a heat of reaction or an amount of a known mineral, the sample should be confined to the same volume and placed in the same position with respect to the thermocouple as the substances used for calibration.

(8) Excellent agreement between determined and known heats of reaction of several substances attested to the accuracy of the heat of reaction scale and also to the validity of the proportionality between the peak area of a thermal break of a *d.t.a.* curve and the heat of reaction responsible for the break.

(9) Ascertaining the temperature scale of the *d.t.a.* apparatus by using the differential thermocouple circuit enables a simplification of the apparatus and thereby also a reduction in its cost.

(10) A heat of reaction calibration enables the assignment of constant parameters to *d.t.a.* curves of pure minerals and consequently *d.t.a.* curves obtained with different instruments become comparable.

(11) One of the most useful applications for the heat of reaction calibration was found in measuring the heat quantities involved in water desorption of hydrated minerals.

References

1. Arens, P. L. (1951), A study on differential thermal analysis of clays and clay minerals. Ph.D. thesis, as Chairman, Dr. A. C. Schuffelen of Landbouw-Hogeschool at Wageningen, Holland.
2. Barshad, I. (1951), Heat of dehydration and desorption of water or organic liquids

from montmorillonite and vermiculite. Abstract of papers, 120th meeting, *Am. Chem. Soc.*, New York, N. Y.
3. Ephraim, F. (1946), Inorganic Chemistry. Interscience Publishers, Inc., New York, N. Y.
4. General-Electric (1951), Tables of thermocouple characteristics (*GET*-1415). Apparatus Department General Electric, Schenectady, N. Y.
5. Grim, R. E. (1951), Method and application of differential thermal analysis: *Ann. New York Acad. Sci.*, **53,** 1031–1053.
6. Kerr, P. F., and Kulp, J. L. (1948), Multiple differential thermal analysis: *Am. Mineral.*, **33,** 387–419.
7. Lange, N. A. (1946), Handbook of Chemistry. Handbook Publishers, Inc., Sandusky, Ohio.
8. Latimer, W. M., and Hildebrand, J. H. (1929), Reference book of inorganic chemistry. Macmillan Company, New York.
9. Lewis, G. N., and Randall, M. (1923), Thermodynamics and the free energy of chemical substances. McGraw-Hill Book Company, Inc., New York.
10. Speil, S. (1944), Application of thermal analysis to clays and aluminous materials: *U. S. Dept. of Int., Bureau of Mines,* **R. I. 3764.**
11. Wittels, M. (1951), The differential thermal analyzer as a microcalorimeter: *Am. Mineral.*, **36,** 615–621.
12. Wittels, M. (1951), Some aspects of mineral calorimetry: *Am. Mineral.*, **36,** 760–767.

Manuscript received Nov. 13, 1951

NOTES AND NEWS

STRUCTURAL TRANSITION IN AlF_3*

R. L. Thakur, E. J. Rock, and R. Pepinsky, *Department of Physics, The Pennsylvania State College, State College, Pa.*

Because of recent interest in structural transitions and electrical properties of WO_3 (1, 2, 3), it has appeared advisable to examine a number of other ionic structures of similar coordination. One purpose of such investigations is to examine the applicability of the criteria for existence of ferroelectric phases in such structures, as these have been presented by Matthias (4). This author has made brief mention of a transition above 400° C. in AlF_3 (5), but no other studies of the thermal or optical properties seem available. Electrical, thermal and optical properties of AlF_3 over a range of temperatures are reported here.

Single crystals were prepared by heating anhydrous AlF_3 in a covered platinum crucible at 1020° C. Crystals 2 to 3 mm. in size were formed by sublimation on the bottom of the crucible cover.

The crystals show domains at room temperature, as illustrated in Figs. 1 and 2. Figure 1 shows a crystal under crossed nicols, and Fig. 2 in unpolarized light. Upon heating, a few crystals developed domains in two directions. A sharp transition occurs at 460° C., at which temperature the domains disappear and the crystals become isotropic. The domains reappear sharply at 460° C., when the temperature drops.

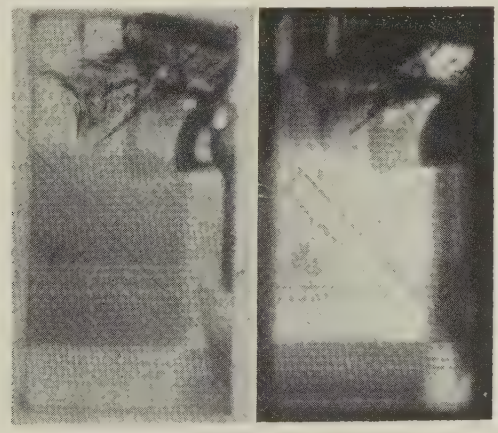

Fig. 1. AlF_3 between crossed nicols.

Fig. 2. AlF_3 in unpolarized light.

* Development supported by Office of Air Research.

The crystals show no measurable piezoelectricity and no anomalies in dielectric constant with temperature variation from −190° C. to 480° C. The dielectric constant is about 6 at room temperature. A thermal analysis was made between 100° and 800° C., and this showed a sharp transition at 460° C. The analysis is illustrated in Fig. 3.

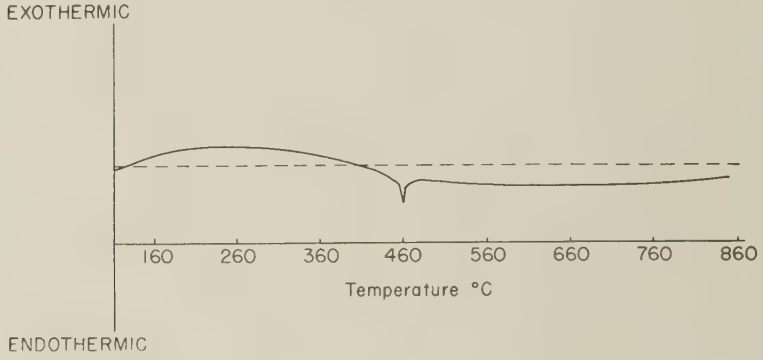

FIG. 3. Differential thermal analysis (AlF_3).

The crystal structure of AlF_3 below the transition point is not firmly established. A reexamination by x-ray diffraction of the structure above and below the transition temperature will be reported shortly.

The participation of Dr. W. Merz in the electrical measurements is gratefully acknowledged.

REFERENCES

(1) MATTHIAS, B. T., *Phys. Rev.*, **76,** 430 (1951).
(2) UEDA, R., AND ICHINOKAWA, T., *Phys. Rev.*, **82,** 563 (1951).
(3) JEFFREY, G. A., KEHL, W., AND WAHL, D., in press.
(4) MATHIAS, B. T., *Science*, **113,** 591 (1951).
(5) MATTHIAS, B. T., *Helv. Phys. Acta*, **23,** 167 (1950).

POWELLITE AND ASSOCIATED PSEUDOMORPHS AT THE ANDERSON MINE, MINERAL COUNTY, NEVADA

HATFIELD GOUDEY, *Yerington, Nevada.*

During and after World War I, the Santa Fe District in Mineral County, Nevada, was an important copper producer and of the producing mines the Champion-Anderson group was one of the largest. The writer had an opportunity in recent years to examine the surface and underground workings of these mines rather extensively. Certain features of the mineralization observed may be of more than passing interest.

The primary metallic minerals observed in the deeper levels of the Champion mine are chalcopyrite, bornite, sphalerite, pyrite, a local occurrence of stibnite, and very sporadic molybdenite. The accessible workings in the adjacent Anderson mine were all in the oxide zone. In these upper levels drusy hemimorphite frequently lines seams in the copper ore and associated with this hemimorphite the crystals described below were found.

Among a number of specimens of the drusy hemimorphite, three were found which showed tiny pyramidal crystals of tetragonal habit implanted upon the hemimorphite crystals. A few square tabular crystals were also found. A few of the crystals, apparently unaltered, were nearly colorless and translucent. Most of the crystals were an opaque white due to partial replacement by hydrozincite which is also present as late crusts on the hemimorphite. A few other crystals of both tabular and prismatic development show partial to complete replacement by chrysocolla. Since both tabular and pyramidal wulfenite crystals had been found in some of the Champion workings, that mineral was suspected here, but both triple nitrite and iodide microchemical tests failed to show any lead. Calcium was proved by precipitating microchemical gypsum and cesium chloride showed the absence of bismuth. Molybdenum was proved by semi-micro reduction to molybdenum blue and confirmation with xanthate. No tungsten reaction was obtained by using reduction tests of both stannous chloride and tin. Thus a calcium molybdate conformable with powellite is indicated. The age sequence in relation to the hemimorphite suggests a relatively low temperature of formation.

Chrysocolla, in addition to replacing the powellite, was observed in various stages up to complete replacement of both hemimorphite and acicular to capillary malachite crystals.

TRICLINIC CALCULATIONS

D. Jerome Fisher, *University of Chicago, Chicago, Illinois.*

To simplify triclinic calculations it may be well to point out certain relations implicit in my recent paper[1] which were not explicitly stated. Here the rectangular coordinate parallel to the $\phi = 0°$ direction of the orthographic projection of unit distance on the axial trace out towards the "right" was expressed as n_0, n_1 or n_2 in the three orientations.[2]

[1] Fisher, D. Jerome (1952), Triclinic gnomonostereograms: *Am. Mineral.*, **37**, 83–94. On p. 91 the denominator of (13) should be cot β.*

[2] Since the m-coordinates (parallel the $\phi = 90°$ direction) are readily derived from the n-values, it would seem that one could dispense with the former. It is stated (*op. cit.*, base p. 88) that the denominator of (9) is n_0.

From (4) and (19) get: $\cos \rho_0 = n_1$ (4′)
From (12) and (28) get: $\cos \rho_1 = n_2$ (12′)
From (21) and (9) get: $\cos \rho_2 = n_0$ (21′)
From (9) and (21) get: $q_0' = c/n_0$ (9′)
From (10) and (28) get: $p_0' = c/(a\ n_2)$ (10′)
From (17) and (21) get: $q_1' = a/n_0$ (17′)
From (18) and (19) get: $r_1' = a/(c\ n_1)$ (18′)
From (26) and (28) get: $p_2' = 1/(a\ n_2)$ (26′)
From (27) and (19) get: $r_2' = 1/(c\ n_1)$ (27′)

Since $\rho_0 = [c] \wedge [c^*]$, it is clear that $\cos \rho_0 = n_1$ is one of the direction cosines of $[c^*]$; another one is $\cos \alpha^* = n_1 y_0'$. Similarly $\rho_1 = [a] \wedge [a^*]$, and so $\cos \rho_1 = n_2$ is one of the direction cosines of $[a^*]$; another is $\cos \beta^* = n_2 z_1'$. And finally $\rho_2 = [b] \wedge [b^*]$, so $\cos \rho_2 = n_0$ is one of the direction cosines of $[b^*]$; another is $\cos \gamma^* = n_0 x_2'$. The last six of the above formulae furnish simple relations between axial units and certain Goldschmidt projection constants, given n_1, n_2, and n_0 [which can be calculated readily from (4), (12), and (21)]. It might be well to include these three values in triclinic angle tables.[3] Of course n_0 becomes unity in the monoclinic (where $n_1 = n_2 = \sin \beta$), and all three are unity in the orthorhombic.

Using these n-values also simplifies several standard formulae,[4] as follows:

$$a^* = 1/(a\ n_2) \quad (54) \qquad a = 1/(a^*\ n_2) \quad (54')$$
$$b^* = 1/(b\ n_0) \quad (55) \qquad b = 1/(b^*\ n_0) \quad (55')$$
$$c^* = 1/(c\ n_1) \quad (56) \qquad c = 1/(c^*\ n_1) \quad (56')$$
$$V^* = a^* b^* c^*\ n_0 \sin \beta^* = a^* b^* c^*\ n_1 \sin \gamma^* = a^* b^* c^*\ n_2 \sin \alpha^* \quad (48\text{–}50)$$
$$V = abc\ n_0 \sin \beta = abc\ n_1 \sin \gamma = abc\ n_2 \sin \alpha \quad (48'\text{–}50')$$

While equations (26′) & (54) seem to say that $p_2' = a^*$, and (27′) & (56) that $r_2' = c^*$, it must be remembered that a, b, & c of (54)–(56) represent unit cell edge lengths. Thus:

$$a^* = p_2'/b_0 = p_0'/c_0 \quad (36)$$
$$b^* = q_1'/a_0 = q_0'/c_0 \quad (37)$$
$$c^* = r_2'/b_0 = r_1'/a_0 \quad (38)$$

where a_0, b_0, & c_0 are a, b, & c of (54)–(56). In short these projection constants (as well as the n_1, n_2, and n_0 direction cosine values) are also con-

[3] For chalcanthite (see *Am. Mineral.*, **37**, 1952, 111) $n_1 = 0.9524$ and $n_2 = 0.9378$. In this table p_0 should $= 0.990$ and p_0' should $= 1.0393$. Other corrections in this paper include: p. 104, base, γ in (31′) should be α; p. 105, lines 10 and 22, *diffraction* should read *precession;* p. 109, Table 6, last line of right column, prime the G_2. The calculated density of the chalcanthite is $499.42/(.6023 \times 361.94) = 2.291$.

[4] Buerger, M. J. (1942), *X*-ray crystallography, New York, pp. 360–361. The numbers are those of Buerger.

stants which relate the lengths of the edges of the direct unit cell to those of the reciprocal unit cell.

The linear[5] elements of the triclinic system may be considered to include a^*, b^*, c^*; $a_0b_0c_0$; also a, b, c; and the six Goldschmidt projection constants listed in the first set of formulae. From the first two "sets of three" of these linear elements one may derive the n_1, n_2, n_0-values [using (54)–(56)], and these put in (9′–10′), (17′–18′), & (26′–27′) yield the listed projection constants.

The angular elements include α, β, γ; α^*, β^*, $\gamma^*(=\lambda, \mu, \nu)$; also ϕ_0, ϕ_1, ϕ_2; and ρ_0, ρ_1, ρ_2. From the last set of three one easily derives d_0', d_1', d_2' (tangent values) or n_1, n_2, n_0 (cosine values). From the first set of three one easily derives $s_0'=z_2'$, $s_1'=x_0'$, and $s_2'=y_1'$ (cotangent values).

From (8) and the value of n_1 in (4) get:	$y_0'=\cos\alpha^*/n_1$	(8′)
From (16) and the value of n_2 in (12) get:	$z_1'=\cos\beta^*/n_2$	(16′)
From (24) and the value of n_0 in (21) get:	$x_2'=\cos\gamma^*/n_0$	(24′)
From (8) and (5) get:	$\tan\phi_0=\cot\beta/y_0'$	(5′)
From (16) and (13) get:	$\tan\phi_1=\cot\gamma/z_1'$	(13′)
From (24) and (22) get:	$\tan\phi_2=\cot\alpha/x_2'$	(22′)

While the n_1, n_2, n_0 values may be calculated easily from either linear or angular elements, there is no way to go from the first six listed angular elements alone to the first six listed linear elements alone. This is most easily comprehended by visualizing the direct and reciprocal unit cells as representing parallelepipeds having definite angles but indefinite (though reciprocal) dimensions. It is possible to calculate the angular elements from the values of the first six listed linear elements. However, this is a tedious process by any method known to the writer; moreover, this is not recognized as being of any practical value.

[5] Goldschmidt uses *linear* as opposed to *polar*. No such meaning is here intended. Goldschmidt's use of the word is outmoded. In his sense the proper word to use is *direct* (as opposed to *reciprocal*) or *primitive*.

Heinrich Laubmann, Bavarian chemist and mineralogist, born October 2, 1865, died February 7, 1951.

Emmanuel Christa, Professor of Mineralogy, University of Erlangen, born March 15, 1874, died February 27, 1948.

MINERALOGICAL SOCIETY (London)

A meeting of the Society was held on Thursday, January 24th, 1952, in the apartments of the Geological Society of London, Burlington House, Piccadilly, W.1 (by kind permission).

The following papers were read:

(1) The Graphitization of Diamond and the Nature of Cliftonite.

By Dr. H. J. Grenville-Wells

Diamond heated in vacuo to about 2000° C. is wholly or partially converted to graphite which has a strong preferred orientation, the [0001] axis of the graphite being associated with the diamond [111] axis irrespective of the original habit of the diamond. The preferred orientation of the graphite in cliftonite, however, has been shown to involve the association of the [0001] axis with the cube axes of the crystal, thus casting doubt on the possibility that cliftonite is a pseudomorph after diamond. The graphite itself appears in both cases to be imperfectly crystallized, and is neither α- nor β-graphite, nor the usual mixture of the two. It has been shown by means of divergent-beam x-ray photographs that the mosaicity of diamonds can be increased by heat treatment.

(2) Sinhalite ($MgAlBO_4$), a New Mineral.

By Dr. G. F. Claringbull and Dr. M. H. Hey

Many of the brown and yellow gemstones supposed for many years to be olivine (peridot) prove to be a new mineral with the composition $MgAlBO_4$. It is orthorhombic with unit cell dimensions $a=4.328$, $b=9.878$, $c=5.675$ Å; space groups D_{2h}^5-Pbmm, C_{2v}^2 $Pb2_1m$ or $C_{2v}^4-Pbm(2)$. The x-ray powder pattern resembles that of olivine.

(3) The Growth and Properties of Large Crystals of Synthetic Quartz.

By Mr. C. S. Brown, Mr. R. C. Kell, Mr. L. A. Thomas, Dr. Nora Wooster and Dr. W. A. Wooster

An outline is given of early experiments on the hydrothermal synthesis of α-quartz, most of which succeeded in producing crystals on a microscopic scale. Experiments aimed at the synthesis of large single crystals are described. These include the Nacken-Wooster method and the modern developments of the Spezia process. A recent technique has enabled high quality quartz crystals weighing up to 150 grams to be grown in about a month.

The physical properties and morphology of synthetic quartz crystals are compared with those of the natural mineral.

(4) On the Occurrence of Turquoise in Cornwall.

By Sir Arthur Russell, Bart., and Dr. E. A. Vincent

(5) The Types of Distribution of Inclusions within Fluorite, Quartz, and Calcite Crystals from Derbyshire.

By Mr. G. Mueller

Inclusions of pyrite, rutile, hydrocarbons, etc., were identified within crystals of gangue minerals from numerous Derbyshire localities. Several examples were found for each of the following modes of distribution: (1) uniform throughout the crystal or within certain growth zones, (2) concentration towards a direction, (3) preferential deposition on certain

faces, (4) concentration along all or some edges, termed "positive edge effect," (5) apparent repulsion from all edges, "negative edge effect," (6) repulsion from the edges and concentration into narrow zones fringing these, "complex edge effect." The proposed explanations of the structures are based on field evidences indicating the mechanical and chemical conditions prevailing during mineralization. The "edge effects" may have also an alternative electrical explanation.

The following papers were taken as read:—

(1) The Decomposition of Afwillite on Heating.

By Mrs. K. M. Moody

Afwillite, $Ca_3(SiO_3OH)_2 \cdot 2H_2O$, loses water when heated, and decomposition takes place in two stages. In an investigation of these processes, the products have been identified by *x*-ray powder methods. The intermediate product is a poorly-crystallized mixture containing $\gamma - Ca_2SiO_4$ and probably CaO and SiO_2. The dehydrated material readily reabsorbs water, but there is no reversion to afwillite or other hydrated silicates. At about 1000° C. a further change occurs and the material recrystallizes as rankinite, $Ca_3Si_2O_7$.

(2) Refractive Indices of Muscovite in the Infra-red.

By Dr. W. Hall and Prof. S. Tolansky (Communicated by Dr. F. A. Bannister)

Refractive indices β and γ of an Australian muscovite have been measured over the wavelength range λ 5870–9410 Å.

(*Titles and abstracts kindly submitted by G. F. Claringbull, General Secretary.*)

Samuel G. Gordon, for thirty years assistant curator at the Philadelphia Academy of Sciences, and more recently associated with the atomic energy plant at Oak Ridge, Tenn., collapsed and died May 18, 1952, in Cincinnati, Ohio. He was 54 years old. For many years he served as one of the associate editors of the *American Mineralogist*, and was a member of several mineralogical expeditions to South America, Greenland, and Africa.

BOOK REVIEWS

IGNEOUS AND METAMORPHIC PETROLOGY, by Francis J. Turner and Jean Verhoogen. McGraw-Hill Book Company, New York. 602 pp., 92 fig., 1951. $9.00.

Once in a while in every field of scientific specialization there is published a work which not only mirrors the complete development of its field but also is so fundamental that it immediately becomes part of that development and serves as solid substance for future expansion. Such a book is *Igneous and Metamorphic Petrology*, in the field of petrogenesis. The book is too advanced for beginning students but is intended, in the authors' words, " . . . for the use of advanced students, research workers and teachers . . . ." To these it may well become indispensable, for it is eminently successful in attaining its goal of presenting " . . . a unified general impression of the origin and evolution of rocks that are generally believed to have crystallized, or to have been profoundly modified, at high temperatures and at pressures such as prevail from the earth's surface to a depth of 15 or 20 km."

The book may be considered as consisting of three parts. The first part contains an introductory chapter and another on principles of chemical equilibrium as applied to rocks. Thereafter follows the section devoted to igneous rocks, and last is the part dealing with metamorphic rocks. The portion on igneous rocks begins with chapters on characteristics and classification, variations in rock associations, crystallization of igneous minerals and crystallization of basaltic and granitic magmas. These are followed by description of the various natural rock associations: (1) the oceanic olivine-basalt—trachyte volcanic association, (2) volcanic associations of nonorogenic continental regions—those with alkaline affinities and the flood basalt—quartz diabase type, (3) volcanic associations of orogenic regions, (4) basic and ultrabasic plutonic associations, (5) granite, granodiorite plutonic association, and (6) pegmatites, lamprophyres and nepheline syenites. Under each group are discussed occurrence based on excellent, well-studied examples, distribution, chemistry, general mineralogy and hypotheses of origin, including a judicial critical review in which the ideas on genesis are examined in the light of *both* field and laboratory evidence. The final chapter on igneous petrology is a succinct summation entitled, "Environment, origin, and evolution of magmas."

In the part dealing with metamorphic petrology the subjects are: scope, classification, chemical principles, correlation of mineral assemblages and metamorphic environment, facies characteristics, special fabric features and the interrelation of metamorphism, magma and orogeny. The facies classification is Turner's modification of Eskola's work (*Geol. Soc. Am., Mem.* **30,** 1948). As is stated in the preface, " . . . Chaps. 15 to 21, dealing with metamorphism, constitute a reduced revised version of *Memoir* **30** . . . ."

The treatment of the individual igneous rock types as parts of a petrologic association is in general an excellent technique for presenting data on occurrence and genesis. Many rock types, however, appear in more than one major association, and thus their descriptions are somewhat decentralized. There are other minor points with which a reader might find fault. Some of the districts cited as examples for igneous rock associations are treated at undue length (Pliocene volcanic association of Eastern Otago, New Zealand—nearly 10 pages!) whereas for some other associations few or no examples are specifically described. On the other hand, the section on the nepheline syenite rocks is in proportion to the quantitative importance of this type, and, on the whole, an equitable balance is maintained between amount of descriptive material and relative abundance of the rock.

Some readers will look in vain for such topics as myrmekite, deuteric processes in general (deuteric is not even listed in the index), the formation of dumortierite with boron metasomatism, agpaitic sequence of crystallization, auto-injection structures, alumina

metasomatism, pegmatite-aplite relations and phenocrysts of the non-marginal plutonic type. Others will no doubt wonder why the authors have insisted on contributing toward perpetuation of many varietal, local, and other minor rock names (e.g., crinanite, atlantite, keratophyre, mangerite, mikenite, allivalite), the mere restatement of which, despite some attached definitions, gives tacit approval to their continued usage.

The line drawings (there are no plates) and tables are uniformly excellent; 41 figures have been repeated from *Memoir* **30**. Typographical errors seem to be at a minimum; a conspicuous example is the topic heading on p. 423. However, the index does not seem to match the text in quality. Some headings do not appear at all (latite, monzonite) and others have been incompletely cited (for dacite pp. 319 and 330 should also be listed). This materially detracts from the value of the book as a reference work. Many of the physical-chemical principles involved are discussed in extensive mathematical equations and formulae; fortunately an adequate understanding and appreciation of the book are not necessarily hinged on a complete comprehension of the complex mathematical notation.

These minor criticisms should not in any way minimize the over-all importance of the work. It will undoubtedly receive a well-deserved and enthusiastic welcome by "hard rock" petrologists everywhere as the outstanding new book in petrogenesis.

E. Wm. Heinrich,
University of Michigan

TABLES FOR MICROSCOPIC IDENTIFICATION OF ORE MINERALS, by W. Uytenbogaardt. Princeton University Press, Princeton, N. J. 242 pp., 1951. $5.00.

Tables for Microscopic Identification of Ore Minerals is another welcome addition to the small group of books dealing with the study and identification of opaque and semiopaque minerals in polished section, mainly under vertically incident light (mineralography, mineragraphy, ore microscopy, Erzmikroskopie). The compiler of the Tables, W. Uytenbogaardt, at the Department of Mineralogy of Stockholm University, follows, in several respects, the work of his distinguished compatriot in the field of ore microscopy, Van der Veen. The first part of the book consists of two lists. List I is an arrangement of the ore minerals in order of increasing polishing hardness (following Van der Veen's technique for comparing the relative hardness of adjacent mineral grains) together with their compositions, % reflectivities (mainly data by Folinsbee) and their optical grouping (I=isotropic, W=weakly anisotropic, D=distinctly anisotropic and S=strongly anisotropic.) In List II the minerals are arranged by increasing % reflectivity, and other data given here are their composition, isotropism-anisotropism and relative grinding hardnesses as compared with those of galena, chalcopyrite, and pyrite. Together these two lists cover about 15 pages. Both give the pages in the subsequent table in which the complete mineral descriptions occur.

Most of the book is made up of a single table in which the minerals are listed by increasing "resistance to polish" (H), as compared to the three standard reference minerals noted above: galena, chalcopyrite and pyrite. For each mineral species much detailed and modern information is presented under the headings: chemistry, crystallography, Talmadge hardness, reflectivity, color, etch tests and miscellaneous. The most valuable information in the entire book is collected in the "miscellaneous" column. Here are notes on polish quality, cleavage, twinning, intergrowths and associations.

The book closes with a list of superfluous mineral names, a bibliography of 441 entries and an index.

The chief virtue of the work is that the author has gathered under one cover and carefully systematized much miscellaneous information and many widely scattered data on ore minerals that have emerged in the literature since the publication in 1940 of Short's,

U. S. Geological Survey, Bulletin **914,** The Identification of the Ore Minerals. One table alone, however, arranged on the basis of the often unobservable property of relative hardness, does not fufill the promise of the title of the book. Using this book and only this book the beginning worker in ore microscopy would indeed be hard pressed to identify ore minerals on the basis of characteristics obtained by means of the standard techniques. The book is a valuable supplement to Short's tables but cannot be considered as supplanting them, even though much of their information is outdated.

What is now needed in ore microscopy is a textbook in English that would encompass not only the *mineralogy* of ore minerals, including preparation of polished sections, optical theory of opaque minerals, mineral identification techniques, data and tables, etc., but also the *petrography* of ore minerals wherein could be found descriptions and examples of textures and microstructural features, their classification and genesis.

E. Wm. Heinrich,
University of Michigan

BULLETIN 3, GEOLOGICAL SURVEY OF GREAT BRITAIN, His Majesty's Stationery Office, *London,* **1951.** 71 pp., 3 plates. Price 4s.6d postpaid ($0.80).

This *Bulletin* is published as a partial record of the work of the Atomic Energy Division of the Geological Survey of Great Britain. It contains four papers:

1. "On thucolite and related hydrocarbon-uraninite complexes, with a note on the origin of the Witwatersrand gold ores," by C. F. Davidson and S. H. V. Bowie. This is the first technical description of the uranium-bearing Rand ores in which both uraninite and a coal-like hydrocarbon, "thucolite," occur, the latter having been formed through polymerization of hydrocarbon gases by means of radioactive radiations. Since the uraninite is clearly of hydrothermal origin and of the same period of mineralization as the gold, its presence is a forceful argument for the hydrothermal origin of these deposits, a thesis long and eloquently advocated by Graton but generally rejected by the Rand mining geologists.
2. "Notes on the photoluminescence of minerals," by J. E. T. Horne, contains a succinct outline on the mechanisms of luminescence, discussions of intrinsic and impurity-activated phosphors, brief developments of some geological applications of luminescence and three appendices: I, an alphabetical list of luminescent minerals with short notes on the species; II(i), an alphabetical list of the fluorescent uranium minerals; and II(ii), a classification of uranium minerals under type of fluorescence or absence of fluorescence.
3. "The chemical determination of uranium, with special reference to its occurrence as a minor constituent of minerals and rocks," by C. O. Harvey. Here are discussed the ferrocyanide method, the peroxide method and uranyl nitrate extraction via ethyl ether. The techniques for uranium determination in siliceous rocks, monazite and other types of material are described.
4. "Autoradiographic techniques in geological research," by S. H. V. Bowie are described under the headings alpha-particle autoradiography, beta-particle autoradiography, exposure, processing, examination and interpretation and quantitative measurements.

E. Wm. Heinrich,
University of Michigan

DIE FESTIGKEITSERSCHEINUNGEN DER KRISTALLE, by H. Tertsch. vii+ 310 pages, 219 text figures. Springer-Verlag, Vienna, 1949. Price, $9.60.

There is a great deal of information in the literature on determination of strength, deformation, working and properties of polycrystalline aggregates, but comparatively

little on single crystals. This is true partly because much information is developed on such materials, especially metals, in the course of processes of fabrication and in experiments on methods of fabrication. Also, it is generally easier to study and describe the properties and behavior of a polycrystalline aggregate that acts as a more or less isotropic medium than a single crystal whose properties and response to stress vary, sometimes quite considerably, with crystallographic direction.

These and other considerations led Tertsch to attempt a synthesis, from the point of view of the mineralogist, of the strength-properties, deformation, etc., of single crystals. He has drawn his material in part from his many years of experience in this field and in part from the literature in mineralogy bearing on this subject. (There are 317 references at the end of the text.) Many of the examples and references are metallurgical. Tertsch assumes that the reader of this volume will have an adequate knowledge of crystallography, including an understanding of the twinning laws of the various crystal systems.

The book consists almost entirely of the description of methods of measuring, expressing, and recording four properties of crystals; (1) cleavage, (2) plasticity, (3) hardness, and (4) impact and pressure figures.

Cleavage is classified as impact-, pressure-, and tension-. Methods are described for measuring and expressing each kind quantitatively. This section closes with a theoretical discussion of cleavage and the cleavage process.

The longest and most complicated section (124 pp.) is that on crystal plasticity. The subject is clearly treated and well illustrated. There is more emphasis on mineral crystals than in other treatments of the subject, but even here a large proportion of examples are drawn from metallurgy. About two-fifths of the illustrations in this section are theoretical diagrams; the other three-fifths are almost equally divided between minerals and metals, the latter taken largely from the works of E. Schmid and his co-workers. An interesting feature on the section on crystal plasticity is a table in which translation elements and/or twin glide elements are tabulated for 85 minerals. This should be very useful for anyone interested in the deformation of minerals and rocks, and especially for those who are undertaking experimental work in this field. So far as the writer is aware this is the largest such compilation ever made. Schmid and Boas[1] give a similar table, but only 15 metal crystals are listed. The section ends with a 29-page theoretical discussion of crystal plasticity.

In the section on hardness twelve different methods of measuring this property are described and the effect of temperature on measurements by various methods is discussed. There are some interesting and instructive tabulations:

(1) The 1500 plus well-defined mineral species are grouped according to hardness, the number being given for each half division of the Mohs scale, and the number in each group that contain combined water. There are approximately 100–200 minerals for each half division between 2 and 6 inclusive, with a maximum of 187 with a hardness of 3. There are no hydrous minerals harder than 6.5.

(2) A similar tabulation is made for minerals containing each of 27 important elements.

(3) A chart shows ionic radii of 64 elements on one side and the maximum hardness of minerals containing each on the other side. In the theoretical discussion at the end of this section there is a further treatment of the relation between hardness and the periodic arrangement of the elements.

In the section on impact and pressure figures the relation of these phenomena to crystal symmetry is pointed out and methods for their production and study are outlined.

The book is bound in paper, but is well put together and is printed on a very good grade paper on which half tones as well as line drawings reproduce nicely. It is the most complete,

[1] Plasticity of Crystals, by E. Schmid and W. Boas (Trans. by L. H. Tripp), F. A. Hughes & Company, London, 1950. Pp. 85.

authoritative and up-to-date treatment of the strength, deformation, and related properties of single crystals of minerals. As such, it is a useful and beneficial compendium not only for those who are working with the deformation of minerals and rocks in Nature or in the laboratory, but also for those who have a broader interest in the physical properties of minerals.

EARL INGERSON,
U. S. Geological Survey, Washington 25, D. C.

MINERALOGY (AN INTRODUCTION TO THE STUDY OF MINERALS AND CRYSTALS), BY E. H. KRAUS, W. F. HUNT, AND L. S. RAMSDELL, 4th Edition, 664 plus vii pages, 735 illustrations, McGraw-Hill Book Co., 1951. Price $8.00.

This is the fourth, revised edition of one of the most widely used textbooks for the teaching of elementary mineralogy in American colleges and universities. Considering the large number of copies sold since it was first published in 1920, and that it is an elementary textbook in a competitive field, the question arises as to the reason for its marked success. This reviewer believes that its success is due to the degree to which it fulfills the requirement as stated by Whitehead[2] that "A student should not be taught more than he can think about. Selection is the essence of teaching." This text presents the basic principles for an elementary course in mineralogy. The selection of the information and data to be included has been uniformly excellent. In addition to the normal topics included in the usual instruction in elementary mineralogy, there are chapters on qualitative blowpipe methods, optical mineralogy, crystal structure and *x*-ray analysis, gemstones, and what is commonly termed mineral economics. All of the special chapters do not have to be included in an elementary course. The selection from this group of topics will depend on the interests of the students, time, and facilities available.

All sections of this book have been revised—some more than others. The illustrations in this edition are much improved over those in earlier editions. A number of illustrations have been omitted and new ones added. Many of those previously used have been reproduced in a much larger size which greatly enhances their value.

The section on "Descriptive Mineralogy" has been radically changed. The arrangement of the species is now based on the classification used in the 7th Edition of *Dana's System of Mineralogy* and on *Strunz's Mineralogische Tabellen*. This is a very desirable change. With the exception of the usage of analcite for analcime, the recommendations of the Mineralogical Society of America's nomenclature committee (1936) have been accepted. *Orthite* has been changed to *allanite* in this edition. The following mineral species have been added to the text (*a*) in large print: aegirite, alabandite, amblygonite, brucite, cordierite, glaucophane, kernite, and prehnite; (*b*) in fine print: annabergite, antlerite, calaverite, covellite, cristobalite, diaspore, dumortierite, erythrite, greenockite, jadeite, microlite, millerite, montmorillonite, nephrite, niter, oligoclase variety—sunstone or aventurine, pentlandite, sylvite, tridymite, triphylite, vermiculite, vivianite, and wurtzite. The list of occurrences for brucite should have included Gabbs, Nevada. Considering the wide distribution of the clay minerals montmorillonite and hydromica (illite group), their description is inadequate.

The chapter on crystal structure and *x*-ray analysis has been rewritten and is both informative and stimulating. It serves to introduce the student to the phenomenological approach to the solid state. The chapters on gemstones and on the classification of the minerals according to the chemical elements have almost a new set of illustrations, in

[2] General Education in a Free Society. Report of the Harvard Committee. Harvard Univ. Press, 1945, p. 63.

keeping with the many changes in these fields in recent years. A selected bibliography of 57 entries has been added.

The determinative tables have been expanded to include the new species added to the text.

This reviewer believes that this fourth edition of Kraus-Hunt-Ramsdell will maintain for this textbook its fine reputation in the field of teaching elementary mineralogy and that it will gain for it many new friends.

GEORGE T. FAUST,
U. S. Geological Survey, Washington 25, D. C.

DIE FELDSPAT-QUARZ-REAKTIONSGEFÜGE DER GRANITE UND GNEISE UND IHRE GENETISCHE BEDEUTUNG BY F. K. DRESCHER-KADEN (1948). Springer-Verlag, Berlin/Göttingen/Heidelberg. xi+259 pp., 210 text figs. Price DM 39.00.

This book is the first of a series to be devoted to monographic treatises on very limited subjects. This series is entitled *Mineralogie und Petrographie in Einzeldarstellungen*, and is under the editorship of F. K. Drescher-Kaden and O. H. Erdmannsdörffer.

The book is organized into four parts. The first part is introductory, and is concerned with the geometrical pitfalls in textural interpretation, classification of reaction textures, a blast at dry diffusion, and nomenclature. The second part contains chapters on myrmekite and its genesis, on graphic granite and granophyre—treated as a single phenomenon—and *its* genesis with generalizations on metasomatism, and on feldspathization of quartz. In each case, some of the older works are adequately reviewed. The third part of the book contains chapters on the space problem of crystalloblasts, the textural relations between crystalloblasts and groundmass, and saussuritization of feldspars. The final section is devoted to a contrast of *truly* igneous and granitic textures, and to a discussion of the source of the substance of aplite and pegmatite dikes. An incomplete summary of the literature is arranged according to year.

Since the book is concerned with the origins of granitic textures, it is in the midst of a lively controversy; the theories will meet approval or disapproval according to the reader's likes. Whether one agrees or disagrees—as do I—with Drescher-Kaden, he deserves full credit for many fertile ideas, only a few of which are considered in this review. Although his conclusions seem to be based too largely on assumption, his book is an important and useful contribution. The excellent descriptions add a wealth of useful information, much serious and sensible doubt is cast on the dogmas of textural interpretation (see also, Niggli, *Schweiz. Min. u. Pet. Mitt.*, Bd. **30,** p. 500, 1950) and the discussion is lively and unusually thought provoking. I wish to urge its reading as exceptionally worthwhile to both magmatist and granitizationist.

Descher-Kaden prefaces his descriptions with the opinion that all granites have a metasomatic origin—and this is a basic assumption in all of his arguments. Although recognizing the described textures to be late stage phenomena produced by the alteration of an earlier fabric, he considers them proof that the entire rock had a metasomatic origin. The crystalloblastic nature of these textures is compared with a *truly* igneous texture (volcanic porphyry), and is argued as proof that granites cannot have crystallized from a melt. It would seem more likely that the crystalloblastic character of many granitic rocks is an expression of a different environment from that of volcanic rocks, an environment more favorable to retention of volatile constituents of the magma and to the presence of exotic hydrothermal solutions, either of which would serve to alter an originally igneous texture into a crystalloblastic one.

A process of "cyclic metamorphism and rheomorphism" is advanced as an integrated

explanation of the several textures described. Although vaguely stated, this hypothesis may be abstracted as follows: metasomatic introduction of potash feldspar during the formation of myrmekite (excellent evidence is presented for the conclusion that potash feldspar is the youngest of the three minerals of myremekite texture) releases soda and lime for granitization of quartz-rich metamorphic rocks; the latter reaction supplies silica to the metasomatizing solutions for use in the formation of myremekite-quartz and of the quartz in graphic granite and granophyre; silica that replaces potash feldspar in the graphic granite reaction releases potash for the formation of the potash feldspar associated with myrmekite and for the sericitization of plagioclase. The hypothesis is too vaguely stated to allow fair criticism. It is surprising that Drescher-Kaden should attribute sericitization of plagioclase to metasomatic solutions. He contends that *all* potash for sericitization of plagioclase is introduced from external sources, overlooking the common presence of sufficient potash feldspar in solid solution to account for the total volume of sericite in a plagioclase crystal.

Noting a common lack of evidence for a channel along which metasomatic solutions were introduced into a partly replaced crystal, the idea of "wet-diffusion" through the structure of the crystal, via structural defects called "intertrunclare" ("lineage" of M. J. Buerger), is advanced and is termed "endeleptonisch." The American literature on this idea is apparently not known to Drescher-Kaden. The idea is intriguing and deserves careful consideration. Its use by Drescher-Kaden seems to be subjective; thus, sericite inclusions in quartz are interpreted in the usual way as inclusions of an older mineral whereas sericite in adjoining plagioclase crystals is interpreted as having been introduced—in light of the endeleptonisch hypothesis. Neither conclusion seems likely as a general rule.

The complete lack of descriptions of field occurrences to supplement and to clarify the microscopic data is unfortunate. To cite an isolated example, the formation of "trains" of liquid inclusions in quartz glyphs in graphic granite is argued for textural reasons—not very convincingly—to precede deformation (disaggregation) of the same glyph (p. 137). Tuttle's (*Jour. Geol.*, 1949, p. 331) careful study of these planes of liquid inclusions, in which field data play a critical part, renders Drescher-Kaden's conclusion very unlikely.

The descriptions of the textures are accurate, unusually detailed, and carefully documented with the numerous drawings and photographs, and, in the case of myrmekite, they are indeed a classic of this kind of study. Many of these illustrations and descriptions —cited as proof of one thing or another—are open to various interpretations. Several of the illustrations contradict Drescher-Kaden's conclusions. For example, photographs cited as showing evidence of auto-catharsis are, in this case, as good textural evidence against the process as one could ever expect to find.

The book is printed on two weights and surfaces of paper; this seems to be a common postwar practice of German publishers. In many instances, letters have failed to register. The covers are paper, and the binding is insecure.

GEORGE J. NEUERBURG